NITRITE AND NITRATE ANALYSIS IN WATER

VIA CHEMILUMINESCENCE

By

RAJESH KUMAR

Bachelor of Engineering

Vinoba Bhave University

Bihar, India

1996

Submitted to the Faculty of the
Graduate College of the
Oklahoma State University
in partial fulfillment of
the requirements for
the degree of
MASTER OF SCIENCE
May, 1998

NITRITE AND NITRATE ANALYSIS IN WATER

VIA CHEMILUMINESCENCE

Thesis Approved:

Randy S. Lewis

Thesis Advisor

Karen A. High

Allen W. Johannes

Wayne B. Powell

Dean of the Graduate College

ACKNOWLEDGMENTS

First of all, I thank God for bringing me to this stage in life and giving me the inner strength and self - belief to tide over the hard times in life. Respectful thanks are due to my parents for their love, guidance and support, and for always being there whenever I needed them. Special thanks are due to my sister, Sunita , and brother-in-law, Sandeep, for their moral support and guidance. I sincerely thank Dr. Randy S. Lewis for providing me academic and inspirational guidance throughout my graduate studies. None of this would have been possible without his active interest and constant encouragement. I am grateful to him and the department of Chemical Engineering for having financially supported me during the period of my graduate studies.

I would like to thank Dr. Arland H. Johannes and Dr. Karen A. High for serving on my thesis committee. I also thank Mr. Charles Baker and the staff of Chemical Engineering for their generous assistance. I am grateful to Anand, Mahendra, Zhang, Steve, Sheena, and all my friends for their help and kindness. I shall always treasure the times we have spent together.

TABLE OF CONTENTS

LIST OF FIGURES

LIST OF TABLES

Table Page

Chapter 1

Introduction

1.1 Biosynthesis and Bioactivity of NO

Nitric oxide (NO) is a highly reactive gas which is toxic in nature at relatively high concentrations. It produces pollutants upon reacting with oxygen and contributes to the ecological damage of acid rain when discharged into the atmosphere.

Moncada *et al.* identified NO as a biological molecule [1989]. NO is synthesized by many mammalian cells including macrophages, neutrophils, endothelial cells and hepatocytes [Conner and Grisham, 1993]. Physiological roles of NO include blood pressure regulation, inhibition of platelet aggregation, regulation of activities of the brain, lungs, liver, kidneys and other organs. The immune system utilizes NO in fighting viral, bacterial, and parasitic infections as well as tumors. The NO molecule has a number of reactive forms, which explains the diversity of its chemistry and the range of biological effects.

1.1.1 NO and the vascular system

NO is an important and versatile messenger in the vascular system. Endothelium derived relaxing factor (EDRF) which causes vasodilation, was discovered by Furchgott [1984], and Moncada *et al.* [1987] identified NO as the most important EDRF. The vasodilating activity of NO has been well established. The major source of NO that causes vasodilation is endothelial NO synthase (NOS). Endothelial NOS is activated by intracellular calcium increases due to acetylcholine exposure [Bredt *et al.*, 1991]. Some blood vessels, especially in the heart, lung, and brain, are seriously damaged when

ischemial reperfusion occurs in conjunction with accelerated NO production [Masini *et al.*, 1991]. The function of NO produced in a reperfusional system is not yet completely understood. In vascular systems, NO diffuses into the blood stream to produce NO-hemoglobin [Iwamoto *et al.*, 1994] or met-hemoglobin and to inhibit platelet aggregation and adhesion [McDonald *et al.*, 1993]. NO can also react with reactive oxygen species, such as superoxide, to form tissue damaging species. Other important sources of NO in the vasodilating system are non-cholinergic and non-adrenergic neurons. The NO from endothelium, non-cholinergic, and non-adrenergic neurons have been related to certain pathological conditions.

1.1.2 Neuronal NO

NO is generated in the nerve system [Grozdanovic *et al.*, 1994]. The presence of neuronal NOS in the skeletal muscle cell [Lobzik *et al.*, 1994] has also been reported. NOS in neurons is activated by calcium increases through agonist-receptor interactions. NO synthesized in the central nervous system (CNS), especially at nerve synapses, is significant because it is closely related to neuronal plasticity (long term potentiation)[Dinerman *et al.*, 1994]. In the cerebellum, NO production is related to the formation of long term depression [Shibuki *et al.*, 1994].

NO modulates the potassium channel [Bolotina *et al.*, 1994] to regulate neuronal transmission. In the peripheral nervous system, the main function of NO is vasoregulation [Toda *et al.*, 1994]. Renal blood flow is likely to be regulated indirectly with NO through the attenuation of sympathetic neuronal activity. The relationship between neuronal NO and excitatory neurotoxicity [Manchester *et al.*, 1993] has not yet

been fully explained. Nerve cells tend to die from overstimulation of excitatory neurotransmitters or agonists. It is unclear whether NO is protective [Dawson *et al.*, 1993] or destructive towards nerve cells [Zhang *et al.*, 1994].

1.1.3 NO and the immune system

Several cells including activated macrophages, nucleophiles, monocytes, and kuppfer cells release a greater amount of NO than endothelial or nerve cells. The origin of this NO is from a NOS different from the endothelial or nerve NOS [Baek, 1993]. The NOS is induced by cytokines or lipopolysaccharides (LPS) and is called inducible NOS (iNOS) [Geller *et al.*, 1993]. The major functions of NO from iNOS are the cytostatic and cytotoxic effects on invading microorganisms or tumor cells [Farias-Eisner *et al.*, 1994]. NO production of iNOS is essential for immune defense, but is sometimes related to pathological conditions, including sepsis, ischemia/reperfusion, acute pulmonary injury, multiple organ failure syndrome, and atherosclerosis. Complete scavenging of the NO is a likely requirement for the improvement of the pathological condition. Some studies show that certain NO scavenging agents like phenyl-4,4,5,5,-tetramethylimidazoline-1-oxyl-3-oxide derivatives (PTIOs) increase the survival rate of animals with NO-related pathological conditions [Yoshida *et al.*, 1994].

1.1.4 NO and the gastrointestinal system

In addition to maintaining vasodilator tone in the gastrointestinal system, NO along with prostacyclin is believed to be responsible for maintaining the integrity of the mucosal layer. NO also mediates some forms of muscular relaxation including the dilation of the stomach to adapt to increases in intragastric pressure [Rand, 1992], the

relaxation of the circular sigmoid muscle of the colon [Tam and Hiller, 1992], and the relaxation of anal sphincter muscle [Burliegh, 1992]. NO may be the key to finding the cure for male impotence as it is responsible for effecting penile erection [Ignarro *et al.*, 1990].

As in the cardiovascular system, NO-dependent dilator tone is essential for proper functioning of the organs. Deficiency of NOS in the pyloric tissue is responsible for hypertropic pyloric stenosis (blockage of the passage connecting the stomach to the duodenum) in infants [Vanderwinden *et al.*, 1992], while a deficiency of NOS in adult gastrophageal tissue seems to be the cause of achalasia (failure of smooth muscle in the gastrointestinal tract to relax) [Maerin *et al.*, 1993]. Inadequate production of NO in the corpus cavenosum (spongy body of the penis) may be the cause for male impotence.

1.1.5 NO as a cytotoxic and cytostatic agent

Macrophages and neutrophils synthesize NO as a defense against microorganisms such as bacteria [Hibbs *et al.*, 1990]. The biochemical basis of the cytotoxicity of NO is its reaction with iron containing moieties in the key enzymes of the respiratory cycle and/or DNA damage in the target cells [Moncada and Higgs, 1993]. NO is thus involved in non-specific immunity and the non-specific nature of its cytotoxicity may prove to be deleterious not only for the tumor cells and invading microorganisms but also for NO generating cells and their immediate neighbors. NO generation stimulated by iNOS could thus be responsible for the damage of healthy and normal tissue leading to the pathogenesis of rheumatoid arthritis, ulcerative colitis [Moncada and Higgs, 1993], insulin dependent diabetes mellitus (IDDM) [Bendtzen, 1989] and asthma [Moncada,

1994]. Inhibition of NO generation by introducing L-arginine analogs is known to alleviate inflammation and adjuvant arthritis in rats [Moncada and Higgs, 1993].

1.2 NO chemistry

NO is a simple hydrophobic gaseous molecule that is highly diffusible and highly reactive. NO is a free radical that has one pair electron in a 2p-π antibonding orbital and thus, is extremely unstable. It cannot maintain its original form for very long in a biological environment. As a result, it undergoes complex changes immediately after being released. The biological actions of NO differ from other major mediators in that (a) its functions are governed by its chemical properties as opposed to its shape, (b) it has a high diffusivity and can easily move from the site of production to the adjacent tissues, and (c) no enzymatic mechanism is needed for its removal [Conner and Grisham, 1995]. Being highly reactive, NO reacts with several species. The byproducts of some of these reactions may also be of physiological and pathological significance.

Although NO is unstable, in ultra pure water it forms a stable solution at room temperature. However, if dissolved oxygen is present in water, NO reacts with oxygen as shown in equations 1.1-1.5. Under most conditions with NO, reaction 1.4 is much faster than reaction 1.2, so an aqueous NO [Stamler *et al.*, 1992] solution gives nitrite (NO_2^-) as a decomposed product.

$$2NO + O_2 \rightarrow 2NO_2 \tag{1.1}$$

$$2NO_2 \Leftrightarrow N_2O_4 \tag{1.2}$$

$$N_2O_4 + H_2O \Leftrightarrow NO_2^- + NO_3^- + 2H^+ \tag{1.3}$$

$$NO + NO_2 \Leftrightarrow N_2O_3 \tag{1.4}$$

$$N_2O_3 + H_2O \Leftrightarrow 2NO_2^- + 2H^+ \tag{1.5}$$

Nitrous anhydride (N_2O_3) is a nitrosating agent and thus a cytotoxin that denatures DNA by nitrosation of the primary amines on DNA bases. It may also nitrosate secondary amines to yield carcinogenic and mutagenic products [Tannenbaum *et al.*, 1991].

Another reactive form of NO is the nitrosonium cation (NO^+). Although it may be formed in aqueous media, a major form of NO^+ equivalent is nitroso compounds in biological environments. Nitroso compounds can be made chemically through the reaction of sodium nitrite and nucleophiles in the presence of an acid. Nitroso compounds can also be directly produced by reacting N_2O_3 with a nucleophile.

$$N_2O_3 + R - XH \Leftrightarrow RS - X = NO + HNO_2 \tag{1.6}$$

NO also reacts with the superoxide anion (O_2^-), to form peroxynitrite.

$$NO + O_2^- \Leftrightarrow ONOO^- \tag{1.7}$$

Peroxynitrite is a strong oxidant that reacts in aqueous medium to form a very highly reactive " hydroxyl-like " radical [Beckman *et al.*, 1990b]. Peroxynitrite and the hydroxyl ion can cause lipid membrane peroxidation [Hogg *et al.*, 1992] and the denaturing of DNA [Delaney and Eizirik, 1996].

NO also forms complexes with transition metals. The interaction of NO with metalloproteins constitute relevant molecular mechanisms accounting for its signal transduction and cytotoxicity. NO readily reacts with the metal centers of proteins

including iron, iron-sulfur, and zinc-sulfur clusters [Radi, 1996]. These interactions with NO lead to the formation of metal nitrosyl complexes resulting in a modification of the structure and/or function of these proteins. In blood, excess of NO is scavenged by oxyhemoglobin to form met-hemoglobin and nitrate, or by deoxyhemoglobin to form a stable iron nitrosyl complex with its iron core. This depletes NO produced in tissues and characterizes NO as a local signal transduction molecule [Radi, 1996]. NO also reacts with the iron core in cytochrome-c oxidase and cytochrome P450 which leads to inhibition of mitochondrial electron transport [Cleeter *et al.*, 1994].

The interaction of NO with the iron-sulfur clusters of mitochondrial aconitase results in the inhibition of the Krebs cycle resulting from enzyme inactivation [Radi, 1996]. The interaction of NO with zinc present in the zinc-sulfur cluster of enzyme alcohol dehydrogenase leads to inhibition of the DNA binding ability of the enzyme [Radi, 1996].

Chapter 2

Trace analysis of nitrite and nitrate

2.1 Significance of nitrite and nitrate measurements

Nitrite (NO_2^-) and nitrate (NO_3^-) are generated in a wide array of natural systems. In the environment, both species are produced in a nitrification process in which ammonia is oxidized by soil bacteria. Humans are exposed to NO_3^- and NO_2^- through the ingestion of vegetables, water, and cured meats [White, 1975]. Analysis of NO_2^- is important due to its role in environmental processes, its toxicity, and its suspected carcinogenicity in humans. NO_2^-, at high concentration levels, can be fatal to infants causing a condition known as methemoglobinemia [Swann, 1975]. Measurement of NO_2^- has recently been examined as a surrogate for in vivo NO production [Termin *et al.*, 1992]. Also of importance is the relationship of NO_2^- and NO_3^- in the formation of N-nitrosoamines [Panalaks *et al.*, 1973].

2.2 Methods of NO_2^- and NO_3^- measurements

Sensitive and selective methods are required to measure NO_2^- and NO_3^- at low levels in the complex matrices found in water, foods, and biological fluids. Generally, calorimetric methods are used for the determination of NO_2^- and NO_3^- [USEPA, 1974]. A common calorimetric method for NO_2^- measurement involves the reaction of NO_2^- with sulfanilamide in acidic solution to yield a diazonium salt which is coupled with an aromatic amine to produce a highly colored azo compound [Sawicki, 1963]. This method can detect up to 0.13 μmol of NO_2^- in the test sample and is a slow process, taking 34

minutes for each sample analysis. Methods for the spectrophotometric determination of NO_3^- are generally based on nitration of phenolic compounds [West, 1960], oxidation of an organic compound by NO_3^-, or reduction of NO_3^- to NO_2^- and determination via the sulfanilamide method [APHA-AWWA-WPCF 14th ed.; Washington D.C.]. These methods require a large volume of sample to generate accurate results. The detection limit is around 1.6 μM. The biggest disadvantage of this method is the interference of chloride ions present in the sample. Since most samples have chloride ions, each sample requires precipitation of the chloride ion before any analysis can be done. This makes the process tedious and requires careful preparation and interpretation when working with biological media [Wegner, 1972]. Ion chromatography has been applied to the determination of NO_3^- in environmental samples [Molik, 1976]. It has a minimum detection limit of 32 nmol of NO_3^- and a sampling time of 1 hour. This method is more selective than those based on calorimetry, but is limited by lack of sensitivity and interference.

NO_3^- can also be determined by reduction to ammonia and its subsequent ultraviolet absorption [Cresser, 1977]. Titanium (III) sulfate rapidly reduces NO_3^- to ammonia at room temperature and provides a sensitive and selective method for the determination of NO_3^-. The detection limit for this method is 80 nmol. However, ions which affect the reduction of NO_3^- by titanium (III) salts interfere with this method and must be removed if present in large amounts.

Nanomolar concentrations of NO_2^- in natural waters have been determined using liquid chromatography [Kieber, 1995]. The NO_2^- reacts with 2,4-dinitrophenylhydrazine to

form 2,4-dinitrophenyl azide under acidic conditions. The azide formed is quantified by HPLC. This method is simple and has a low detection limit of 0.1 nM. However, it is limited by interference from other ions present in the azide formed. The separation of interfering substances makes this method slow with only eight samples being analyzed per hour. Methods have also been described in which NO_2^- and NO_3^- have been determined by thermal reduction to NO followed by chemiluminescence detection [Moskowitz, 1977].

Increasingly, chemiluminescence methods are being applied for determining very low concentrations of NO_2^- in water. Flow injection analysis has been used in many studies for the detection of NO_2^- and NO_3^-. The difference mostly lies in the choice of reducing agents. One flow injection method [Pavel, 1995] used hydrogen peroxide (H_2O_2) in acidic medium to convert NO_2^- to peroxynitrous acid. Peroxynitrous acid is converted to peroxynitrite by the chemiluminescence reaction with alkaline solution of luminol. The detection limit of NO_2^- is 1 nM for 50 µl sample (0.05 pmol) and the calibration curve is linear up to 10 µM NO_2^-. This method requires a cation-exchange column as it is limited by interference effects of the cations. Aoki *et al.* [1995] used Ti(III) as a reductant for a sample containing both NO_2^- and NO_3^-, and iodide solution for a sample containing NO_2^- only. The difference between the peak heights obtained for the two reducing solutions corresponded to the NO_3^- present in the sample. This method has a detection limit of 80 nmol for NO_3^- and 65 nmol for NO_2^-. NO_2^- has also been determined in environmental and biological samples by using Vanadium(III) in acidic medium at room temperature. NO_3^- can also be rapidly reduced to NO at 80 -90 ^{0}C in this

solution[Braman, 1989]. Sodium iodide in a mild acidic media reduces NO_2^- to NO at room temperature and NO_3^- to NO under stronger reducing conditions [Cox, 1980]. Aqueous NO_2^- has been determined using sodium iodide in phosphoric acid in a flow system [Dunham, 1995].

2.3 Research Methods

The chemiluminescence method was adopted for the analysis of NO_2^- and NO_3^-. Since chemiluminescence detection is selective for the measurement of NO, and since the detection occurs in the gas-phase, neither sample coloration nor turbidity interfere with the measurement. However, ions may affect the conversion of NO_2^-/NO_3^- to NO.

Two different reducing agents were studied. Potassium iodide (KI) in glacial acetic acid (CH_3COOH) rapidly reduces NO_2^- to NO [Cox, 1980]. For NO_3^- determination, solutions of 4% ferrous ammonium sulfate [Aldrich Chemical Co.] and 2% ammonium molybdate [Aldrich Chemical Co.] were used to convert NO_3^- to NO[Cox, 1980]. NO_3^- reduction occurs rapidly between 80-90 ^{0}C. NO_3^- reductors, which are small screw capped vials having cadmium coated inner walls, were also used to reduce NO_3^- to NO_2^-, after which the NO_2^- is converted to NO using the glacial acetic acid solution. These vials reduce NO_3^- to NO_2^- at room temperature.

Two systems were developed and studied for the analysis of NO_2^- and NO_3^-. The first experimental setup was a flow system with a continuous flow of the reducing agent, a mixing chamber, and a permeation chamber connected to the chemiluminescence detector (Figure 2.1). In the permeation chamber, generated NO diffuses through the semi-

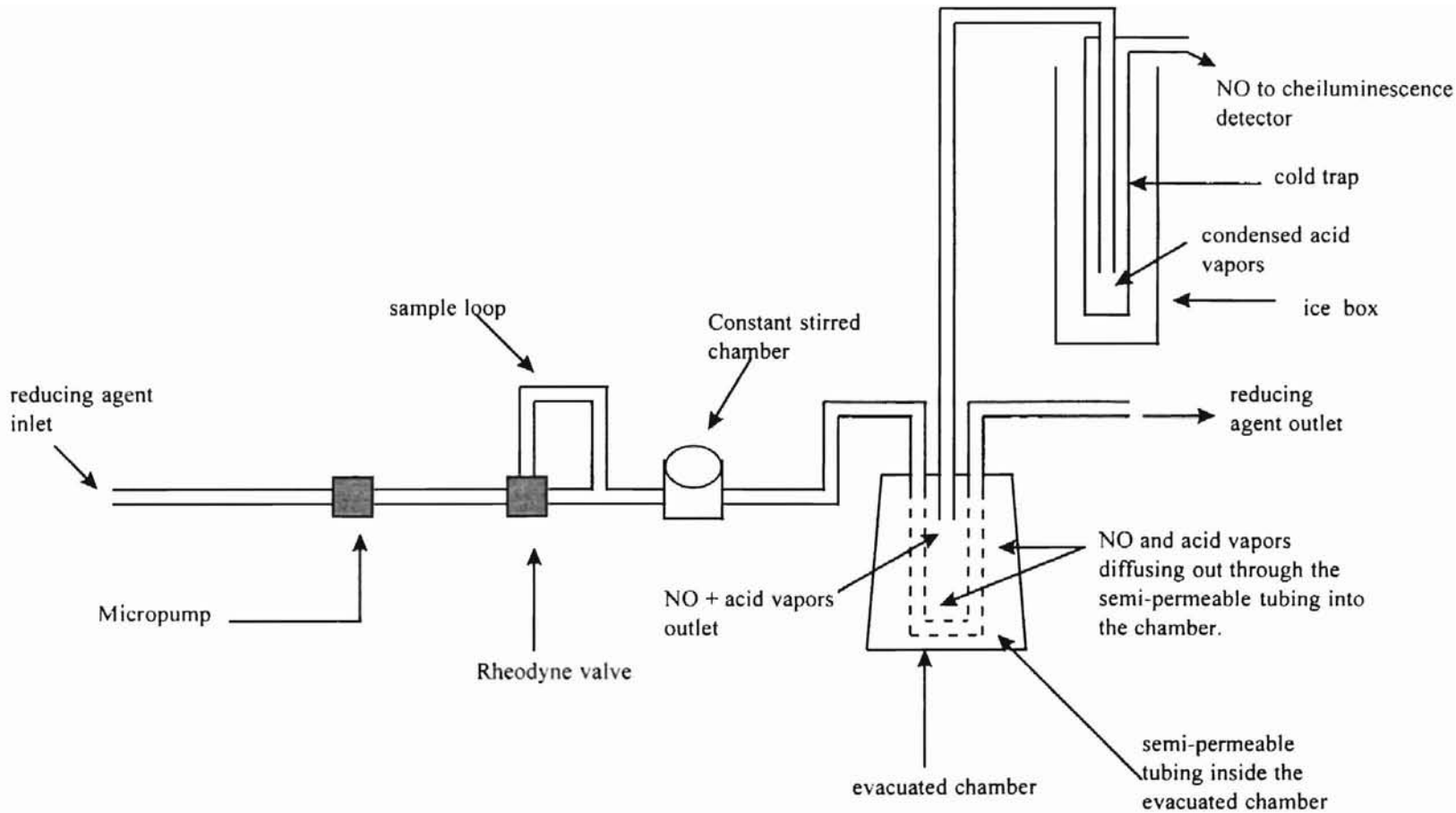

Figure 2.1 : Flow system for the analysis of nitrite and nitrate - permeation method.

permeable membrane and into the detector, whereupon reaction with ozone produces a response which is recorded on a chart recorder. The second system consisted of a small vial containing 10 ml reducing agent. The reducing solution is continuously purged with ultra pure nitrogen and the NO generated by injecting a sample into the solution is transferred to the nitrogen and transported to the detector (Figure 2.2). The response is recorded on a chart recorder. The NO passes through a cold trap so that the acetic acid vapors can be condensed and only NO and nitrogen go into the detector. Condensation of acid vapors is necessary to prevent any damage to the detector.

Though micromolar detection limits of NO_2^- have been achieved previously, reaction kinetics of NO_2^- and NO_3^- have not been determined with the two reducing agents. Dunham [1995] used a long reaction coil in his flow system to allow sufficient time for the reaction to occur with a reducing agent consisting of freshly prepared 0.1 M sodium iodide and 0.1 M phosphoric acid. However, the kinetics and transport issues have not been studied or optimized to determine the optimal design for measuring NO_2^- and NO_3^- samples. This project takes into consideration the mass transfer and kinetics of NO in the two systems described above.

The methods employed in this study are potentially applicable to the analysis of other nitrogen-containing trace species in aqueous or biological samples via reactions which form NO, NO_2^-, or NO_3^-.

2.4 Thesis Objectives

The overall objective of this research was to develop and implement an optimized method for measuring both NO_2^- and NO_3^- concentrations via chemiluminescence

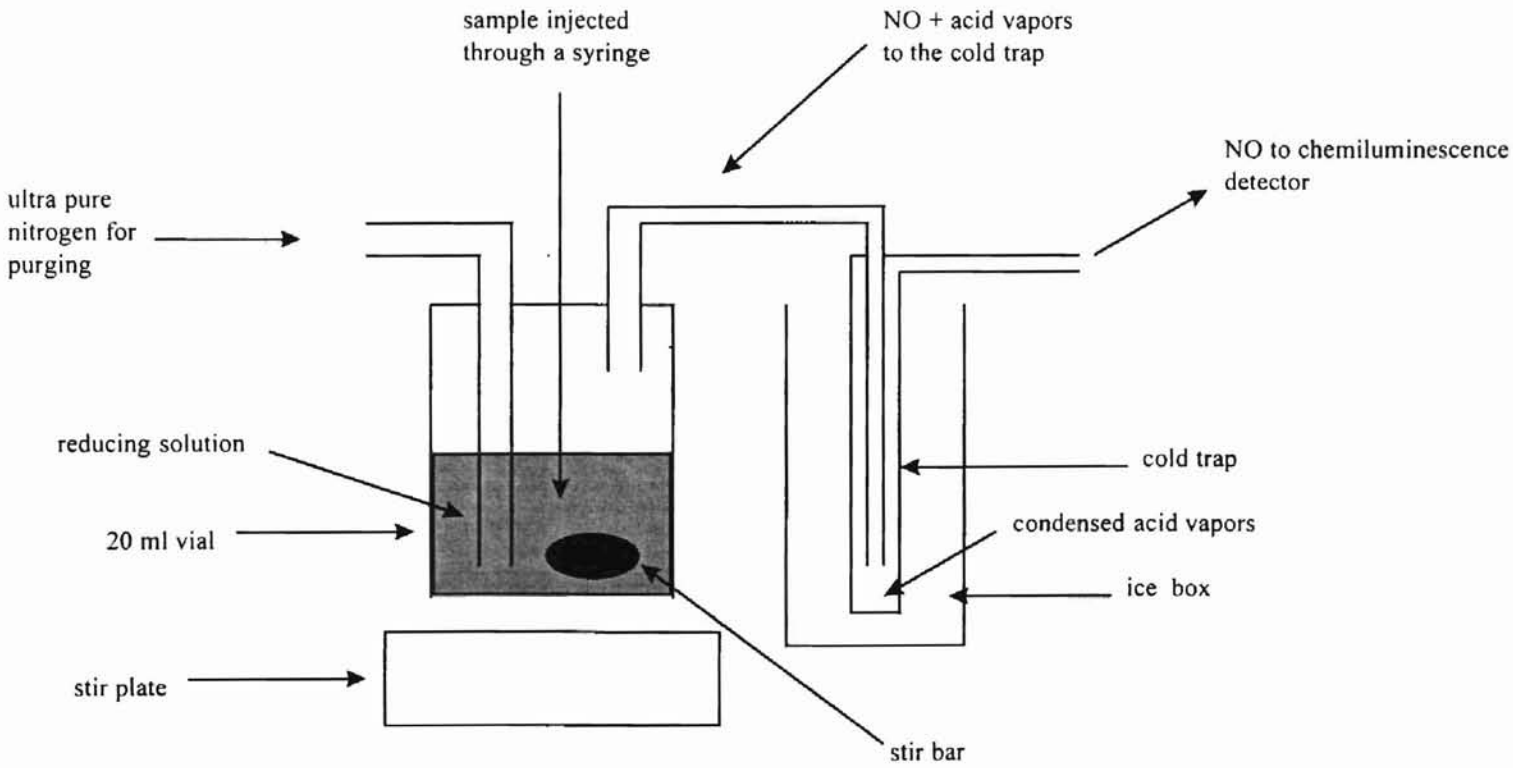

Figure 2.2 : Flow system for the analysis of nitrate and nitrite - purge method.

detection. This method was applied for multiple samples analysis. The overall objective was achieved through the completion of three specific aims given below:

2.4.1 Aim # 1: Study of the reaction kinetics of NO generated from NO_2^- and NO_3^-.

The objective of this aim was to kinetically characterize the rate of formation of NO and the degree of conversion of NO_2^- or NO_3^- in the given reducing agent. The reducing agent for NO_2^- was glacial acetic acid and 0.2M potassium iodide [Fisher Chemical Co.] in the ratio 1:3. The reaction rates of NO_2^- and NO_3^- were also studied in a second reducing agent consisting of 4% ammonium ferrous sulfate and 2% ammonium molybdate and concentrated phosphoric acid in the ratio 1:1:5.

All reactions were performed in a stirred chamber with a semi-permeable membrane at the bottom to continuously measure the NO concentration via chemiluminescence [Lewis *et al.*, 1994]. Rates of reaction at different temperatures were studied to determine optimum reaction conditions. The NO rate of formation was utilized for optimization of NO_2^- and NO_3^- analysis.

2.4.2 Aim # 2: Design and optimization of a NO_3^- and NO_2^- analytical apparatus.

The objective of this aim was to develop and optimize the design of a method for measuring both NO_2^- and NO_3^- concentrations. The system incorporated a continuous flow of the reducing agent as previously described in section 2.3. To minimize the residence time for sample analysis, the flow rate, temperature, and apparatus dimensions were optimized using a model for mass transfer in small capillaries [Davis, 1970]. The

minimized residence time allows the optimum number of samples to be analyzed within a given time period.

2.4.3 Aim # 3: Evaluation of the sensitivity of NO_2^- and NO_3^- measurements.

The objective of this aim was to evaluate the accuracy and sensitivity of the NO_2^- and NO_3^- measurements. Calibration standards of deoxygenated solutions with a known NO concentration were prepared and injected for comparison with samples of different concentrations of NO_2^- and NO_3^- prepared in deionized water. Minimum detection limits were obtained and methods to further increase the sensitivity and accuracy were studied. The effect of solution flow rate and tube dimensions on the sensitivity of the analytical apparatus were studied and limitations of the system identified.

The second system (purge method), as previously described in section 2.3, was also studied and compared with the flow system. The effect of the rate of mass transfer on the sensitivity and sampling time for the second system was determined.

Chapter 3

Determination of reaction kinetics of NO generated from nitrite & nitrate

Reaction kinetics describe the rate of a reaction under a given set of conditions. Kinetic experiments can determine the rate of a reaction, the equilibrium conditions if they exist, and the activation energy of a reaction. Once the kinetics are determined, the parameters governing the rate law are identified. The reaction kinetics of NO_2^- and NO_3^- in the glacial reducing agent and the phosphoric reducing agent were evaluated. A rate law was hypothesized for the conversion of NO_2^- and NO_3^- to NO and the data obtained was fit to the rate equation to test the validity of the hypothesis. The study of reaction kinetics and the determination of reaction parameters was necessary to meet the following objectives:

1) Development of a highly sensitive analytical system to measures trace amounts (preferably in the nanomolar ranges) of NO_2^- and NO_3^- . The sensitivity of the chemiluminescence analytical system depends on the NO flux going into the detector which depends upon the rate and percent of conversion of NO_2^- and NO_3^- to NO. The rate of conversion can be assessed by measuring NO formation in solution.
2) Achievement of a small sampling time which allows samples to be assayed quickly. A quick assay requires a rapid reaction and a high transfer rate of NO from solution into the detector. The rate of a reaction can be determined only through the study of reaction kinetics. Once the reaction kinetics are known and the reaction parameters determined, the analytical system can be optimized to give maximum sensitivity in a minimum sampling time.

3.1 Theory

The reduction of NO_2^- or NO_3^- in acidic media, such as phosphoric acid or sulfuric acid, is achievable with many reducing agents including urea, titanium (II), iron (III), molybdenum (VI), and/or vanadium(III) [Cox, 1980]. The chemical reduction of NO_3^- requires highly acidic conditions except when vanadium(II) is used as a reducing agent. Reduction of NO_2^- can be achieved at room temperature, but NO_3^- reduction requires temperatures in the range of 80^0 - 90^0C [Aoki *et al.*, 1985]. Experiments at room temperature only reduce the NO_2^-. Once the NO_2^- content of the sample is determined, the total NO_2^- and NO_3^- content can be determined using stronger reducing conditions and a higher temperature. Thus, the NO_3^- is determined by difference [Cox, 1980].

The basic approach towards the development of an analytical methodology for NO_2^- and NO_3^- was reduction of these species to NO and subsequent determination of NO via the chemiluminescent reaction with ozone. Equations for the respective reactions are:

$$NO_3^- + 2H^+ + 2e \Rightarrow NO_2^- + H_2O \qquad (3.1)$$

$$NO_2^- + 2H^+ + e \Rightarrow NO + H_2O \qquad (3.2)$$

NO_2^- can be reduced under much milder conditions than NO_3^- [Hassan, 1972]. Although NO_3^- is reduced to NO_2^- at temperatures in the range of 80^0 - 90^0C, NO_3^- can also be converted to NO_2^- at room temperature via a cadmium coated vial [World Precision Instrument Inc.]. The cadmium acts as a catalyst which is capable of reducing NO_3^- to NO_2^- without any reducing agent. The NO_2^- formed can then be reduced to NO in an acidic reduction medium. Thus, the amount of NO_3^- originally present in the sample is

determined. This study uses a NO_3^- reducing agent as well as cadmium reduction for the determination of NO_3^-.

3.2 Reagents used for analysis

Ideal reagents for conversion of NO_2^- and NO_3^- to NO for analysis would have the following criteria:

1) A 100% conversion to NO should be achieved,
2) The reaction must be rapid and quantitative at low NO_2^- and NO_3^- levels, and
3) The reagent should be of low volatility to minimize acid vapors going to the detector and to minimize solution loss via evaporation.

Cox reports [1980] that iodide ion in a weakly acidic medium is a very efficient reducing agent for NO_2^-. The reaction product is NO there is no interference from the reagent ions, and the solution can be easily prepared. Fe(II) and Mo(VI), and Ti(III) in highly acidic medium at around 80^0 - 90^0C allows for the reduction of NO_3^- to NO at the parts-per-billion level [Cox, 1980].

NO_2^- reducing agent was prepared by mixing 0.2 M potassium iodide [Fisher Chemical Co.] and glacial acetic acid [Fisher Chemical Co.] in the ratio 1:3. For NO_3^- reducing agent, solutions of 4% ferrous ammonium sulfate and 2% ammonium molybdate [Aldrich Chemical Co.] were added to concentrated (85%) phosphoric acid (H_3PO_4) in the ratio 1:1:5. Distilled water was used for the preparation of samples and the reducing solutions.

3.3 Experimental setup and procedure

Experimental setup: All reactions were performed in a modified 200 ml ultrafiltration chamber adapted to continuously measure the NO concentration via chemiluminescence

(Figure 3.1). The chamber has a stirring rod to provide quick mixing of the injected sample with the reducing solution in the chamber. A thermometer inserted in the lid shows the temperature of the reacting solution. The chamber has a gas inlet port to allow continuous purging of the head space and a gas outlet port to allow the purged gases to leave the chamber. The bottom of the chamber has a perforated plate covered with a NO-permeable silastic membrane. The side of the membrane not exposed to the solution is connected to the chemiluminescence detector which provides a vacuum to create a driving force to transport NO from solution and into the detector. The NO, upon reaction with ozone, produces a signal which is recorded on a chart recorder. A cold trap was placed in the vacuum line to condense acidic vapors.

Procedure: For the NO_2^- analysis, 100 ml of glacial reducing agent was freshly prepared and added to the reaction chamber and continuously stirred. The stirring speed was maintained at 220 rpm in all the studies. The head space was continuously purged with argon to remove oxygen to minimize the reaction of NO with O_2 to form NO_2^-. However, the presence of oxygen did not affect the analysis as the reducing agent would convert NO_2^- back to NO. After purging with argon for 45 minutes, 1 ml samples of solutions containing known concentrations of NO and NO_2^- in .01 M phosphate buffer were injected into the reducing agent at room temperature. Three injections of each sample were analyzed. Due to the continuous purging, the concentration of NO in the head space was always maintained at zero. The chemiluminescence detector response for different concentrations of NO and NO_2^- were compared. The areas under the response curves for different concentrations were also calculated and compared.

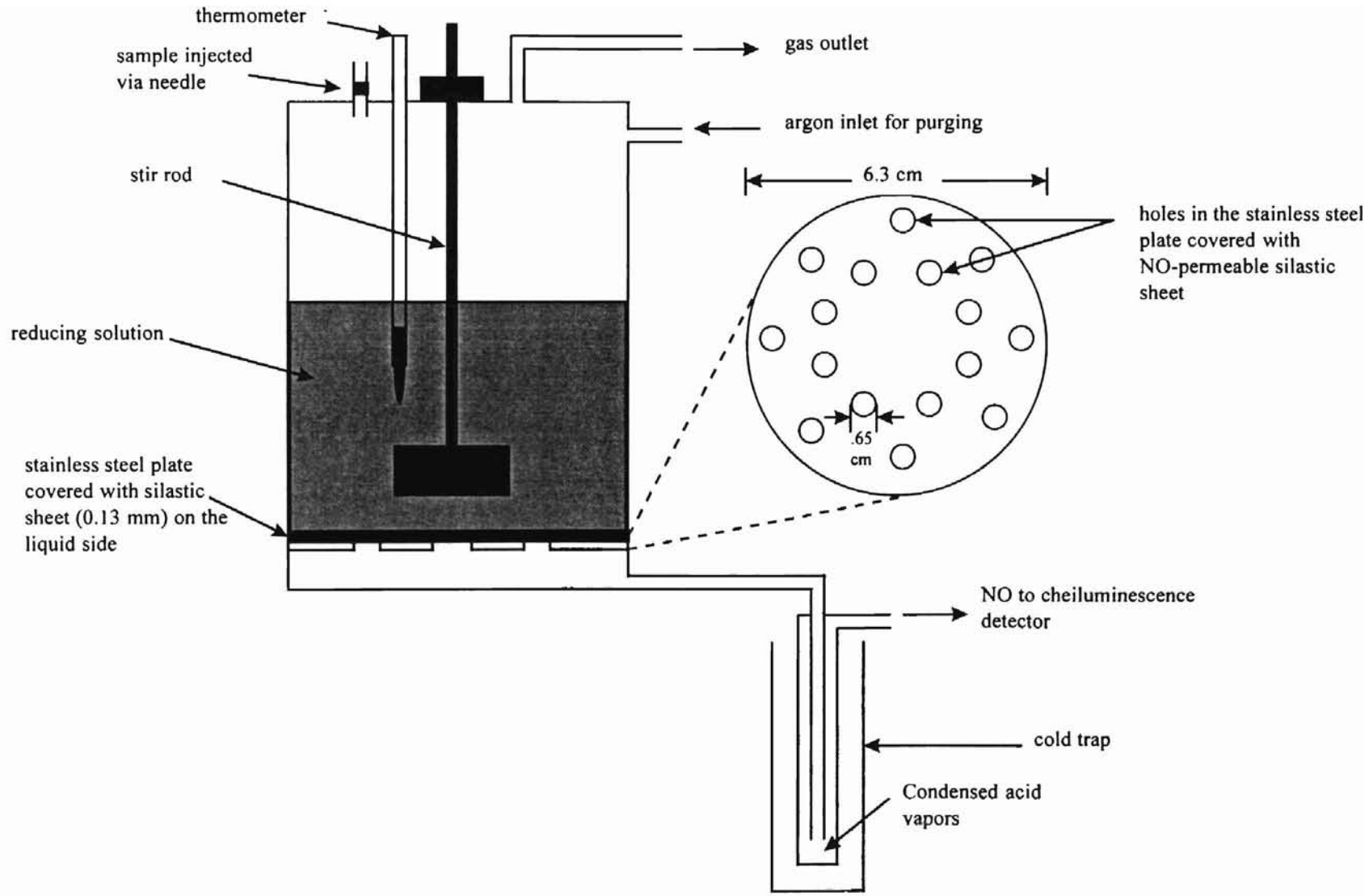

Figure 3.1 : Schematic of apparatus used to study reaction kinetics

For the study of reaction kinetics in the phosphoric reducing agent , the same set up and procedure was used. Since NO_3^- is converted to NO at high temperatures [Cox 1980], the NO_3^- study was done at temperatures of 35°C, 50°C and 77°C. Studies were not done at temperatures higher than those mentioned as the volatility of the reducing agent caused a significant amount of acid vapors to be produced. This required the volume change to be taken into account and also required the cleaning of the acid trap frequently to prevent any acid vapors from entering the detector.

The use of cadmium reduction involved an extra step in which the NO_3^- was reduced to NO_2^- in 1 ml cadmium vials. Ammonia buffer (0.5 M) of pH 9 was prepared with 0.5 M ammonium chloride salt solution and adding sodium hydroxide until the pH was adjusted to 9. Equal volumes of NO_3^- sample and ammonia buffer were added to the vial and allowed to react for up to 90 minutes. After reaction, the sample was injected into the reducing agent for NO_2^-. This method eliminated the use of the stronger reducing agent for NO_3^- and did not require heating of the solution for conversion to NO.

3.4 Reaction Model

In order to analyze the kinetics of NO_2^- and NO_3^- conversion to NO, a model was developed. The continuity equation of NO for a well-mixed system is

$$\frac{d[NO]}{dt} = R_{NO} - \left(\frac{k_L a}{V}\right)_{NO} [NO] \tag{3.3}$$

where $(k_L a/V)_{NO}$ is the combined volumetric mass transfer coefficient for the gas/liquid interface and the semi-permeable membrane. The above equation states that the rate of

change of NO concentration in the solution is equal to the rate of NO produced from NO_2^- minus the rate of NO transporting out of the solution into the gas phase and detector. The rate of change of NO_2^- concentration in the stirred chamber is

$$\frac{d[NO_2^-]}{dt} = R_{NO_2^-} \tag{3.4}$$

NO_2^- is converted to NO in the glacial reducing agent according to the following equation

$$NO_2^- \rightarrow \alpha NO + \textit{ other potential products} \tag{3.5}$$

where α is the ratio of NO produced to NO_2^- reacted. To determine the reaction kinetics of Eq.3.5, it is hypothesized that the rate of reaction of NO_2^- is proportional to the concentration of NO_2^- thus,

$$-R_{NO_2^-} = \frac{R_{NO}}{\alpha} = k_1[NO_2^-] \tag{3.6}$$

Integrating Eq.3.4 and substituting into Eq.3.3 yields

$$\frac{d[NO]}{dt} = \alpha k_1[NO_2^-]_0 e^{-k_1 t} - (\frac{k_L a}{V})[NO] \tag{3.7}$$

where $[NO_2^-]_0$ is the initial NO_2^- concentration. The objective of this study is to evaluate the parameters α and k_1 for optimization of the analytical measuring system using kinetic analysis. In order to do so, the value of $(k_L a/V)_{NO}$ must be determined. Once the parameters of the equation are determined, a good fit of the experimental NO data with Eq.3.7 would validate the hypothesized rate law of Eq.3.6.

3.5 Determination of model parameters

Evaluation of (k_La/V) : The volumetric mass transfer coefficient $(k_La/V)_{NO}$ can be calculated by injecting NO into the reducing solution. When NO is injected into the reducing solution, the R_{NO} term of Eq.3.3 is zero and the equation reduces to

$$\frac{d[NO]}{dt} = -\left(\frac{k_L a}{V}\right)_{NO}[NO] \tag{3.8}$$

This equation on integration with respect to time is

$$\frac{[NO]}{[NO]_0} = e^{-\left(\frac{k_L a}{V}\right)t} \tag{3.9}$$

where $[NO]_0$ is some initial concentration of NO. If the value of $[NO]/[NO]_0$ is known as a function of time, then $(k_La/V)_{NO}$ can be calculated.

Evaluation of α for NO_2^- conversion: The value of α can be determined from equal concentration injections of NO_2^- and NO into the reducing solution. The total amount of NO generated from NO_2^- relative to the total amount of NO added is;

$$\alpha = \frac{[\int_0^\infty \left(\frac{k_L a}{V}\right)_{NO}(NO)dt]_{NO_2^-}}{[\int_0^\infty \left(\frac{k_L a}{V}\right)_{NO}(NO)dt]_{NO}} = \frac{\left[\int_0^\infty (NO)dt\right]_{NO_2^-}}{\left[\int_0^\infty (NO)dt\right]_{NO}} \tag{3.10}$$

Thus, by injecting equal concentrations of NO_2^- and NO (in separate experiments), and calculating the response area under the NO curves, the value of α can be determined.

Evaluation of k_1 for NO_2^- conversion: After determining the values of $(k_La/V)_{NO}$ and α, the rate constant k_1 can be determined by substituting the values for $(k_La/V)_{NO}$ and α in Eq.3.7 and fitting the *(NO) vs t* data to the equation. The value of k_1 which best fits the equation to the data is the value of k_1 for the reaction assuming the hypothesized reaction kinetics of Eq.3.6 are correct. Having determined the three parameters, $(k_La/V)_{NO}$, α, and k_1, the reaction kinetics of NO_2^- are completely determined.

For the determination of α and the rate constant k_2 for NO_3^-, a rate law was hypothesized. Since earlier studies [Aoki *et al.*, 1985] showed that NO_3^- conversion was incomplete, then a hypothesized reaction is

$$\begin{aligned} NO_3^- &\xrightarrow{k_2} NO \\ NO_3^- &\xrightarrow{k_3} X \end{aligned} \tag{3.11}$$

where X is an unknown species produced by the reaction. Assuming first-order rate kinetics, the rate of change of NO and NO_3^- according to Eq.3.12 is represented by the following equations

$$\frac{d[NO]}{dt} = k_2[NO_3^-] - \left(\frac{k_La}{V}\right)_{NO}[NO] \tag{3.12}$$

$$\frac{d[NO_3^-]}{dt} = -(k_2 + k_3)[NO_3^-] \tag{3.13}$$

On substituting the integral of Eq.3.13 in Eq.3.12, Eq.3.12 becomes

$$\frac{d[NO]}{dt} = R_{NO} - \left(\frac{k_La}{V}\right)_{NO}[NO] \tag{3.14}$$

$$R_{NO} = k_2[NO_3^-]_0 e^{-(k_2+k_3)t} \tag{3.15}$$

Since the initial concentration of NO_3^- and $(k_La/V)_{NO}$ are known, a plot of $\ln(R_{NO})$ vs t would yield a slope of $-(k_2+k_3)$ and an intercept of $\ln(k_2[NO_3^-]_0)$. The value of R_{NO} is calculated from NO vs t data according to Eq.3.14

Evaluation of α for NO_3^- conversion: The value of α is the ratio of NO formed to the initial amount of NO_3^- present. R_{NO} integrated over time from zero to infinity gives the total NO formed.

$$\alpha = \frac{\int_0^\infty R_{NO}}{[NO_3^-]_0} = \int_0^\infty k_2 e^{-(k_2+k_3)t} = \frac{k_2}{k_2+k_3} \tag{3.16}$$

Thus, the ratio gives the value of α based upon the hypothesized kinetics. The value of α is also determined by calculating the area under the response curve as described in the section for evaluating α for NO_2^-conversion. This latter method could also be used for determining α for NO_2^- conversion.

3.6 Results

3.6.1 NO_2^- kinetics.

The experiments were performed as described in the previous sections and the data obtained was analyzed to establish the reaction parameters. On injecting 1ml of 1μM NO at room temperature into the glacial reducing solution a response was obtained (Figure 3.2). With proper calibration the curve gives the concentration of NO in the reducing solution with respect to time. Although the initial response was rapid, the slight lag is

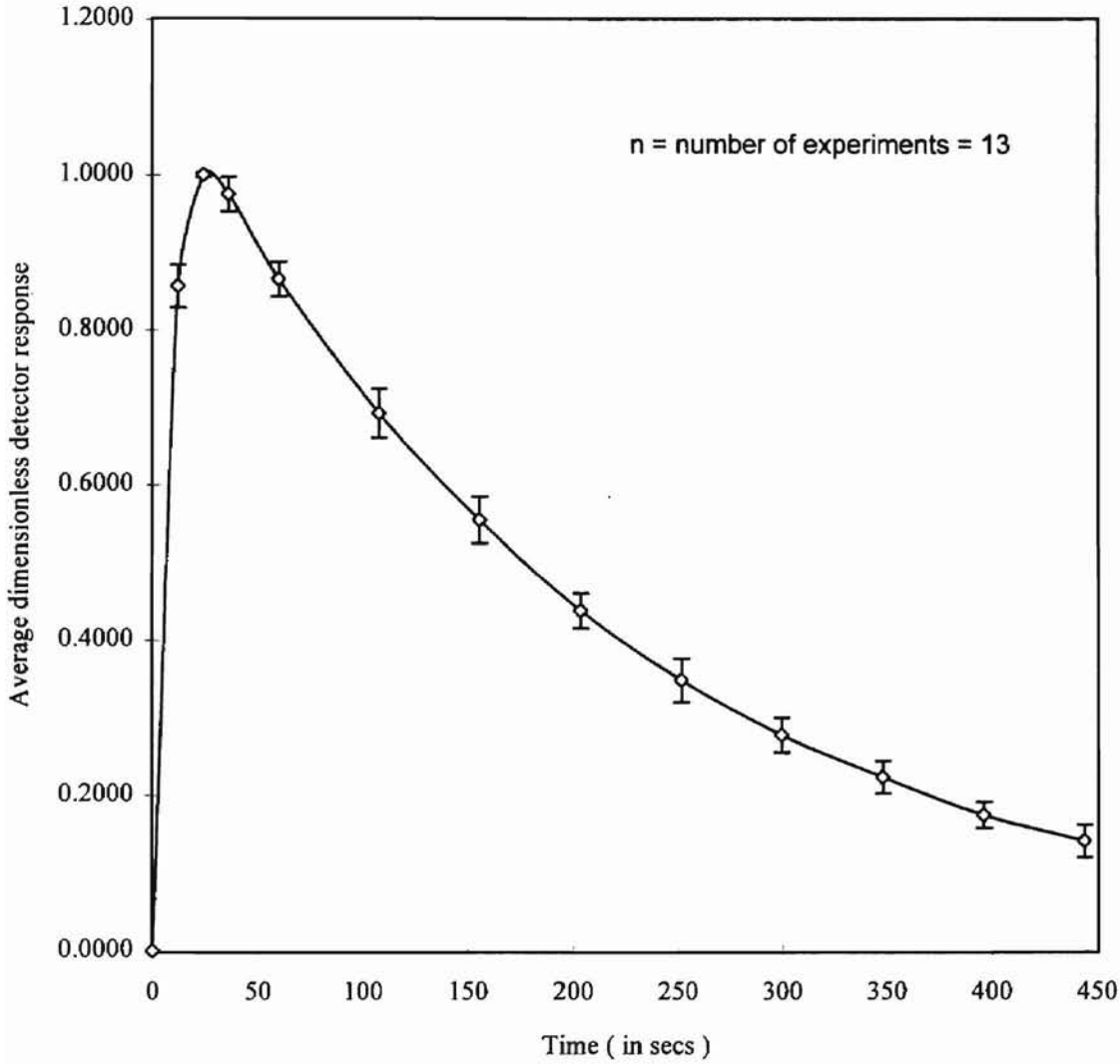

Figure 3.2 : NO Profile

likely attributed to a contribution of the response time of the detector, the mixing of the sample in the solution, and the variability of injection location. Preliminary studies using a dye solution showed that the mixing is essentially complete within 5 seconds following injection of a dye. Eq.3.9 shows that approximately 2%-3% of NO could be lost from the solution in 5 seconds, which is well within the limits of experimental error. However, the peak height of the NO response curve depended on the position of injection of the sample in the reducing solution. When the sample was injected closer to the silastic membrane at the bottom of the reaction chamber, the peak height was higher than when the sample was injected higher up. The difference in peak heights for the different positions of injections was significant and hence not suitable for calibration purposes. The NO_2^- samples did not show variation in peak heights with change in injection position. Thus, if there is instantaneous and complete conversion of NO_2^- to NO, the NO_2^- sample could be used for NO calibration of the analytical system.

Evaluation of (k_La/V) : The volumetric mass transfer coefficient, (k_La/V), was calculated from the decay data of NO and Eq.3.9 and was .0043 sec^{-1}. For NO_2^-, a 1 μM sample was injected and a concentration profile was obtained. The volumetric mass transfer coefficient for NO following formation from NO_2^- was also calculated using Eq.3.9 and was .0043 sec^{-1}, which is the same as that obtained for NO (Figure3.3).

Evaluation of α : The calculation of α required the area under the NO_2^- and NO response curves (Eq.3.10). However, it was observed that the NO sample was contaminated with NO_2^- likely due to incomplete purging of oxygen and subsequent reaction of NO with oxygen to form NO_2^-. To properly compare the area under the NO_2^-

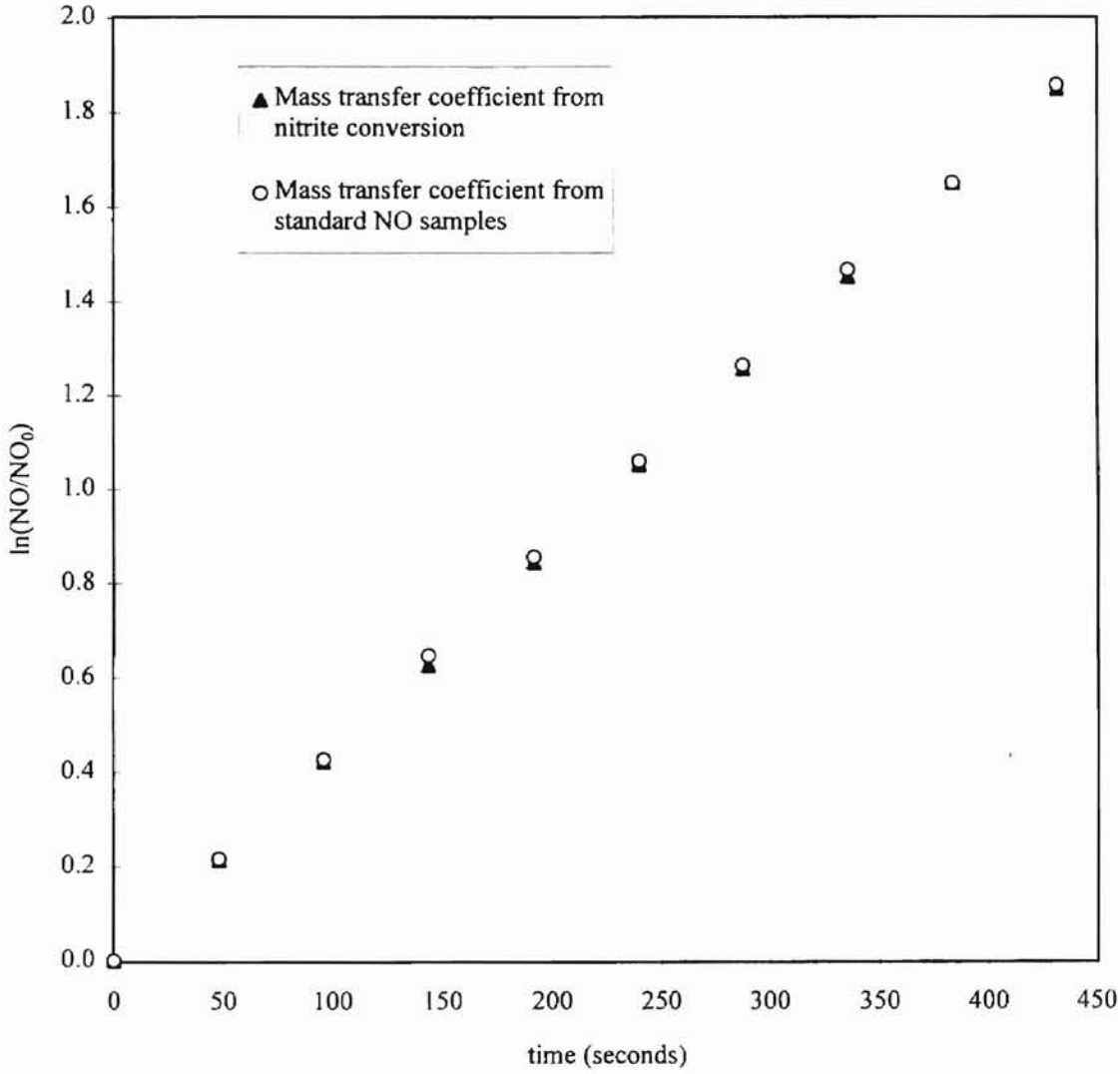

Figure 3.3 : Mass transfer coefficient in glacial reducing agent at 25^0C.

and NO response curves, the area resulting from NO_2^- contamination of the NO sample has to be subtracted from the response curve following the injection of NO. To find the area due to NO_2^- present in the NO sample, the NO saturated phosphate buffer solution was purged with argon for 15 minutes to remove NO from the solution. The purged solution was then injected into the glacial reducing agent and a response curve obtained. The area under the curve represented the contribution of NO_2^- in the NO sample. This area was subtracted off from the area of the NO response curve to obtain the area due only to the NO.

The areas obtained for NO_2^- and NO samples were within 10% of each other (Figure 3.4). The conversion factor α for the glacial reducing agent was determined by taking the ratio of the area under the NO_2^- and NO curves. The value of α was calculated for experiments performed on three different days. For 1 μM sample injections of NO_2^- and NO, the value of α was 0.99 ± 0.1.

The value of α obtained in the phosphoric reducing agent for 1 μM NO_2^- was 1.07 ± 0.06. The area of NO curve and NO_2^- curve were within 10% of each other at all the three temperatures. Thus, NO_2^- conversion was essentially complete within measurement errors likely due to the difficulty of adding an exact amount of NO to solution.

Evaluation of k_1 : The value obtained for α in both the reducing agents indicates that NO_2^- is essentially all converted to NO. To compare the behavior of NO_2^- sample with NO, the detector response versus time for NO_2^- and NO injections was plotted. Since the peak height changed from day to day, a direct comparison of plots obtained on different days would have lead to erroneous results. Hence, to make these plots independent of

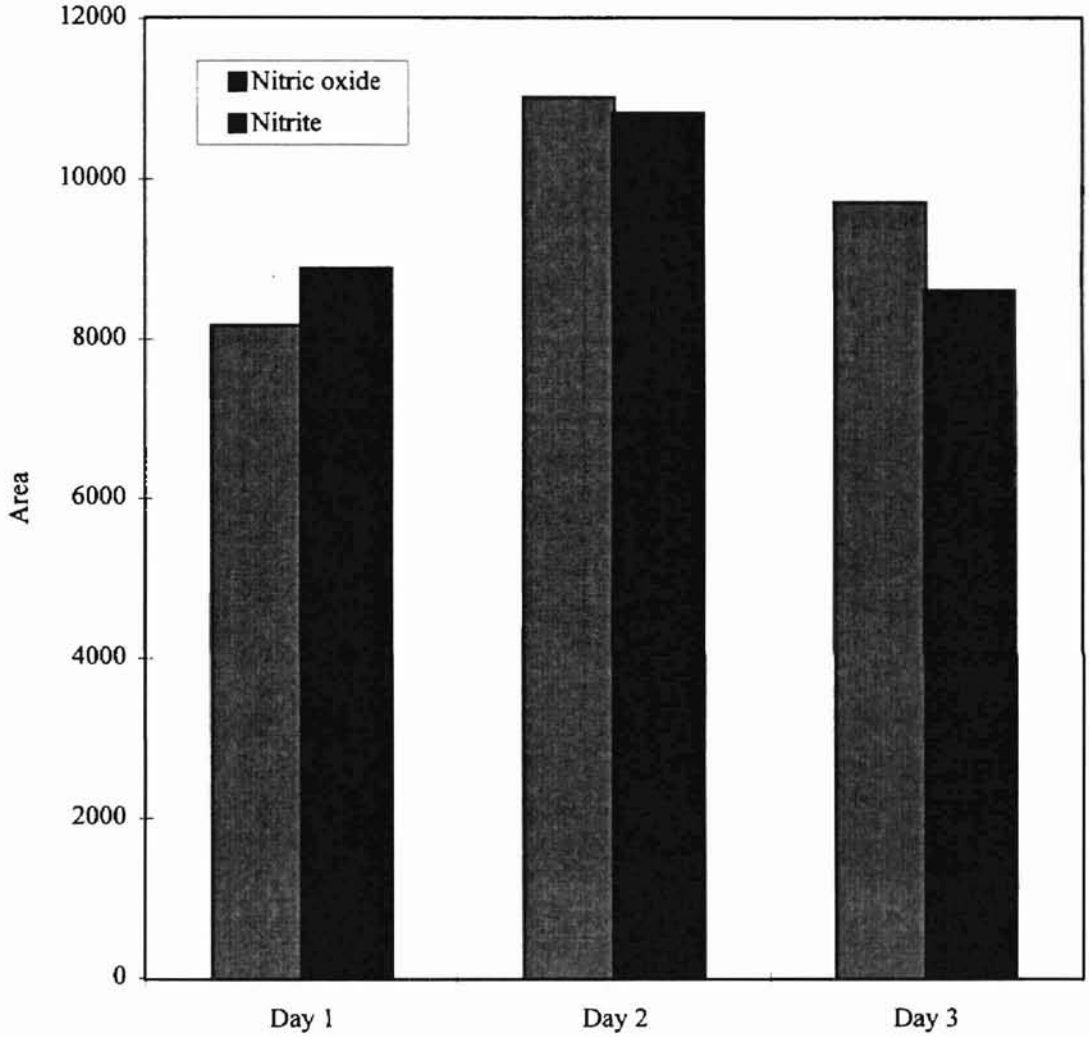

Figure 3.4 : Comparison of area under the curve for NO and NO_2^- at 25^0C.

day to day variations, the profiles were made dimensionless by dividing all points on one profile with the peak of the profile. Points at fixed time intervals were plotted and compared. The dimensionless profile of NO_2^- agreed closely with the dimensionless profile of NO (Figure 3.5). Therefore, NO_2^- essentially behaves as NO upon addition to the reducing agent. For this to occur, NO_2^- must be instantaneously converted to NO. Complete and instantaneous conversion of NO_2^- to NO meant that NO_2^- essentially behaved as NO, and, for this to be true, Eq.3.7 and Eq.3.8 must be the same. This requires the term $\alpha k_1 \left[NO_2^- \right]_0 e^{-k_1 t}$ in Eq.3.7 to be zero. Since, α and $[NO_2^-]_0$ have a constant finite value, and since k_1 cannot be zero, k_1 must approach infinity to reduce the term to zero. Since NO_2^- mimics NO, NO_2^- injections would be useful for NO calibration of the analytical system.

3.6.2 NO_3^- kinetics.

The experiments were performed at 35°C, 50°C and 77°C. The dimensionless NO concentration profiles following injections of NO, NO_2^-, and NO_3^-, were plotted. The NO and NO_2^- sample profiles matched each other very closely for the three temperatures at which the experiments were performed. However, the dimensionless concentration profile for NO_3^- sample showed wide variation from the profile of NO. These variations decreased with increase in temperature and the profile at 77°C began to approach the NO profile (Figure 3.6-3.8).

Evaluation of ($k_L a/V$) : Using the methods previously described in section 3.5, ($k_L a/V$) was evaluated. The value of ($k_L a/V$) in the phosphoric reducing agent, at all the three temperatures, was less than that obtained in the glacial reducing agent. However,

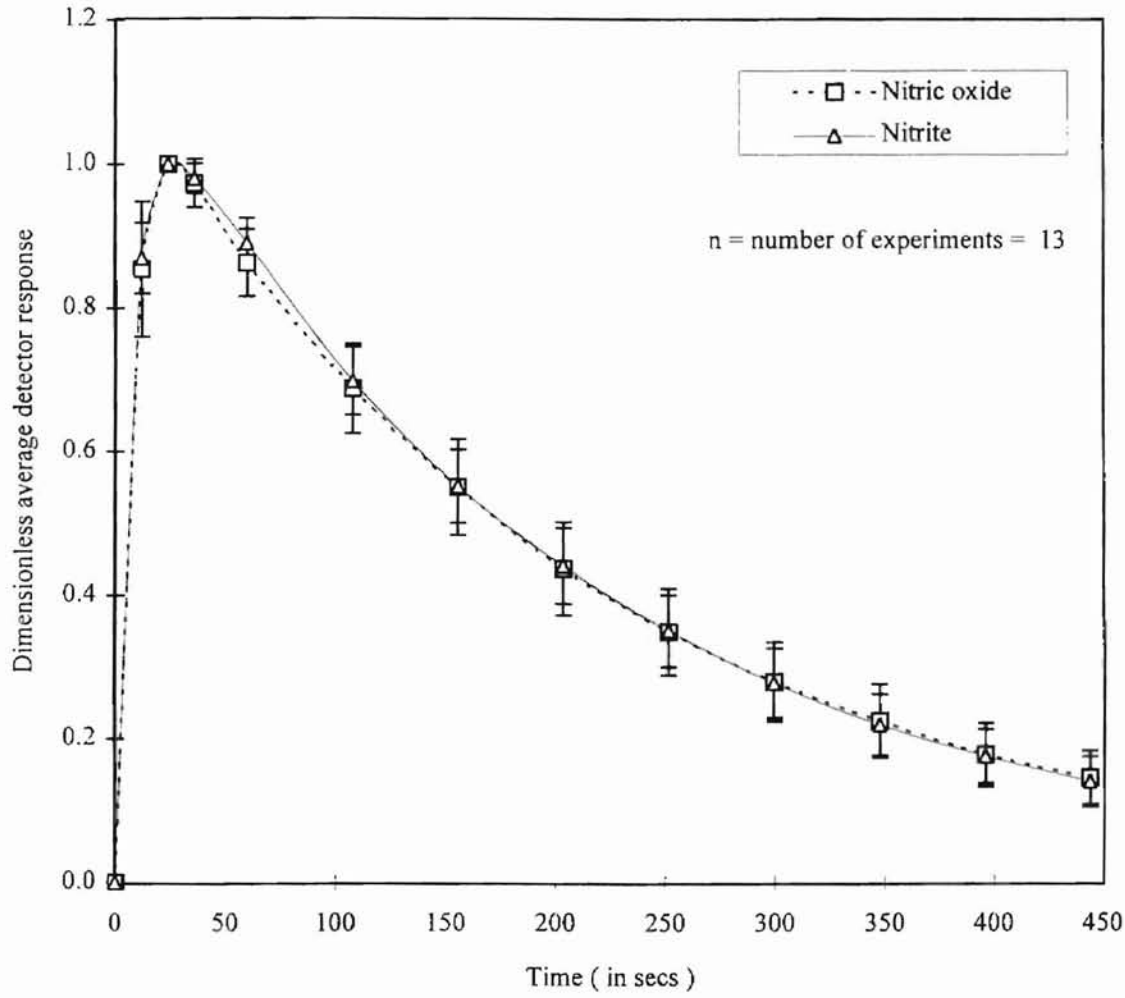

Figure 3.5 : Dimensionless profiles of NO and NO_2^- at 25^0C.

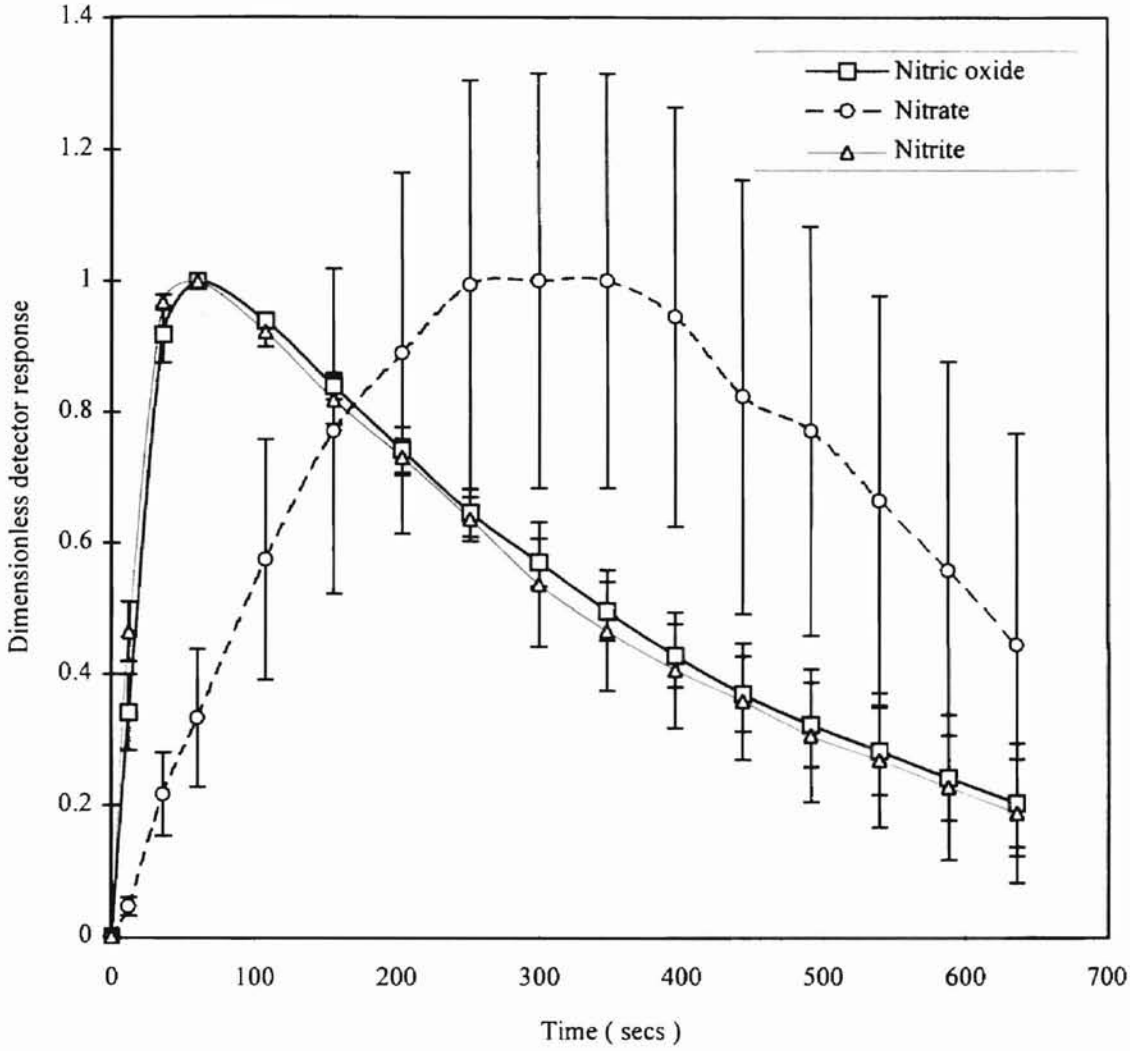

Figure 3.6 : Profiles of NO, NO_3^- and NO_2^- at 35^0 C

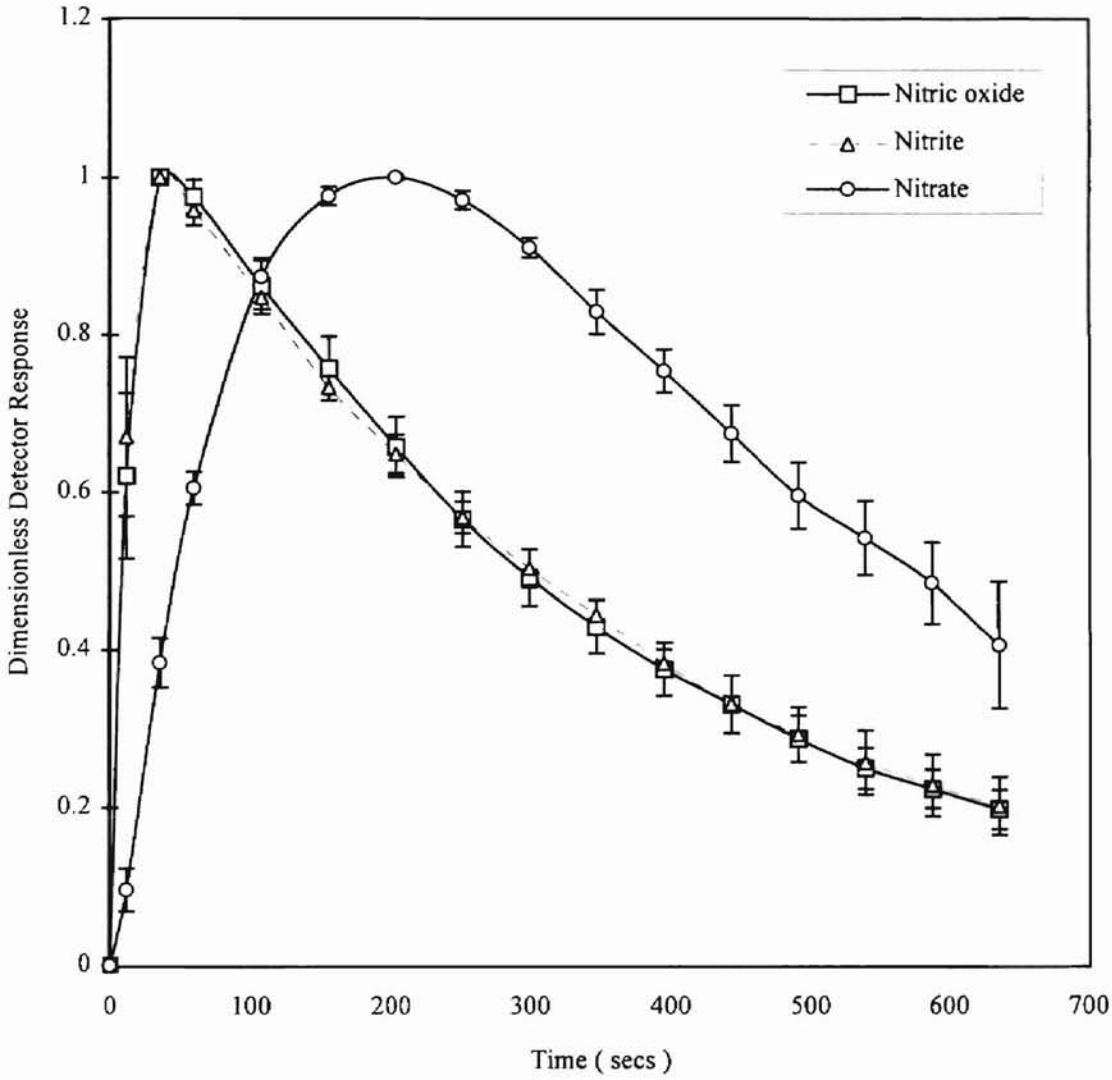

Figure 3.7 : Profiles of NO, NO_3^- and NO_2^- at 50^0 C

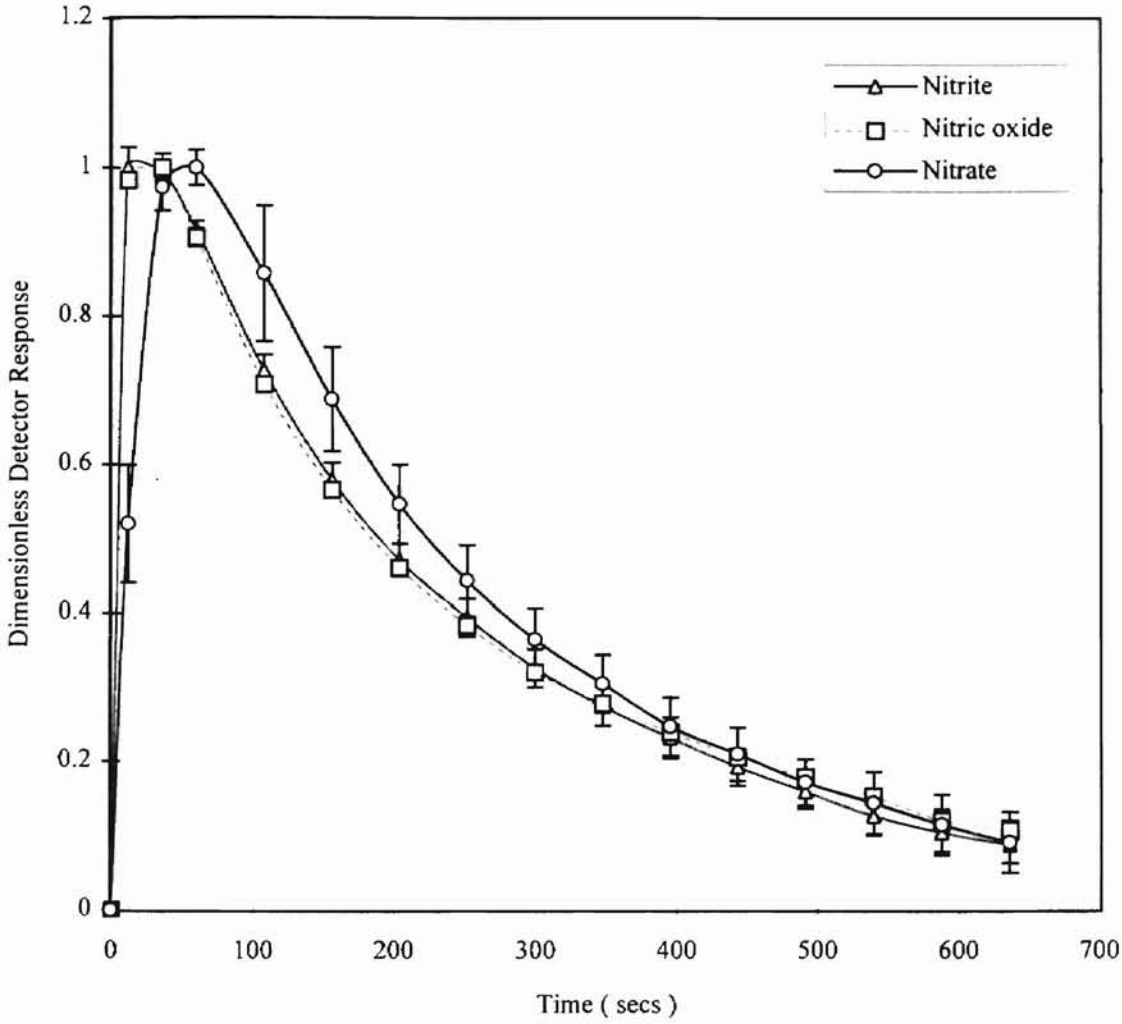

Figure 3.8 : Profiles of NO, NO_3^- and NO_2^- at 77^0 C

the values of (k_La/V) obtained from NO_2^- response curve and NO response curve were within 10% of each other at 35°C and within 4% at 50°C and 77°C (Figure 3.9-3.11). Figures 3.9-3.11 show that the value of (k_La/V) increased with increase in temperature, indicating that the mass transfer rate increases at higher temperatures as expected.

Evaluation of k_2 *&* α : The value of α for 1 μM NO_3^- was determined graphically from the area under the response curve. The values of α were 0.39, 0.79, and 0.84 at 35°C, 50°C, and 77°C, respectively. The area under the curve increased with increase in temperature.

Eq.3.16 was also used to evaluate α. The straight line fit to the $\ln(R_{NO})$ vs t curve provided values for k_2 and k_3, and thus α. Figures 3.12 and 3.13 show the $\ln(R_{NO})$ vs t curve at 35°C and 50°C, respectively. The values of k_2 and k_3 are 0.0023 s^{-1} and 0.0021 s^{-1} at 35°C, and, 0.0035 s^{-1} and 0.0020 s^{-1} respectively at 50°C. Thus, values of α are 0.52 and 0.63 at 35°C and 50°C, respectively. The value obtained is 33% higher than the value obtained graphically at 35°C, and 21% lower than the value obtained graphically at 50°C. The poor fit of the data shows that the hypothesized reaction kinetics are not very accurate, and the values of α, k_2, and k_3 obtained by Eq.3.16 provide only a rough estimate.

Figure 3.14 is a comparison of the areas under the NO, NO_2^- and NO_3^- response curves at the three temperatures for 1 μM injections of each sample. The areas of NO_2^- and NO are within 10% of each other at all the three temperatures showing that NO_2^- is completely converted to NO. However, the area under the NO_3^- curve is 70% less than

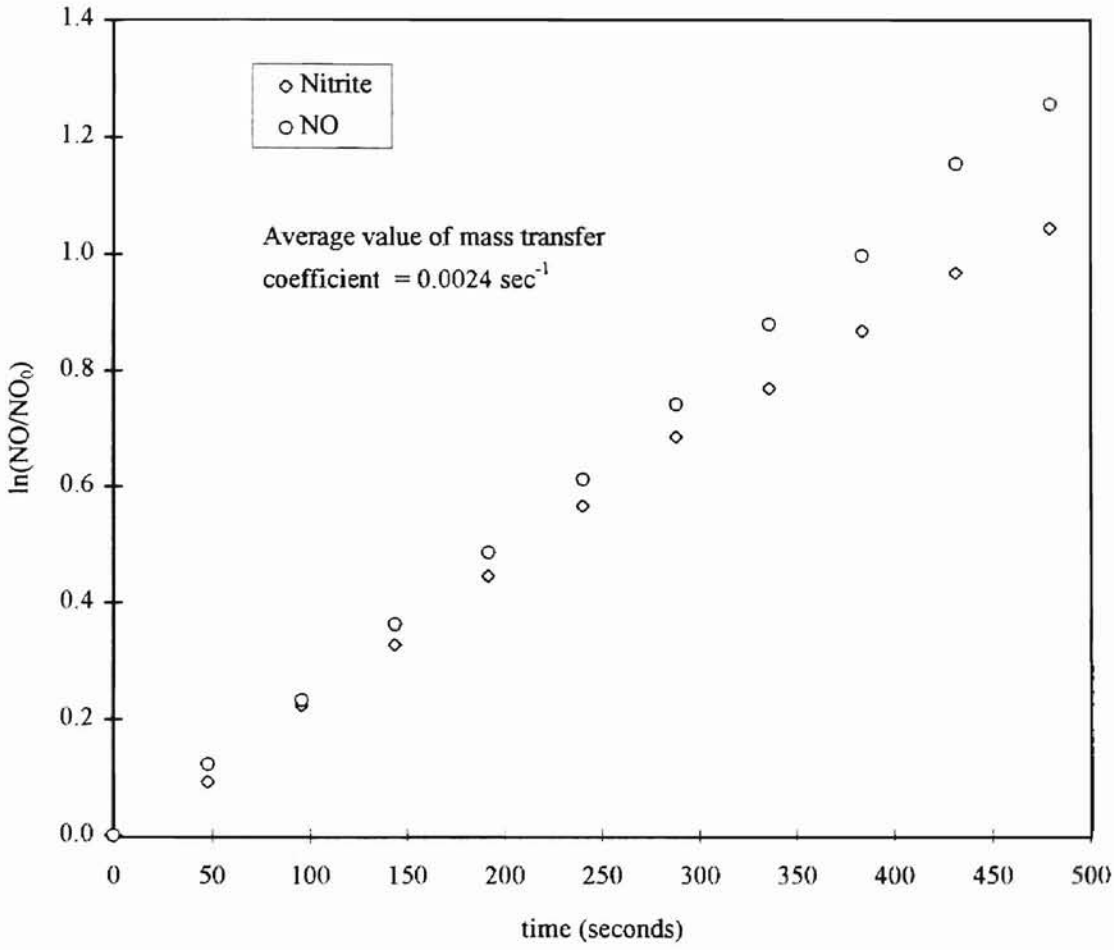

Figure 3.9 : Mass transfer coefficient in phosphoric reducing agent at 35^0C.

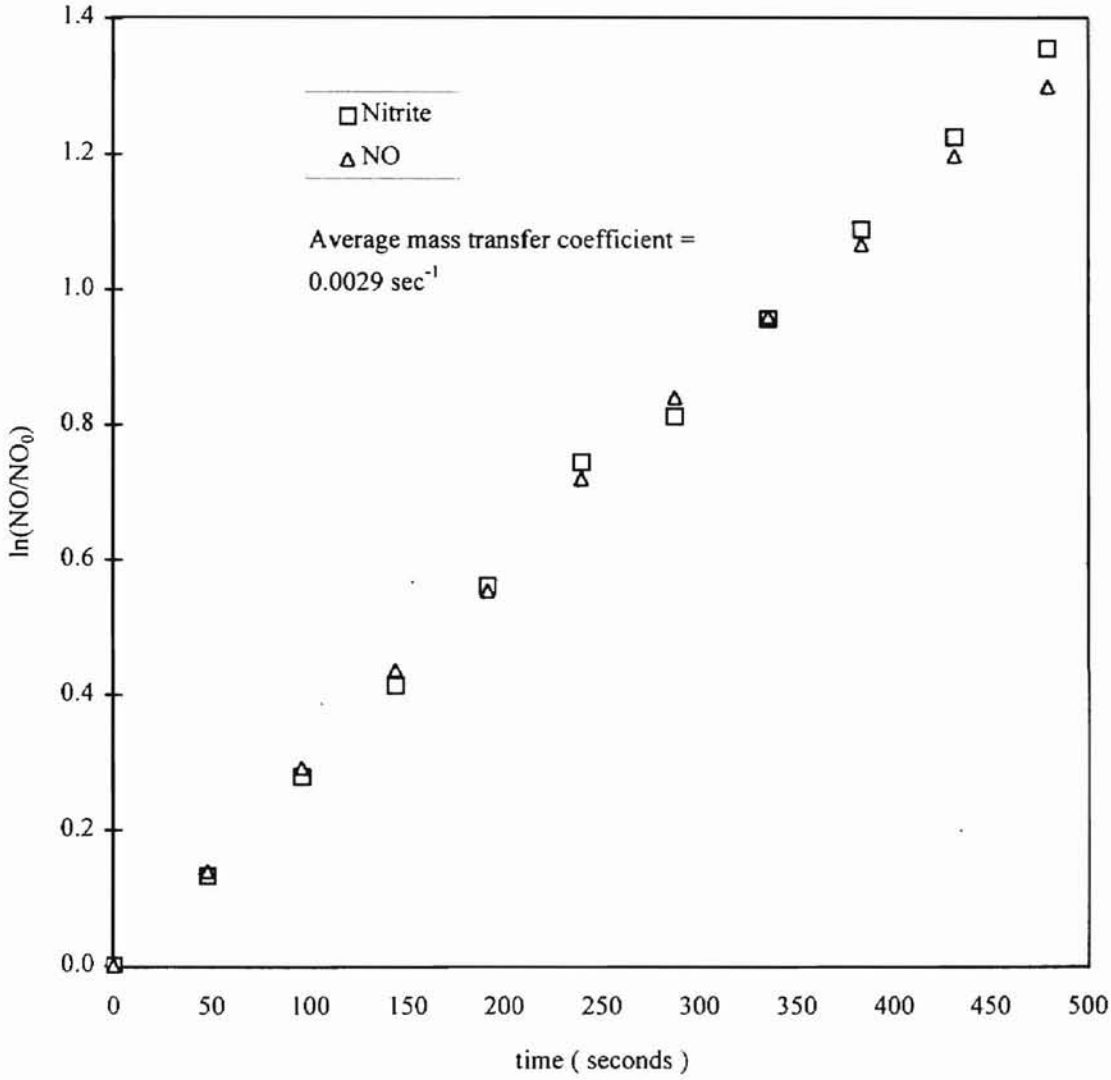

Figure 3.10 : Mass transfer coefficient in phosphoric reducing agent at 50^0C.

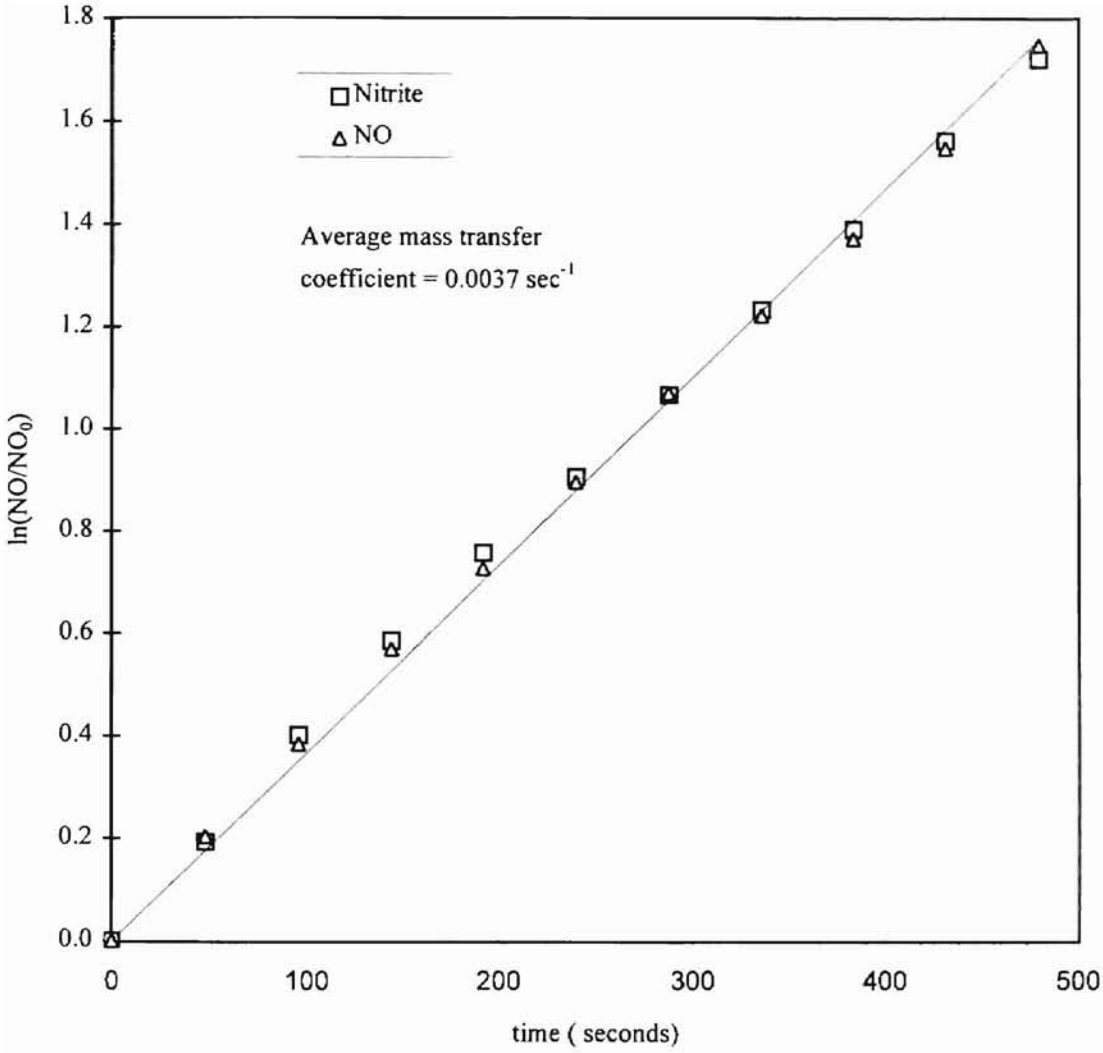

Figure 3.11 : Mass transfer coefficient in phosphoric reducing agent at 77^0C.

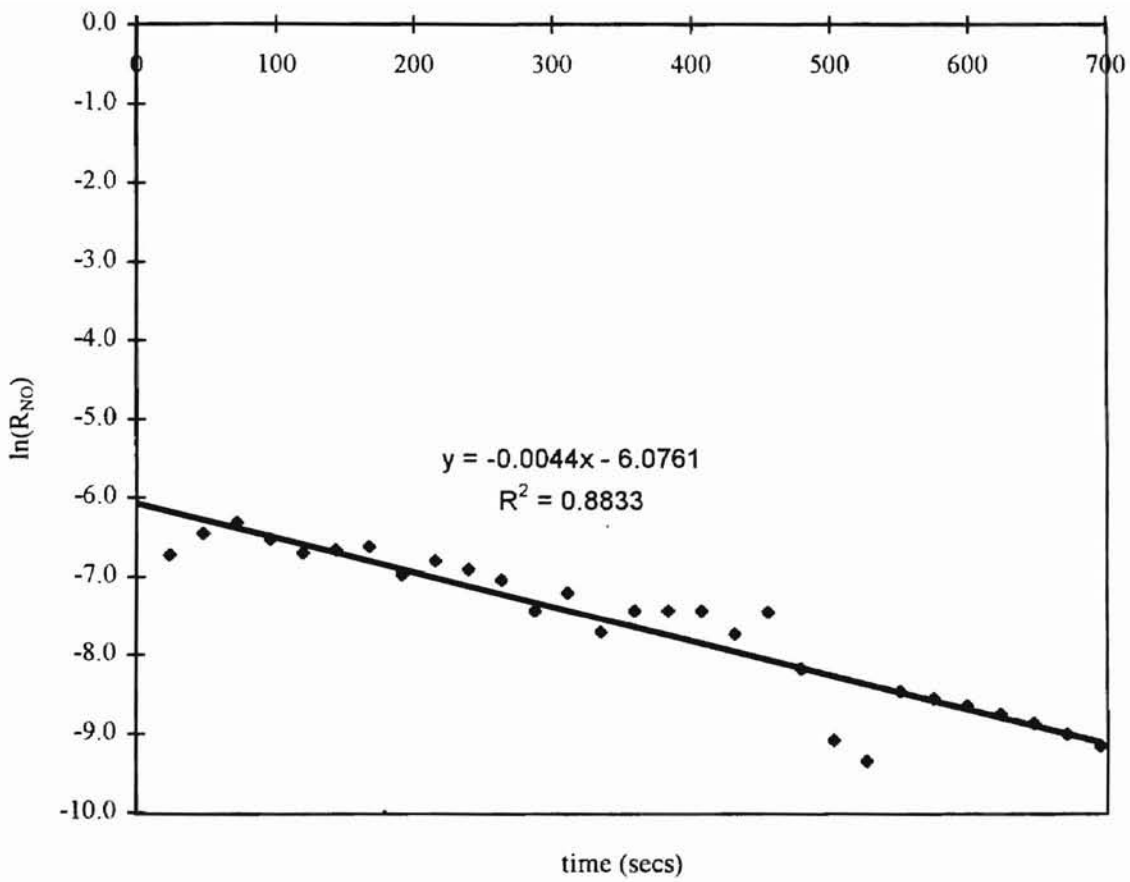

Figure 3.12 : $\ln(R_{NO})$ vs t at 35^0C for NO_3^- addition to phosphoric reducing agent.

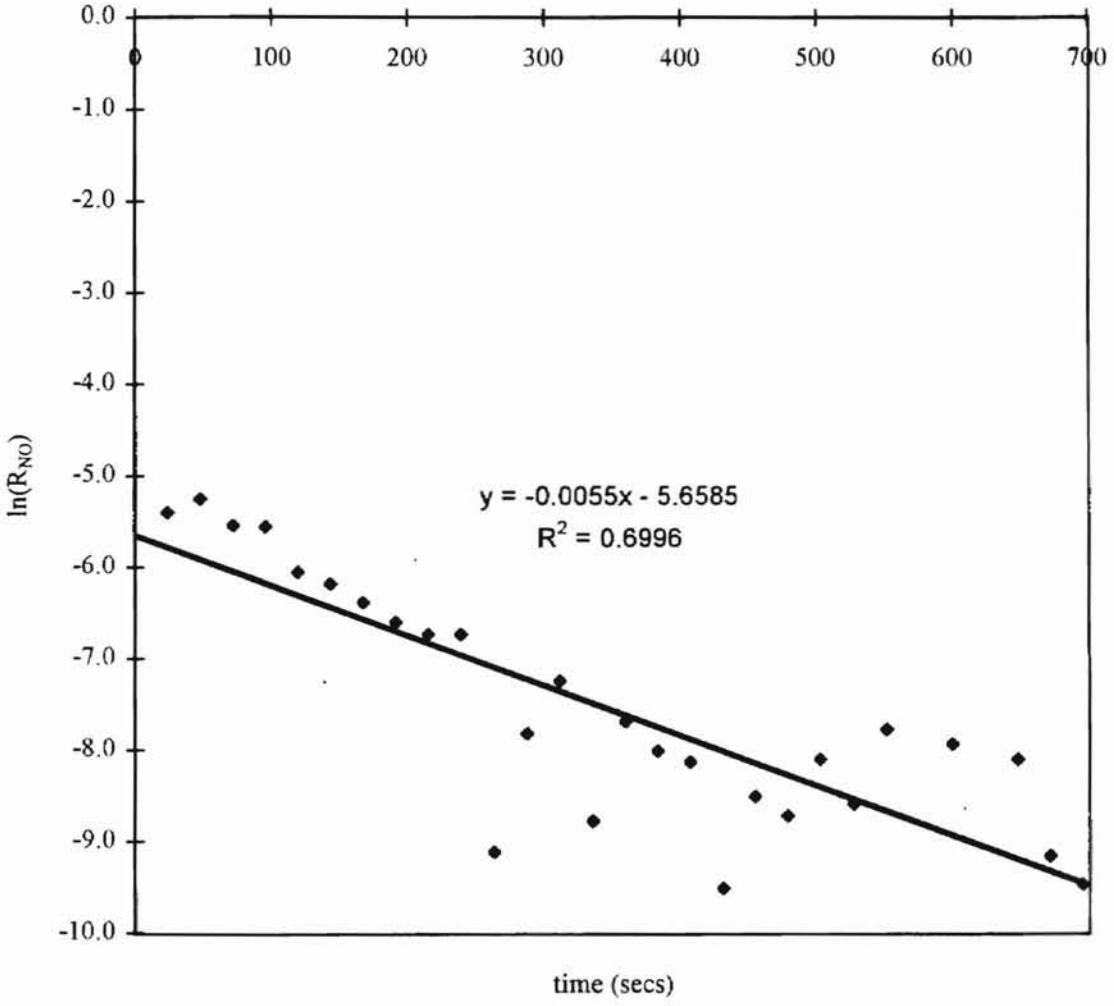

Figure 3.13 : $\ln(R_{NO})$ vs t at 50^0C for NO_3^- addition to phosphoric reducing agent.

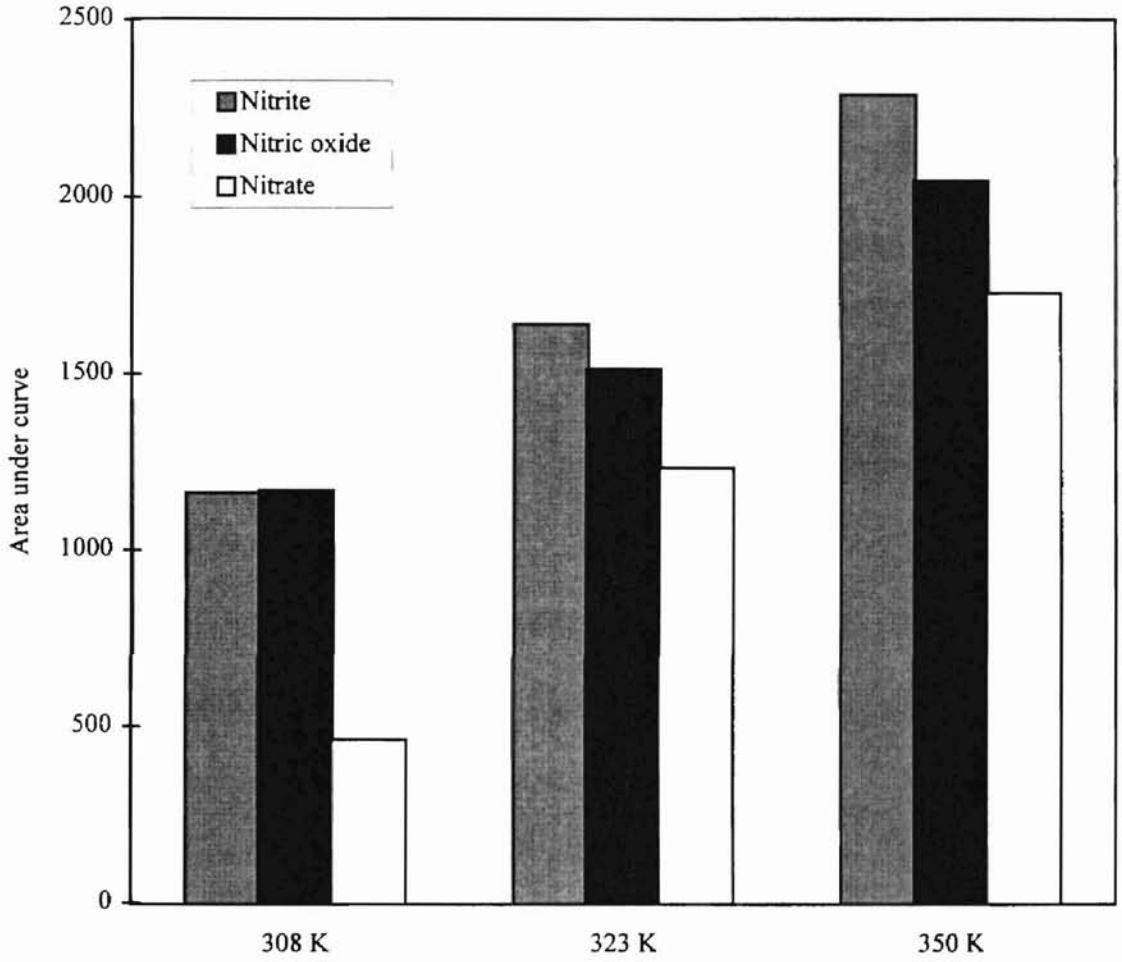

Figure 3.14 : Comparison of area under the curve for NO, NO_2^- and NO_3^- at different temperatures.

the NO_2^- curve at 30°C, 25% less at 50°C, and 20% less at 77°C. The area under the NO_3^- curve approaches that of NO and NO_2^- with increase in temperature, indicating that higher conversion of NO_3^- to NO is achieved as the temperature is increased.

3.6.3 NO_3^- analysis via cadmium reduction.

With cadmium reduction of NO_3^-, there was no need of high temperatures for the reduction of NO_3^- to NO. The NO_3^- sample, after being reduced to NO_2^- by the cadmium vials, was injected into the glacial reducing agent. The peak height and area under the response curve was obtained and compared with the peak height and area under the response curve for standard NO_2^- concentrations. Figure 3.15 shows that the peak heights of NO_3^- and NO_2^- agree closely. The area under the response curves were within 10% of each other for all concentrations of NO_3^-. The dimensionless profile of NO_2^-, formed via reduction of NO_3^-, duplicated the NO_2^- and NO profiles (Figure 3.16). The peak heights, dimensionless profiles, and area under the response curve show that NO_3^- is essentially completely converted to NO_2^- in the cadmium vials.

Complete reduction of NO_3^- to NO takes approximately 90 minutes and not 5 minutes as claimed by the manufacturer (World Precision Instruments, Inc.). Figure 3.17 shows the percent conversion of NO_3^- vs time. There is 35% conversion in 5 minutes, approximately 75% in 30 minutes, and 99% conversion in approximately 90 minutes.

3.7 Conclusions

The dimensionless profiles of NO and NO_2^- in the glacial reducing agent matched very closely, indicating that NO_2^- essentially behaves as NO. The steep rise in the profile indicates that the NO sample mixes with the reducing agent very fast, and a uniform

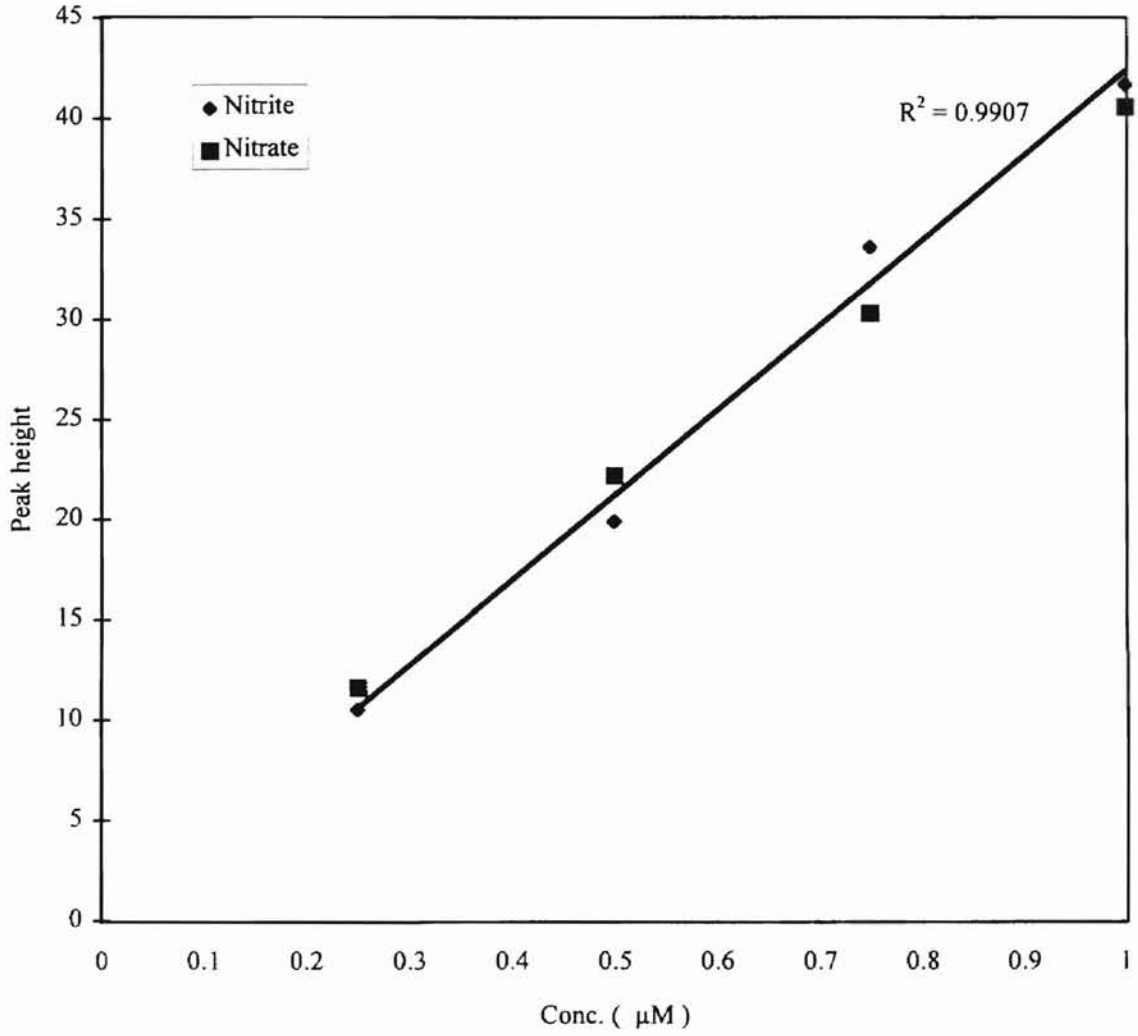

Figure 3.15 : Comparison of peak heights of nitrate reduced via cadmium reduction with standard nitrite sample

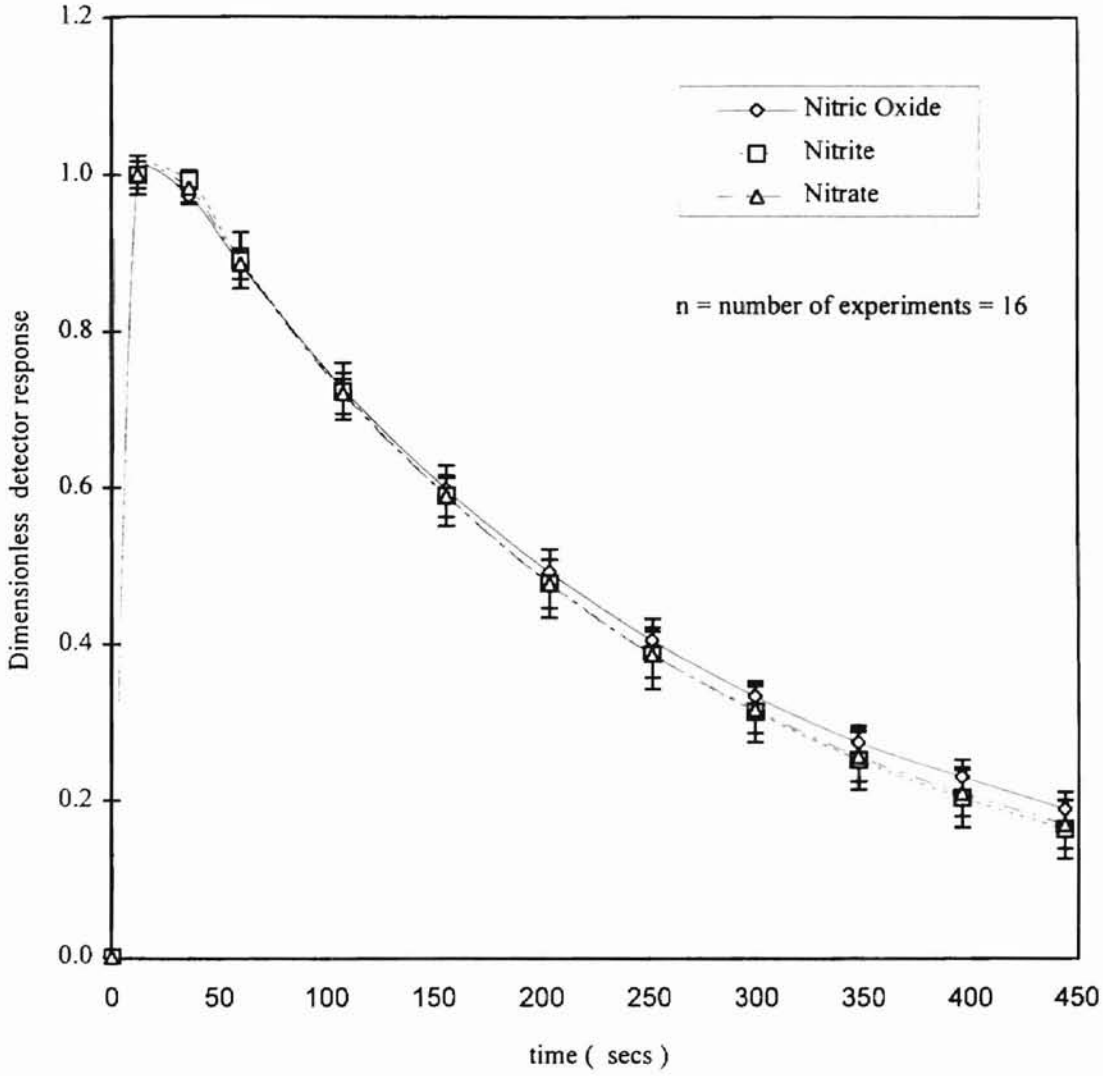

Figure 3.16 : Profiles of NO, NO_2^- and NO_3^- samples at 25^0C.

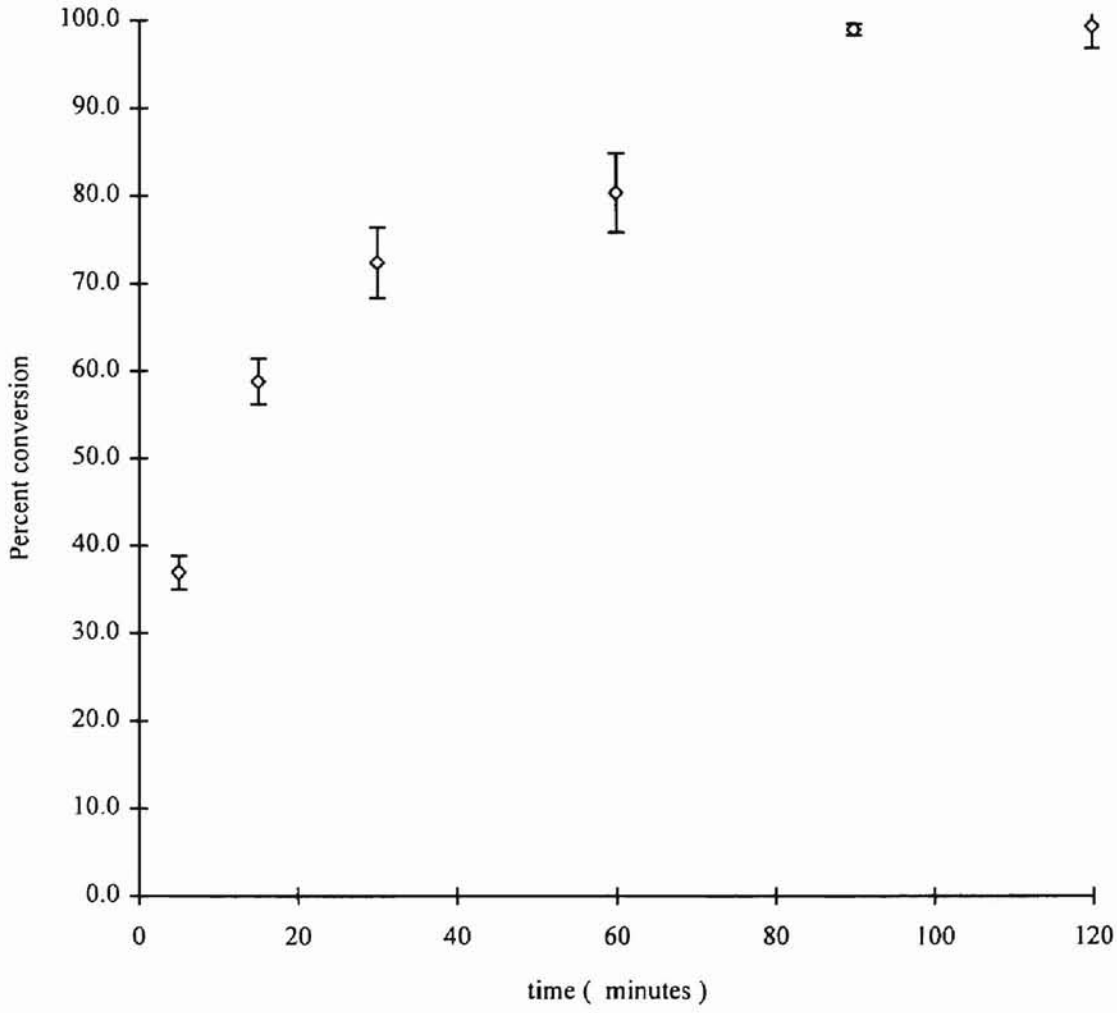

Figure 3.17 : Conversion of nitrate to nitrite via cadmium reduction at 25^0C.

concentration is obtained in the chamber. The value of $(k_La/V)_{NO}$ obtained from the NO_2^- and NO profiles in glacial reducing agent were the same, indicating that the species produced by the reduction of NO_2^- is NO.

The value of α in glacial reducing agent was very close to one. From the analysis of the results it is safely concluded that NO_2^- is instantaneously and completely converted at room temperature to NO in glacial reducing agent.

In the phosphoric reducing agent, the dimensionless profiles of NO_2^- and NO duplicate each other at all the three temperatures, showing that NO_2^- is again converted instantaneously to NO and behaves as a NO sample. The value of α showed that NO_2^- is completely converted to NO at all the three temperatures.

The dimensionless profile of NO_3^- showed wide variation from the NO profile at 35°C. However, the NO_3^- profile approached the NO profile as the temperature was increased and approached NO profile at 77°C showing that with the increase in temperature, the behavior closely resembles NO.

The value of α determined graphically showed that the conversion of NO_3^- is not complete and the profile showed that the conversion, though faster than that at 35°C and 50°C, is still not instantaneous. However, the trend indicates that with further increase in temperature, NO_3^- can be instantaneously and completely converted to NO. Complete conversion of NO_3^- was achieved in the cadmium reduction vials at room temperature in approximately 90 minutes. Working at room temperature reduced the loss of reducing agent through vaporization, and eliminated the use of an incubator to maintain a high temperature. Since the cadmium reduction method provides a convenient and simple

method for reducing NO_3^- at room temperature, the phosphoric reducing agent was discontinued for further studies.

Chapter 4

Design and optimization of a nitrate and nitrite analytical apparatus

Sensitive and selective methods are required to measure NO_2^- and NO_3^- at low levels in the complex matrices found in water, food and biological fluids. Several methods have been used to measure NO_2^- and NO_3^- at low levels (Section 2.2). However, the optimization aspect of the methods has not been studied. Having studied the reaction kinetics of NO_2^- and NO_3^- samples in the reducing agents, a novel system for their detection was developed and optimized.

4.1 Proposed method

Experimental setup : The detection system developed was based upon the method developed by Dunham [1995]. The experimental setup consists of a continuous flow system connected to the chemiluminescence detector (Figure 4.1). The NO_2^- reducing agent is continuously pumped through the flow system. An injection valve (Rheodyne Injection Valve 7010) is connected in the flow line to allow samples to be injected into the reducing agent. A mixing chamber (0.5 ml) with a tiny stir bar is connected after the injection valve and the solution goes from the mixing chamber and into a semi-permeable silastic tubing. The semi-permeable portion of the tubing is placed in a conical flask with a rubber stopper. Approximately 5 cm length of the semi-permeable tubing at each end is covered with heat shrink tube. Holes are drilled into the rubber stopper for the two ends of the semi-permeable tubing to pass through. The teflon tube of the flow system is connected to one end of the silastic tubing with stainless steel fittings and the other end is

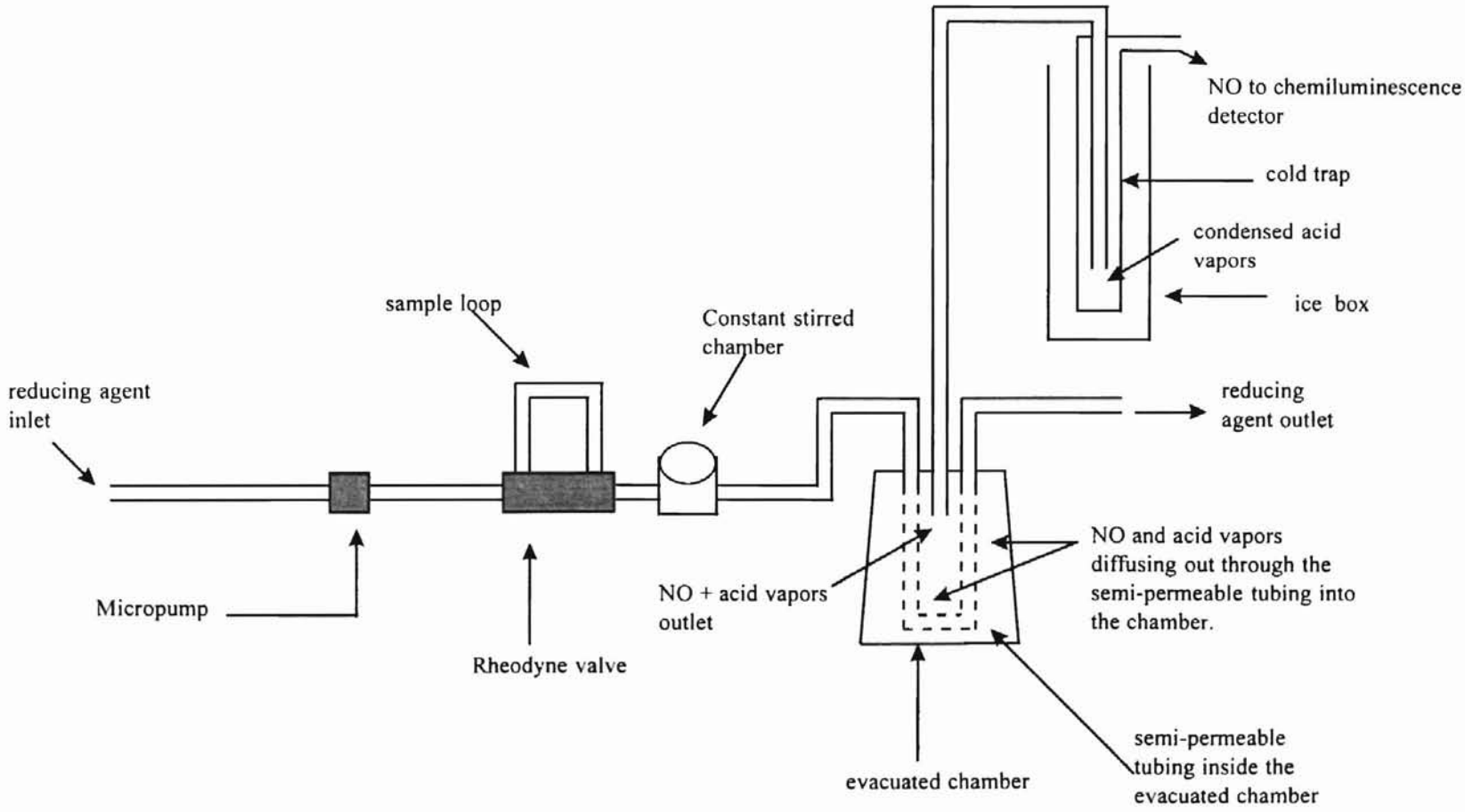

Figure 4.1 : Flow system for the analysis of nitrite and nitrate - permeation method

connected to a waste bottle into which the used solution is discarded. A vacuum line connects the conical flask to the chemiluminescence analyzer.

The reducing agent was allowed to continuously flow through the flow system. A constant flow rate of 3 ml/min was maintained throughout the experiment. 100 µl samples of different concentrations of NO_2^- and NO_3^- were injected into the sample loop of the injection valve and the direction of flow was switched to make the reducing agent flow through the sample loop. The mixing chamber mixed the sample with the reducing agent to ensure complete conversion of NO_2^- to NO since mixing time, rather than reaction time, is the important parameter. The vacuum in the conical flask creates a driving force which causes NO in the solution to diffuse into the flask. The acid vapors are condensed in the acid trap. NO passes through the acid trap and into the detector. Upon reaction with ozone, NO produces a response which is recorded on a chart recorder. Standard NO_2^- solutions were used to evaluate the efficiency of the flow system. Samples containing NO_3^- were also injected into the flow system and their concentration determined.

The detection and determination of NO_3^- concentrations required an additional step. The NO_3^- sample was first converted to a NO_2^- sample by cadmium reduction. 1 ml cadmium vials were used for the purpose. Equal volumes of NO_3^- sample and ammonia buffer of pH 9 were added to the cadmium vial. The cadmium vial reduces NO_3^- to NO_2^- as described in Chapter 3. The NO_2^- solution was then injected into the flow system to determine the concentration of NO_3^-.

4.2 Design considerations

The optimization of the apparatus required the study of the factors affecting the transport of NO from the flow system and into the detector. Mass transfer through a tube containing a flowing solution has been studied [Davis *et al.* 1970]. The resulting model includes solutions for non-newtonian fluids, such as blood, and is based upon the following assumptions:

1) The inlet concentration is uniform,
2) The physical properties of the fluid are constant,
3) The concentration outside of the semi-permeable tubing is constant, and
4) The wall permeability is constant.

All the above assumptions are applicable to the proposed system. Complete mixing of the reducing agent with the injected sample makes the inlet stream to the semi-permeable membrane of uniform concentration. The physical properties of the fluid are constant and the concentration outside of the semi-permeable tubing is essentially zero due to the vacuum of the detector. The permeability of the semi-permeable tubing is constant at a given temperature.

4.2.1 Model of NO transfer to detector.

The steady state dimensionless diffusion equation with the above assumptions is

$$\frac{\partial^2 c}{\partial \rho^2} + \frac{1}{\rho}\frac{\partial c}{\partial \rho} = \frac{u(\rho)}{2}\frac{\partial c}{\partial \xi} \tag{4.1}$$

where the dimensionless variables are defined as

$$c = \frac{C(r,x) - C_d}{C_{in} - C_d} \quad , \quad \rho = \frac{2r}{Di} \quad , \quad \xi = \frac{2x}{DiPe} \quad , \quad u(\rho) = \frac{u(r)}{U_m} \tag{4.2}$$

Di is the inner tube diameter, c is the dimensionless concentration, C_{in} is the inlet aqueous concentration, C_d is the concentration outside the tubing, r is the inside radius, ρ is the dimensionless radius, x is the length of the semi-permeable tubing, ξ is the dimensionless length, $u(\rho)$ is the dimensionless velocity, and Pe is the Peclet number defined as

$$Pe = \frac{U_m Di}{D} \tag{4.2a}$$

where D is the diffusivity of NO in solution and U_m is the average velocity. The boundary conditions are

$$c(\rho) = 1, \quad 0 \le \rho \le 1 \quad \xi = 0 \tag{4.2b}$$

$$\frac{\partial c(\rho)}{\partial \rho} = 0, \quad \rho = 0 \tag{4.2c}$$

$$\frac{\partial c(\rho)}{\partial \rho} = -Sh_w c(\rho), \quad \rho = 1 \tag{4.2d}$$

Sh_w can be calculated using the permeability, diameter of the silastic membrane, and the diffusivity of NO in the reducing agent. Sh_w is given by the expression

$$Sh_w = \frac{k_w Di}{2D} \tag{4.3}$$

where k_w is the mass transfer coefficient characterizing transport through the wall, Di is the inner diameter of the semi-permeable tubing, and D is the diffusivity of NO in the reducing agent. The mass transfer coefficient at the wall is given by the expression

$$k_w = \frac{P^*}{H\delta} \tag{4.4}$$

where P^* is the permeability of the semi-permeable membrane (mol $cm^{-1}s^{-1}cmHg^{-1}$), H is the Henry's constant (mol $1000^{-1}cm^{-3}cmHg^{-1}$) and δ is the thickness of the wall (cm). Thus, Sh_w can also be written as

$$Sh_w = \frac{P^* Di}{2H\delta D} \tag{4.5}$$

The permeability, Henry's constant, and the diffusivity being constant at a given temperature, Sh_w becomes a function of the diameter and thickness of the semi-permeable tubing at a given temperature. The solution to this problem is presented by Davis and Parkinson [1970] from which an overall mass transfer coefficient, k_0, can be calculated. k_0 is used in optimizing the detection system and is useful in analyzing the sensitivity of the system. The coefficient k_0 is related to k_w by

$$\frac{1}{k_0} = \frac{1}{k_w} + \frac{1}{k_f} \tag{4.6}$$

where k_f is the mass transfer coefficient characterizing transport through a fluid boundary layer. If the transport resistance is mainly due to the wall, such that $k_0 = k_w$, then the thickness of the tube wall may be reduced to increase the value of k_0 (Eq.4.4). If the

resistance is mainly due to the fluid, the flow rate may be increased to reduce the boundary layer resistance such that k_0 approaches the value of k_w. In all cases k_0 is never greater than k_w.

4.2.2 Sampling time.

Sampling time is the time required to assay a given sample. The smaller the sampling time, the faster the analysis. For the purpose of fast analysis, the sampling time of the flow system has to be optimized. The sampling time which can be related to the residence time depends on the volume through which the solution flows, the solution flow rate, and flow characteristics (i.e. plug flow, well-mixed flow, etc). The ideal sampling system would be the minimization of the sampling or residence time.

For the flow system, the residence time is given by the expression

$$\tau_{sys} = \tau_{cstr} + \tau_{tube} + \tau_{silastic} + \tau_{other} \qquad (4.7)$$

where the residence time for the system is the sum of the residence time of the mixing chamber (observed as a continuous stirred tank reactor (CSTR)), the residence time of the teflon tubing in the system, the residence time of the semi-permeable tubing and the residence time due to the extra volume of unions at tube connections. The residence time of the injection valve should also be included for a complete assessment. The residence times of the CSTR, tube, and silastic are given by the following expressions:

$$\tau_{cstr} = V_{cstr}/Q \qquad (4.8)$$

$$\tau_{teflon} = \pi d_t^2 L_t/(4Q) \qquad (4.9)$$

$$\tau_{silastic} = \pi d_s^2 L_s n/(4Q) \quad (4.10)$$

where V_{cstr} is the volume of the mixing chamber, d_t is the inner diameter of the teflon tubing in the flow system (0.16 cm), L_t is the length of the teflon tubing , L_s is the length of the silastic, n is the number of parallel silastic tubes, d_s is the inner diameter of the silastic tubing, and Q is the total volumetric flow rate.

Since the sampling time depends on the length of the silastic tubing, it is to be noted that the length of the silastic required would be determined by the time required to get 90% of the sample out of the CSTR. The time required to get 90% of the sample out of the CSTR would be determined by the CSTR design equation as described in section 4.3.1.

4.2.3 Sensitivity.

Sensitivity is related to the smallest measurement a system can accurately measure. The usefulness of any analytical system is determined by its sensitivity. For the flow system, the sensitivity depends on the amount of NO going into the detector. The NO flux going to the detector depends on the overall mass transfer coefficient (k_0), the mass transfer area (A_s), and the concentration gradient (c). The product $k_0 A_s$ should be maximized to maximize the sensitivity for a given concentration. The mass transfer area is the surface area of the tube and is given by the expression

$$A_s = \pi D_{avg.} L \quad (4.11)$$

where D_{avg} is the average of the inner and outer diameter of the semi-permeable tube and L is the length of the semi-permeable tube.

4.3 Design calculations

The flow rate of the reducing agent and the total volume of the flow system determines the residence time of the analytical apparatus. The amount of NO going into the detector is determined by the product of the overall mass transfer coefficient (k_0), the exposed surface area of the silastic (A_s), and the concentration (c). To develop an optimized system, design calculations were performed at different flow rates and different lengths and diameters of the silastic tubing using the methods discussed in the previous section. The flow rate, length, and diameter which gives the maximum sensitivity and minimum sampling time is the optimized flow system.

4.3.1 Concentration effects on detector sensitivity.

Since the detector sensitivity depends on the concentration of NO, the NO concentration exposed to the silastic should be maximized. Therefore, the time it takes for 90% of the NO in the mixing chamber to enter the silastic tubing was equated with the residence time in the silastic tubing to determine a maximum tubing length to which the aqueous NO will essentially all be in the tubing following injection into the CSTR. The concentration of the sample leaving the mixing chamber, assuming a pulse injection into the CSTR, is calculated using the design equation for a CSTR which is

$$c = c_0 e^{-\frac{t}{\tau_{CSTR}}} \tag{4.12}$$

The inlet concentration is c_0, c is the outlet concentration, and τ is the residence time of the CSTR. The residence time of NO in the mixing chamber at different flow rates was calculated using Eq.4.8. The time for the NO concentration in the mixing chamber to reduce to 10% of the original value (injected concentration) is 2.3 τ_{CSTR} as calculated using Eq.4.12. Thus, for $\tau_{silastic} = 2.3\ \tau_{CSTR}$, the length of the silastic is

$$L = \frac{4(2.3)\tau_{CSTR} Q}{\pi d_s^2 n} = \frac{9.2 V_{CSTR}}{\pi d_s^2 n} \qquad (4.13)$$

where n is the number of silastic tubes and d_s is the inner diameter of the silastic tube. For the calculations, silastic tubing of inner diameter 0.15 cm and 0.03 cm were used.

Table 4.1 shows the length of silastic tube required for 90% of the injected NO to be exposed to the silastic tube as based on residence time calculations. For the 0.15 cm diameter tubing, approximately 65 cm length of silastic was required for a single tube. As the number of tubes was increased, the length of tubes decreased by the same factor as evidenced in Eq.4.13. For 0.03 cm diameter tubing, the length required for a single tube was approximately 15 m. This is because the small area of cross section of the tube requires a very large length to provide the adequate volume for the NO profile. Since a length of 15 m is impractical, multiple tubes of 0.03 cm diameter are more appropriate. The lengths required for 16 tubes and 20 tubes are less than 100 cm, which is more reasonable.

It should be noted that the above calculations are based on the assumption that the mixing chamber behaves as a perfect CSTR and the injection valve injects the sample

Table 4.1: Calculation of silastic tubing length for 0.03 cm and 0.15 cm diameter tubes.

Total Q (ml/min)	# tubes	Q/tube (ml/min)	τ_{cstr} (seconds)	L (cm) @ d_s = 0.15 cm		L (cm) @ d_s = 0.03 cm	
				residence time method	% lost method	residence time method	% lost method
1	1	1	30	65	133	1578	131
3	1	3	10	65	397	1578	393
3	8	0.375	10	8	50	197	50
3	16	0.1875	10	4	25	99	25
3	20	0.15	10	3	20	79	20
4	1	4	7.5	65	529	1578	524
4	8	0.5	7.5	8	67	197	66
4	16	0.25	7.5	4	34	99	33
4	20	0.2	7.5	3	27	79	27
6	1	6	5	65	793	1578	786

into the CSTR as a pulse. Experiments with a dye showed that the injection system does not inject the sample as a pulse, but discharges the sample over a period of up to 7 seconds. This behavior will increase the time required for 90% of the NO to clear out of the CSTR and thus increase the calculated lengths shown in Table 4.1. Also, according to Eq.4.12, the time required for 99% of the NO to clear out of the CSTR is double the time required for 90% of the NO to clear out of the CSTR. Thus, the calculated length of silastic based on the time required for 99% of NO to clear out of the CSTR would also be double. However, for the present study, all the calculations are based on 90% of NO.

To validate the use of the theoretical residence times used above, the residence time of the flow system without the injection valve was compared with theoretical values calculated for the CSTR and the tubing. The experimental setup consisted of a three-way valve connected to the mixing chamber with a teflon tube. The mixing chamber was then connected to a spectrophotometer. A step input of ethanol, followed by a step input of water at a flow rate of 3 ml/min, resulted in a change in the absorbance as shown in Figure 4.2. The residence time for this system was calculated from the data following the step input of water according to the following equation

$$\tau_{sys} = ((\sum t*(abs^0 - abs) / abs^0) \tag{4.14}$$

where abs^0 is the steady-state absorbance following the step input of ethanol, and t is the time at which the absorbance occurs following the step input of water. The residence time was compared with the theoretical value which is

$$\tau_{sys} = \tau_{cstr} + \tau_{tube} + \tau_{spectrophotometer} + \tau_{other} \tag{4.15}$$

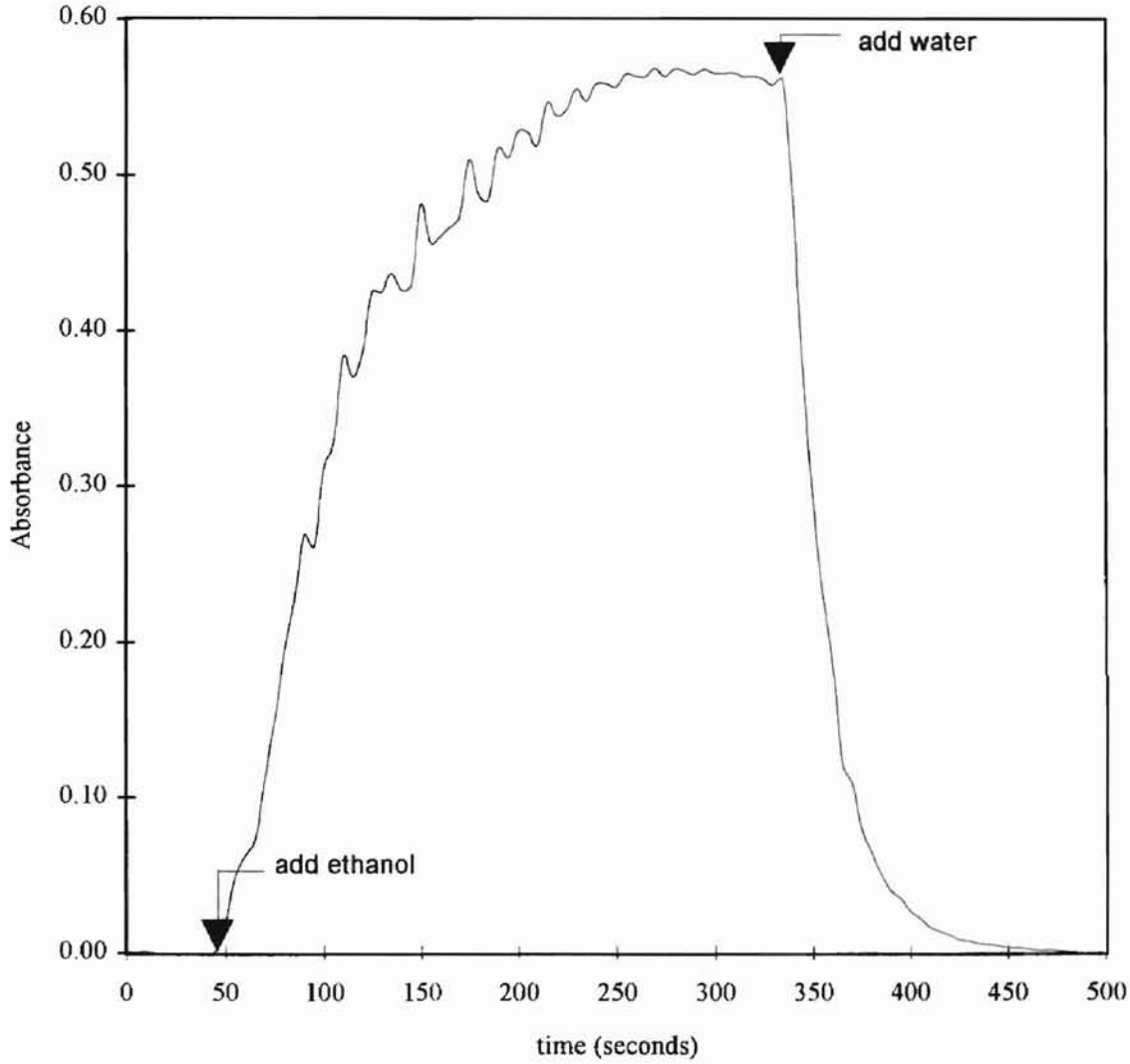

Figure 4.2 : Absorbance vs time for a step input of ethanol followed by a step input of water.

where τ_{tube} is the residence time of ethanol in the tubing connecting the CSTR (0.5 ml) to the spectrophotometer (V=1.8 ml), $\tau_{spectrophotometer}$ is the residence time in the spectrophotometer (V=0.3 ml) and τ_{other} is the residence time due to the extra volume of the three way valve and all the fittings in the system (0.9 ml). The residence time of the system calculated using Eq.4.14 and Eq.4.15 was 69 seconds and 70 seconds, respectively. This essentially shows that without the injection valve, the system behaves as theoretically expected. As noted before, the injection valve would increase the residence time of the system due to the time lag in injection of the sample. Thus, the length calculated using Eq.4.13 represents a smaller length than required. Since the time lag is difficult to quantify, the lengths could be increased from the calculated values in Table 4.1. However, the lengths shown in Table 4.1 would at least be a minimum requirement to maximize the amount of NO in the silastic tubing.

Another aspect to consider for the optimal tube length is the NO lost from solution as it travels through the silastic tube. The fraction of NO entering the silastic tubing which is lost to the detector can be calculated from the following differential mass balance equation assuming plug low

$$U_m A_C \frac{dc}{dz} = -k_0\left(\pi D_{avg.}\right)c \qquad (4.16)$$

where U_m is the average velocity, A_c is the area of cross-section, dz is the differential length, $D_{avg.}$ is the average diameter, and c is the average inlet concentration in the tube. The integration of Eq.4.16 over a given length gives the fraction of c which is remaining at the outlet of the silastic tubing which is

$$\frac{C_{out}}{C_{in}} = e^{-\left(k_0 \frac{\pi D_{avg}}{U_m A_c}\right) L} \qquad (4.17)$$

The length of silastic tubing required for 90% of the NO entering the tubing to be lost can be calculated using Eq.4.17. This length is representative of the maximum length of the silastic tubing required as any greater length would not be as beneficial since very little NO would be exposed to the remaining tube. The length of the silastic for which 90% of the NO in the solution is lost was determined at different flow rates. The value of k_0 used in Eq.4.17 was calculated as described in section 4.2.1. The wall thickness of the 0.15 cm tube was 0.024 cm and the wall thickness of the 0.03 cm tube was 0.016 cm. The permeability of the semi-permeable tubing at 25^{0}C is 2.3 x 10^{-12} mol $cm^{-1}s^{-1}cmHg^{-1}$ [Robb, 1968] and the diffusivity of NO in water at 25^{0}C is 2.3x10^{-5} cm^2s^{-1}[Reid, 1977]. The Henry's constant for NO in water at 25^{0}C is 2.5x10^{-5} M $cmHg^{-1}$[Lange, 1967] and this value was used for acetic acid as an approximation. Table 4.1 gives the length of the silastic required for 90 % of the entering NO in the solution to diffuse from the solution and into the detector. For the 0.03 cm diameter tubing, the NO is lost in a much shorter length than calculated using the residence time method. On the other hand, the reverse is true for the 0.15 cm tube.

As shown in Table 4.1, the maximum length for a single 0.15 cm diameter tube is 65 cm at all flow rates analyzed. With the 0.03 cm diameter silastic tubing, a 50 cm length of eight tubes at a flow rate of 3 ml/min is sufficient to loose 90% of the NO in the solution. Thus, Table 4.1 shows that the optimum length of the tube is determined by the residence time method for 0.15 cm diameter tubing and is determined by the amount lost

method for the 0.03 cm diameter tubing. Any extra length would only serve to increase the residence time of the analytical system without increasing the sensitivity very much. Again, it should be noted that if the calculations are based upon 99% of NO being lost to the detector, then according to Eq.4.17 the calculated length would be double of the value calculated for 90% being lost. Also, the non-ideality introduced by the injection valve will further increase these lengths. Nevertheless, this analysis gives a basis for approximating tube lengths.

The maximum tube length at other flow rates and number of tubes can be analyzed in a similar manner. Based on the shortest length given in Table 4.1 for a given set of conditions, the sampling time was calculated. The calculations were based on the time for 90% of NO to clear out of the CSTR plus the residence time in the silastic tubing of the given length plus the residence time in the connecting teflon tubing. It should be noted that the actual sampling time will be greater since only 90% removal from the CSTR was included and the effect of the injection valve on the sampling time was excluded. Nevertheless, the current analysis is sufficient for comparison.

A comparison of the sampling time in Table 4.2 shows that at a given flow rate and number of tubes the sampling time for 0.03 cm silastic tubing is less than the sampling time for the 0.15 cm silastic tubing. The sampling time at 1 cc/min for 0.15 cm silastic tubing is 181 seconds, whereas for 0.03 cm silastic tubing the sampling time is 117 seconds for the same flow rate. The sampling time decreases as the flow rate is increased. For the 0.03 cm tube, at a flow rate of 3 cc/min, the sampling time is approximately 50 seconds, whereas for the 0.15 cm tube, the sampling time at the same flow rate is approximately 65 seconds. The sampling time is also affected by the

Table 4.2: Comparison of the length, modified mass transfer coefficient, and sampling time for 0.03 cm and 0.15 cm tubes.

Q	# tubes	Q/tube	τ_{cstr}	d_s = 0.15 cm			d_s = 0.03 cm		
(ml/min)		(ml/min)	(seconds)	L (cm)	$k_0 A_s$ cc/sec (cc/sec)	Sampling time seconds	L (cm) (cm)	$k_0 A_s$ cc/sec (cc/sec)	Sampling time (seconds)
1	1	1	30	65	0.020	181	131	0.038	117
3	1	3	10	65	0.025	65	393	0.115	47
3	8	0.375	10	8	0.025	65	50	0.117	48
3	16	0.1875	10	4	0.025	65	25	0.117	48
3	20	0.15	10	3	0.025	65	20	0.117	48
4	1	4	7.5	65	0.026	50	524	0.154	39
4	8	0.5	7.5	8	0.026	50	66	0.155	39
4	16	0.25	7.5	4	0.026	50	33	0.155	39
4	20	0.2	7.5	3	0.026	50	27	0.158	39
6	1	6	5	65	0.029	36	786	0.230	30

injection valve. Though the injector in theory is supposed to inject a pulse, the actual injection is not a pulse as the sample takes approximately 7 seconds to clear out of the injector. Due to the lag time of the injector the NO concentration profile deviates from the ideal plug flow profile in the tube and this adds to the sampling time of the flow system.

4.3.2 Modified mass transfer coefficient(k_0A_s) effects on detector sensitivity.

The product of the mass transfer coefficient and the mass transfer area (k_0A_s) is referred to as the "modified mass transfer coefficient". The detector sensitivity depends on k_0A_s. The higher the value of k_0 and A_s, more NO goes into the detector and the sensitivity of the system increases.

Figure 4.3 shows the change in the values of k_0 with length and flow rate for a 0.15 cm diameter tube. For the optimum lengths given in Table 4.1 at a given flow rate, the value of k_0 for 0.15 cm diameter tube can be determined from Figure 4.3. The value of k_0 for a 5 cm length of tubing increases from 0.0007 cm/sec to 0.0016 cm/sec as the flow rate is increased from 0.15 cc/min to 6 cc/min. The change in k_0 decreases as the length of the tube is increased with relatively little change in k_0 for tube lengths greater than 50 cm at a given flow rate.

Figure 4.4 shows the change in the modified mass transfer coefficient with length. For the optimum lengths given in Table 4.1 at a given flow rate, the value of k_0A_s can be determined from Figure 4.4. The plot for all the flow rates is essentially a straight line for tube lengths greater than 50 cm. This is due to the fact that there is very little change of

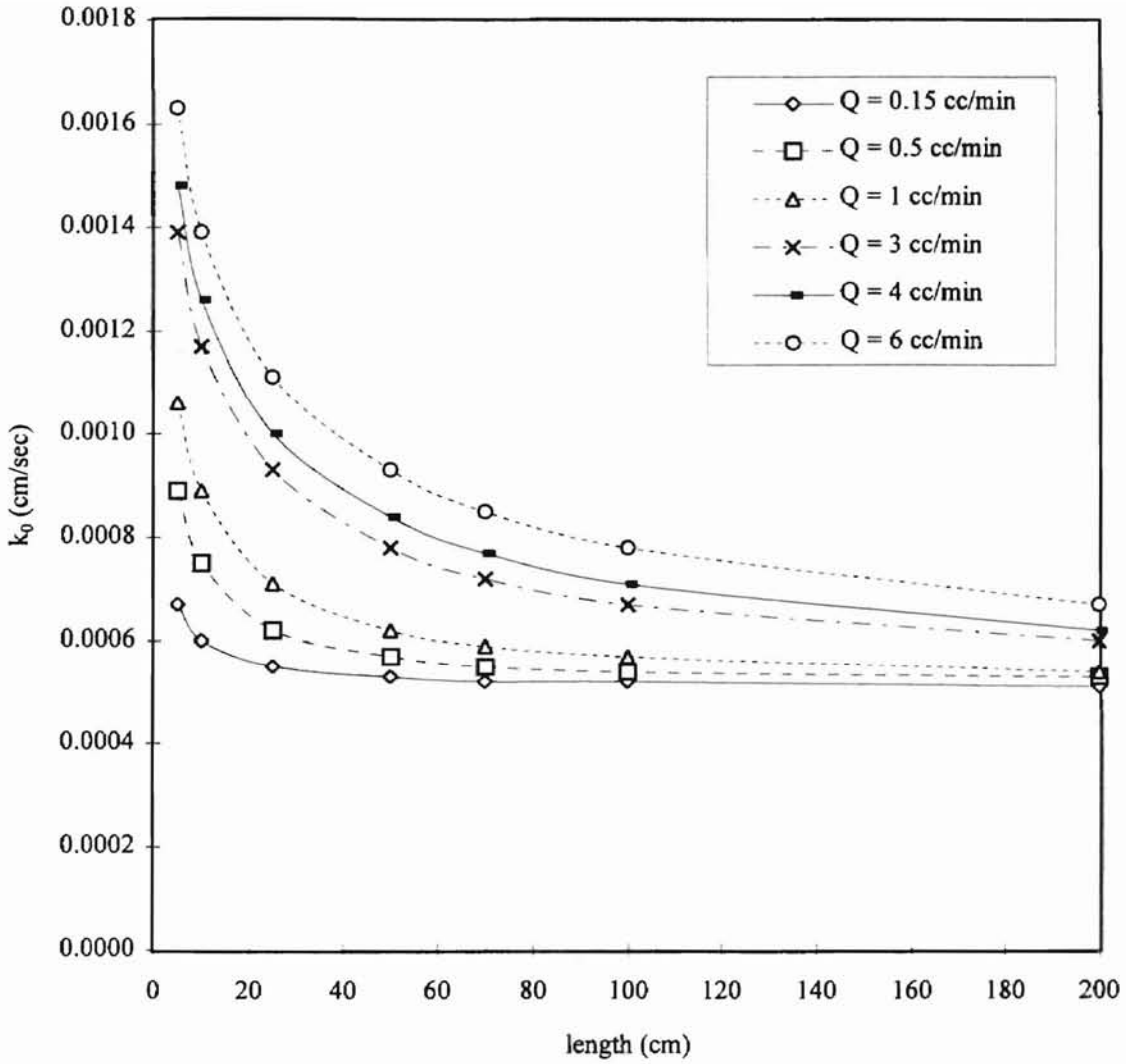

Figure 4.3 : k_0 vs L for a 0.15 cm diameter single tube

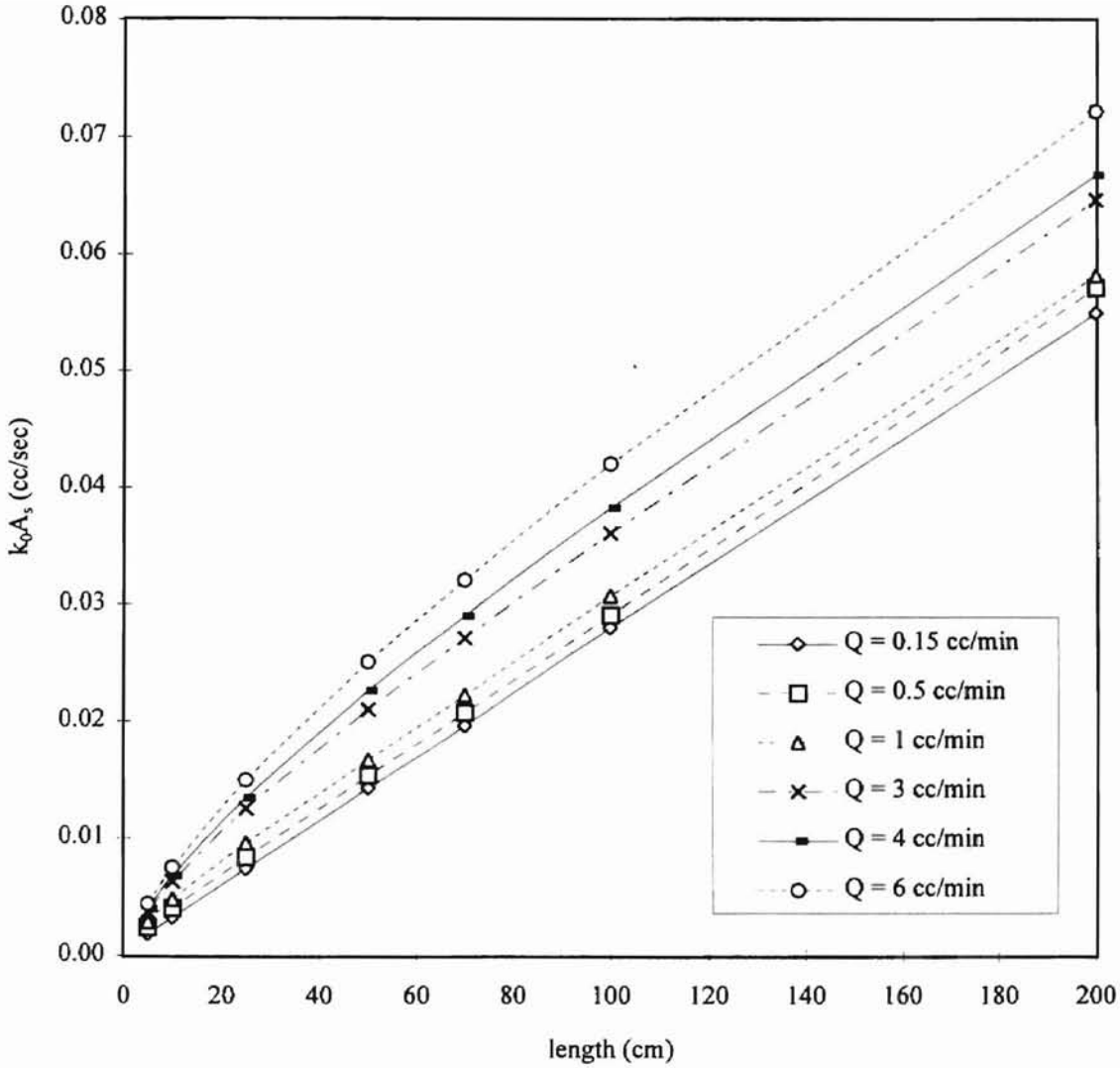

Figure 4.4 : k_0A_s vs L for a 0.15 cm diameter tube with the given flow rate through the tube.

k_0 in that region. The modified mass transfer coefficient increases with increase in length as expected.

Figure 4.5 shows the change in k_0 with length for a 0.03 cm diameter tube. The values of k_0 varies between 0.0023 cm/sec and 0.0037 cm/sec for flow rates between 0.15 cc/min and 6 cc/min at 5 cm length. For lengths greater than 50 cm, the change in k_0 is less than 5% for flow rates up to 1 cc/min and between 10% - 15% for flow rates between 1 cc/min and 6 cc/min. Figure 4.6 shows the change in k_0A_s with length for 0.03 cm diameter tube. The plot for all the flow rates is essentially a straight line for tube lengths greater than 50 cm since little change in k_0 occurs above 50 cm. k_0A_s was calculated for the optimum lengths determined in Table 4.1. Table 4.2 shows the value of k_0A_s for 0.15 cm as well as 0.03 cm diameter tubing at different flow rates. k_0A_s at optimum lengths, for all flow rates, is greater for 0.03 cm tubing. With an increase in flow rate, k_0A_s increases for the 0.03 cm tube and the 0.15 cm tube. For the 0.03 cm tube, k_0A_s at 4 cc/min is approximately 4 times the value of k_0A_s at 1 cc/min, primarily due to the difference in A_s. The maximum value of k_0A_s for the 0.15 cm tube is less than the smallest value of k_0A_s for the 0.03 cm tube.

4.3.3. Summary of k_0A_s and concentration effects on detector sensitivity.

From the above calculations and discussions, the importance of the concentration of NO in the silastic tubing and the modified mass transfer coefficient in designing the apparatus is obvious. Both quantities have to be maximized to optimize the sensitivity of the detection system. The length required for maximum sensitivity based upon the residence time of CSTR was calculated for 0.03 cm and 0.15 cm diameter tubes. The

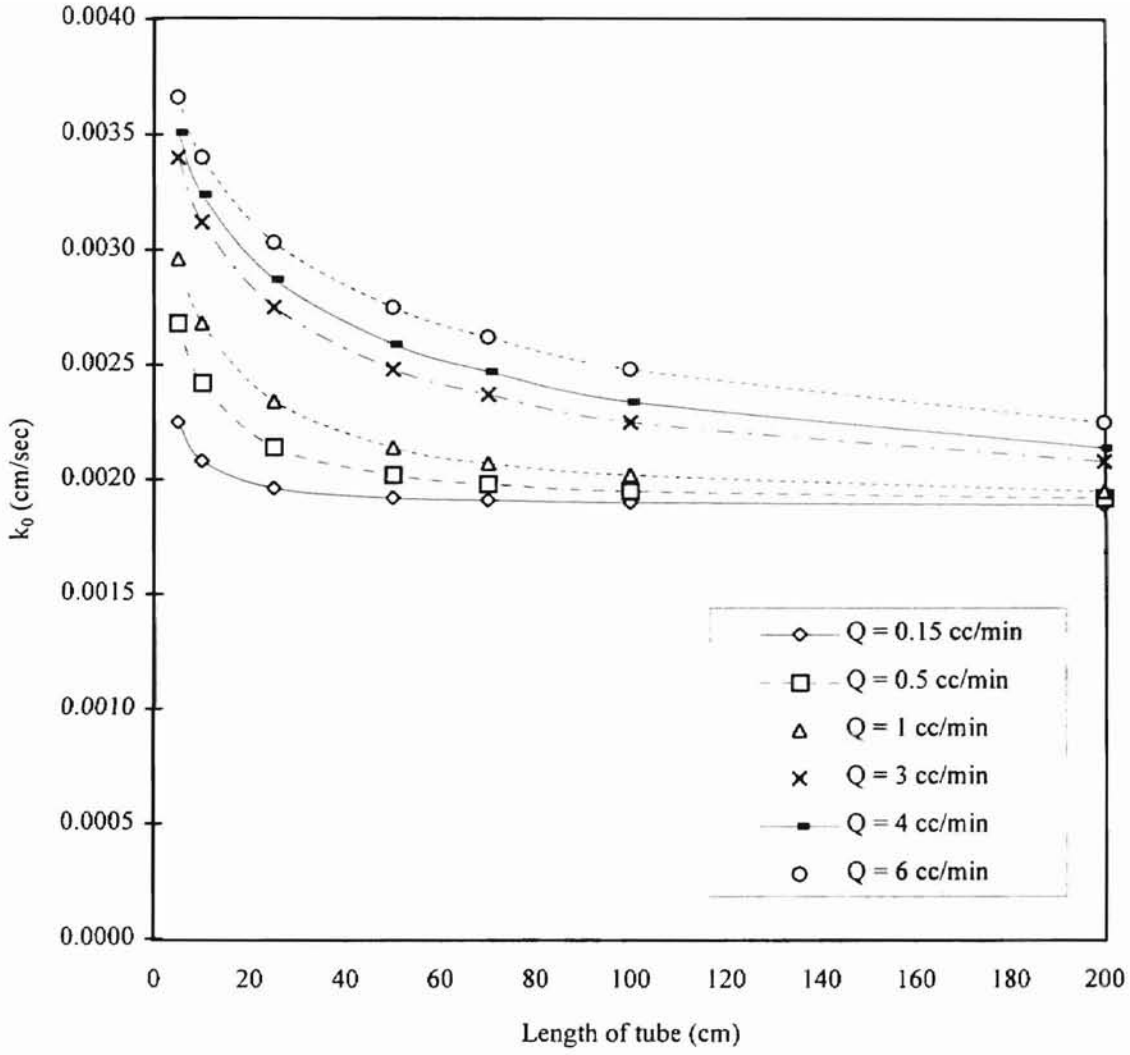

Figure 4.5 : k_0 vs L for a 0.03 cm diameter tube with the given flow rate through the tube.

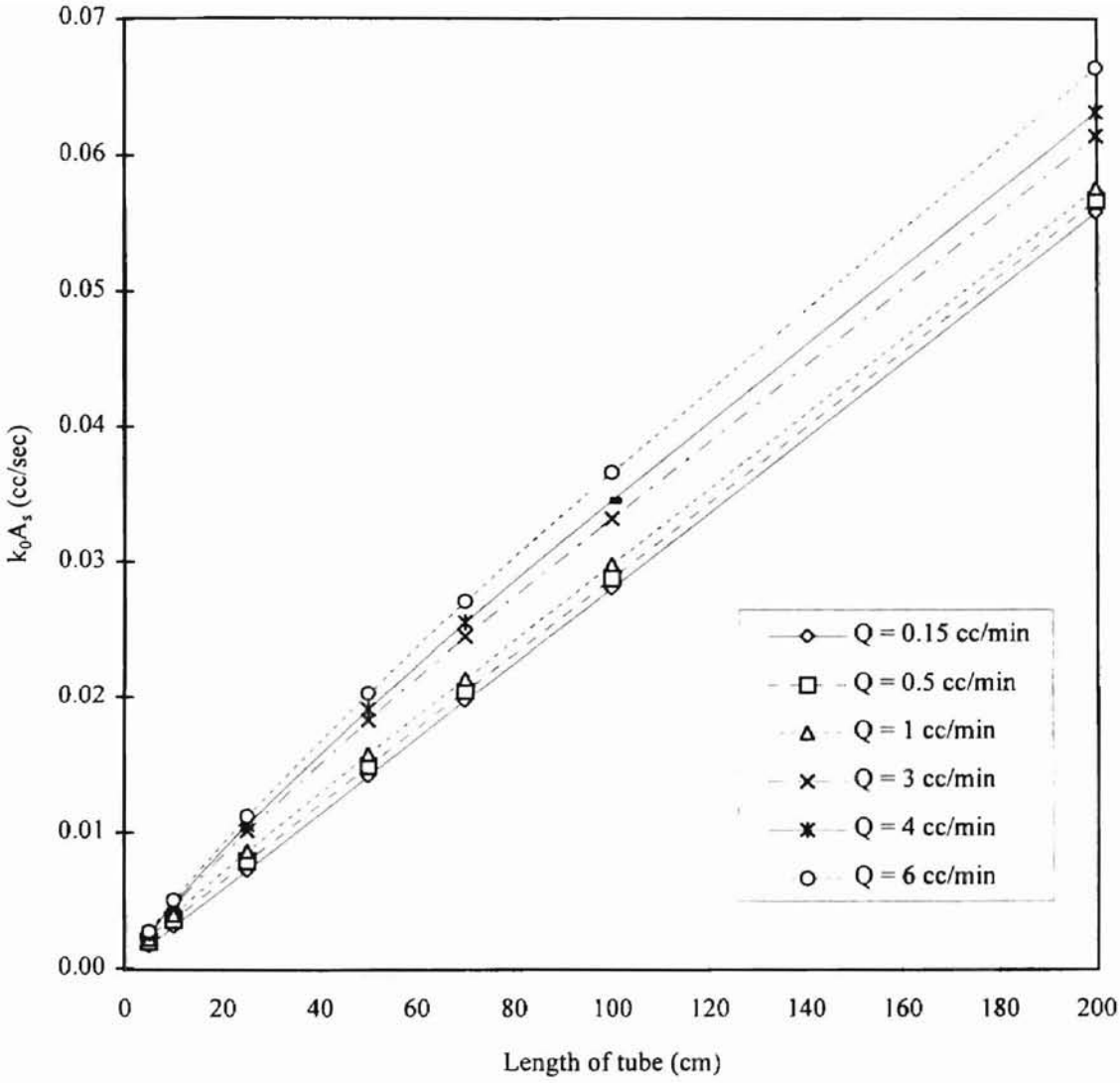

Figure 4.6 : k_0A_s vs L for a 0.03 cm diameter tube with the given flow rate through the tube.

length required to lose 90 % of NO to the detector was also calculated. The smaller of the two lengths was the optimum length although this length can also be shorter based on the combined effects of NO being lost as the complete NO profile enters the silastic. The length would be double if the calculations were based on 99% of NO going into the detector instead of 90%. The length can still be longer due to the non-ideality of the injection valve. The modified mass transfer coefficient and sampling time was also calculated for the optimum length of the tube. The flow rate and length of the tube for which the modified mass transfer coefficient was high and the sampling time was small was the optimized system.

A study of Table 4.2 shows that the analytical system can be optimized better with the 0.03 cm diameter silastic tubing. For determining the optimum flow rate and length of the 0.03 cm tubing, the length, modified mass transfer coefficient, and the sampling time were compared. Table 4.2 shows that the modified mass transfer coefficient for 6 cc/min is the highest and the sampling time is the smallest, but the length required is approximately 8 meters which is unreasonable. Also, a flow rate of 6 cc/min is a high flow rate for a system designed to measure trace amounts of NO_2^- and NO_3^- and would result in the wastage of reducing agent. The flow rates of 3 cc/min and 4 cc/min present a sampling time of less than a minute, and a reasonable length of 50 cm and 66 cm for 8 tubes. The modified mass transfer coefficient is 0.12 cc/sec at 3 cc/min and 0.15 cc/sec at 4 cc/min, which is more than 3 times of the value obtained at 1 cc/min for a single tube. Shorter tubes and a greater number of tubes is just as efficient as one long tube of 131 cm length for a flow rate of 1 cc/min. Thus, at a flow rate of 3 cc/min, flow systems with 8 tubes of 0.03 cm diameter and 50 cm length and 20 tubes of 0.03 cm diameter and 20 cm

length represented an optimized system of equal sensitivity. Though the theory calculated length of the tube for 8 tubes at 3 cc/min was 50 cm, extra length was used in experiments to account for the non-ideality of the injection system. Similarly, extra length was provided with 20 tubes also. Again, it should be noted that the calculated optimal length of the tube for 8 tubes and 20 tubes at 3 cc/min would be 100 cm and 40 cm respectively, if the calculations were based on 99% of NO lost instead of 90%.

To verify the optimization method, three systems were developed. The first system consisted of 8 tubes of 0.03 cm diameter tube and 65 cm length, the second system had 20 tubes of 200 cm length and the third had 20 tubes of 40 cm length. According to Table 4.2, 20 tubes of 0.03 cm diameter at a flow rate of 3 cc/min gives an optimum silastic tube length of 20 cm based on 90% (or 40 cm based on 99%).

4.4 Experimental results

Experiments were performed with the proposed flow system. With the 8 tube system (0.03 cm diameter and 65 cm length) a linear response was obtained for different concentrations of NO_2^- (Figure 4.7). The slope in Figure 4.7, which is 4.8, is the ratio of the detector response to the amount injected. The sampling time for this system was between 70-80 seconds at a flow rate of 3 cc/min. This sampling time was based on 90% of the NO lost. The increase in sampling time as compared to the calculated value in Table 4.2, which is 48 seconds at 50 cm length, is likely due to the 10% NO not being accounted in the calculations as well as the additional length. The calculated value would have been closer to the experimental value had the length of the silastic been double to allow 99% of NO to be lost. The increase in sampling time is also likely caused by the

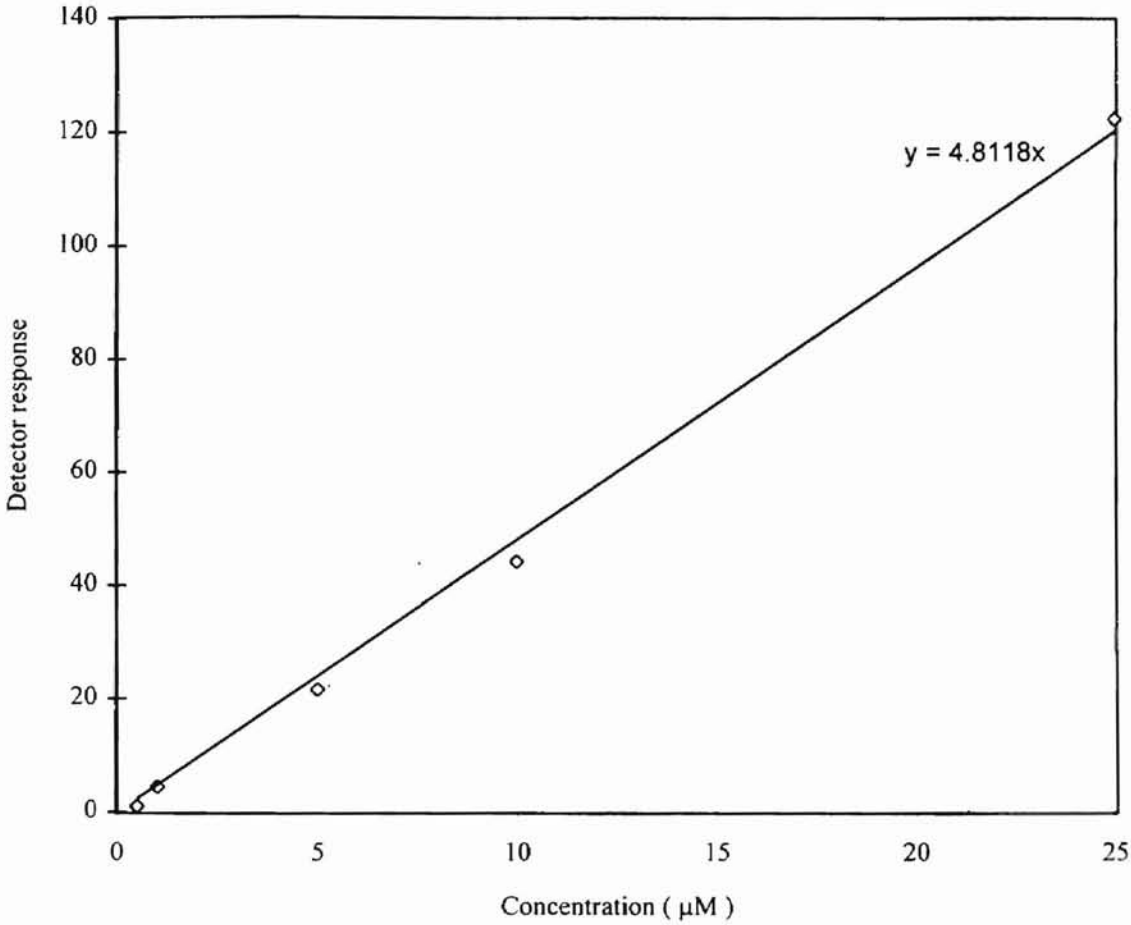

Figure 4.7 : Detector response vs. injected concentration for 8 tubes of 0.03 cm diameter and 65 cm length at a flow rate of 3 cc/min.

lag time of the injection valve. The minimum detector response was 0.5 μM for a 100 μl sample. However, the response below 1 μM was not consistent.

With 20 tubes and 200 cm length the mass transfer area was increased approximately 7.5 times that of the experiment with 8 tubes. However, Figure 4.8 shows that the detector response only increases approximately three-fold since the slope is 2.9 times that of Figure 4.7. This could be due to the fact that all the NO produced is not transported to the detector with the previous system of 8 tubes and 65 cm length. The detection limit of the 20 tube system was still approximately the same with uncertainty in measurements below 1 μM. The sampling time increased from 70-80 seconds to 130-140 seconds for the 200 cm length of tubing at the flow rate of 3 cc/min. This was due to the drop in flow rate through individual tubes and the increase in the tube length. The residence time through the silastic tube for 65 cm length was approximately 8 seconds, whereas for 20 tubes of 200 cm length, the residence time was approximately 57 seconds which is a difference of approximately 49 seconds. This explains the increase in sampling time.

Since 200 cm long tube was an excessive length as compared to optimized values in Table 4.2, system of 20 tubes and 40 cm length at a flow rate of 3 cc/min was examined. Figure 4.9 shows that the detector response for 40 cm length system was approximately 70% of that obtained for the 200 cm length tubes. This indicated that all the NO produced was not going into the detector. Hence, another system of 20 tubes of 0.03 cm diameter and 75 cm length and a flow rate of 3 cc/min was examined. The detector response obtained was within 2% of the response obtained for 200 cm length flow system. This indicates that the optimum length is between 40 cm and 75 cm, and the

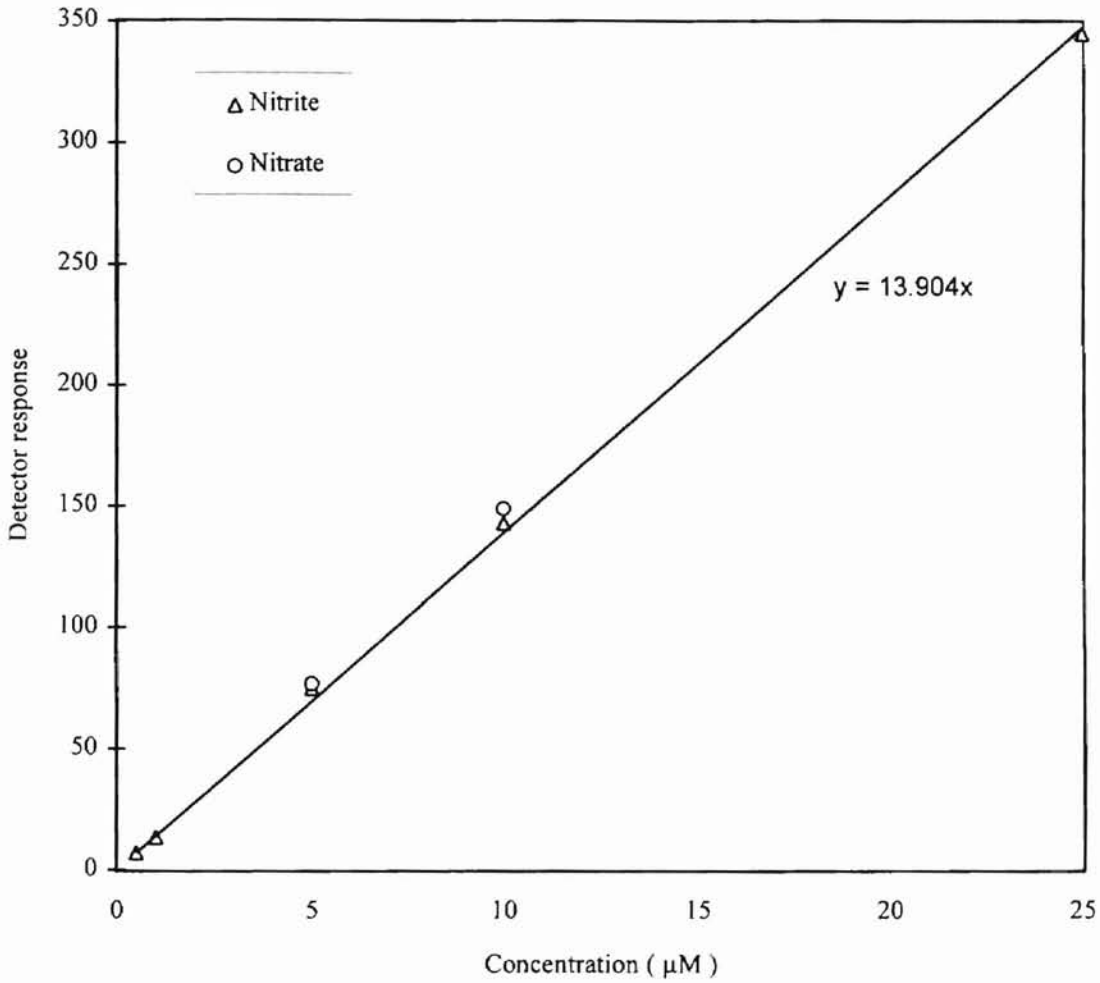

Figure 4.8 : Detector response for nitrite and nitrate samples with the flow system of 20 tubes (0.03 cm diameter) and 200 cm length at a flow rate of 3 cc/min.

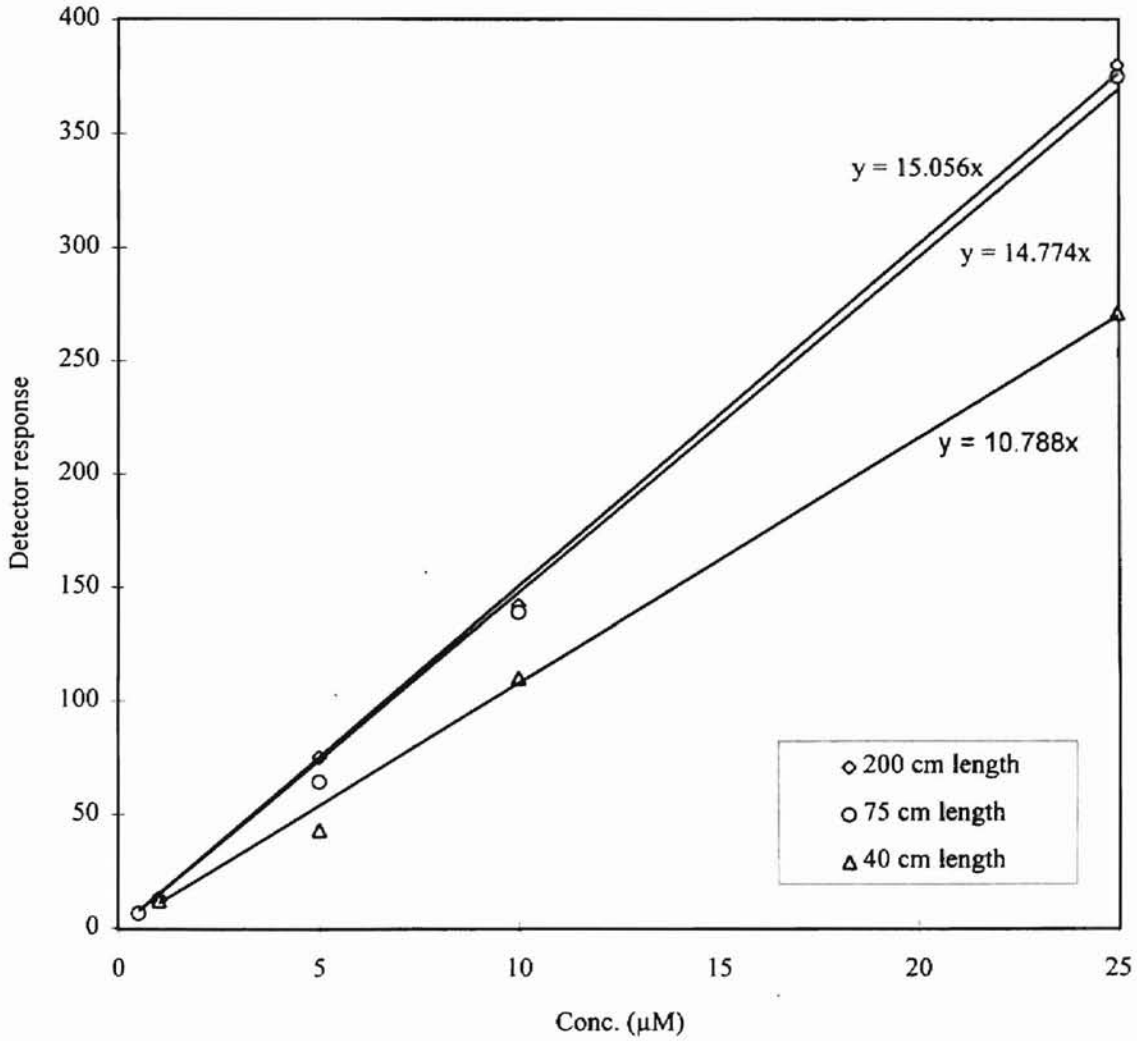

Figure 4.9 : Detector response vs concentration for different tube lengths.

remaining length of the silastic tubing is redundant. The optimum length being approximately 3 times of the theoretical calculated length can be due to a number of factors. Likely factor includes the non-ideality of the injection valve (i.e. the sample is not injected as a pure pulse into the CSTR) and the calculations were based on a 90% removal rate and not a 100% rate. The optimum length would be 40 cm on the basis of 99% of NO being lost, which is more consistent with the above experiments.

The optimum length being approximately 3 times the length given in Table 4.1 also explains the low detector response of the 8 tube system. The theoretical length from Table 4.1 was 50 cm and the 65 cm length was insufficient to remove more than 90% of the NO from solution and into the detector. A length of more than 150 cm would likely give the same response as the 20 tube system of 75 cm length.

NO_3^- samples were also tested in the flow system. After conversion to NO_2^- via cadmium reduction, the NO_2^- samples were injected into the flow system and the detector response obtained was compared with NO_2^- samples of the same concentration. The detector response obtained was within 4% of that obtained for NO_2^- (see Figure 4.8).

4.5 Conclusions

The results of the experiments performed with the flow system validated the optimization method. The results demonstrated the effects of concentration (c) and modified mass transfer coefficient (k_0A_s) on the sensitivity of the detection system.

The length of the silastic tubing required for maximum sensitivity was determined in two ways. The first method was based on the time required to remove 90% of NO from the CSTR thus exposing 90% of the NO to the detector. The second method was based

on the length of silastic tubing required to lose 90% of the NO produced in the solution due to mass transfer. The smaller of the two lengths was chosen because having a greater length than that required to expose 90% of the NO profile would not increase the detector response significantly as almost the entire concentration profile would already be exposed to the detector. Also, having a length greater than that required to remove 90% of NO from the solution would not have increased the sensitivity as there would be very little NO left in the solution to cause any significant increase in detector response.

The conclusion of the design calculations and optimization method were well supported by the results of the four experiments performed. As shown in Table 4.3 the experimental systems with 20 tubes and 200 cm length and 20 tubes and 75 cm length provided the same detector response. The system with 20 tubes and 40 cm length gave approximately 70% of the detector response as compared to 20 tubes of 200 cm length. These results indicate that the optimum length was between 40cm and 75 cm and the extra length in the 200 cm system only served to add to the sampling time. According to Table 4.2, the required length of the tubing for 20 tubes of 0.03 cm diameter was 20 cm based on 90% of NO being lost, and 40 cm for 99% of NO being lost. The fact that the optimum length was greater than the theoretically calculated length can be attributed to the reasons previously discussed. For this same reason, the detector response for the experimental system with 8 tubes and 65 cm gave a detector response which was only 33% of the response obtained for the experimental system with 20 tubes and 200 cm length. A length of over 150 cm would have been closer to the detector response of the 20 tube and 75 cm length flow system.

Table 4.3 : Comparison of the detector response for the 0.03 cm diameter flow systems based upon 20 tubes and 200 cm flow system.

# of tubes	Length (cm)	% detector response	Theoretical length for 90% of NO lost (cm)	Theoretical length for 99% of NO lost (cm)
20	200	100	20	40
20	75	100	20	40
20	40	70	20	40
8	65	33	50	100

The optimization method discussed above presents a sound system for the optimization of flow systems with semi-permeable tubing and a gaseous diffusing component in the mobile phase. Further studies in the optimization of the system can be performed since the above method serves to provide the boundaries only. The length based upon the residence time of the CSTR and the length based upon the amount of NO being lost provide a guideline for the tube length. In an actual unsteady state analysis, the rate of loss of NO from the solution with time would also be taken into consideration, and this would further reduce the length and sampling time of the system. The low detection limit of the system may partially be attributed to NO being trapped in the CSTR and the injection valve. It may also be due to the limitation of the detector. Also, to narrow the differences between the theoretical and actual lengths a more detailed model needs to be tested.

Since the detection limit of the flow system was not up to the desired limit, an alternate method which would allow faster and complete transfer of NO into the detector was required. Faster mass transfer would help reduce the sampling time of the detection system.

Chapter 5

Alternative method for nitrite and nitrate measurement

The lack of good sensitivity and large sampling time for the flow system resulted in the analysis of an alternative method for NO_2^- and NO_3^- measurements. The aim was to achieve a lower detection limit and improve upon the sampling time obtained with the optimized flow system.

5.1 Experimental setup and procedure

Experimental setup: Figure 5.1 shows the experimental setup of the system. The set up is based upon Cox's (1980) batch reactor method. A glass vial of 20 ml volume containing 10 ml of reducing agent formed the mixing and the reaction chamber. A tiny stir bar provided thorough mixing of the injected sample with the reducing solution. The reducing solution is continuously purged with ultra pure nitrogen and the NO generated by injecting a NO_2^- sample is transferred to the gas phase. The vacuum of the detector creates a driving force which transports the NO to the detector. The cold trap condenses the acid vapors transported along with NO. The reaction of NO with ozone produces an electrical signal which is recorded on a chart recorder.

Procedure: 10 ml of glacial reducing agent was added to the glass vial and sealed with a rubber septum. The reducing solution was continuously purged with ultra-pure nitrogen at a flow rate of 0.1 SCFH for 10-15 minutes to remove the oxygen present in the solution. The stirring speed was 1330 rpm. Care was taken to see that the stirring speed was not increased so much as to cause entrainment of the liquid into the vacuum line. Also, a very high stirring speed and high nitrogen flow rate was avoided to prevent

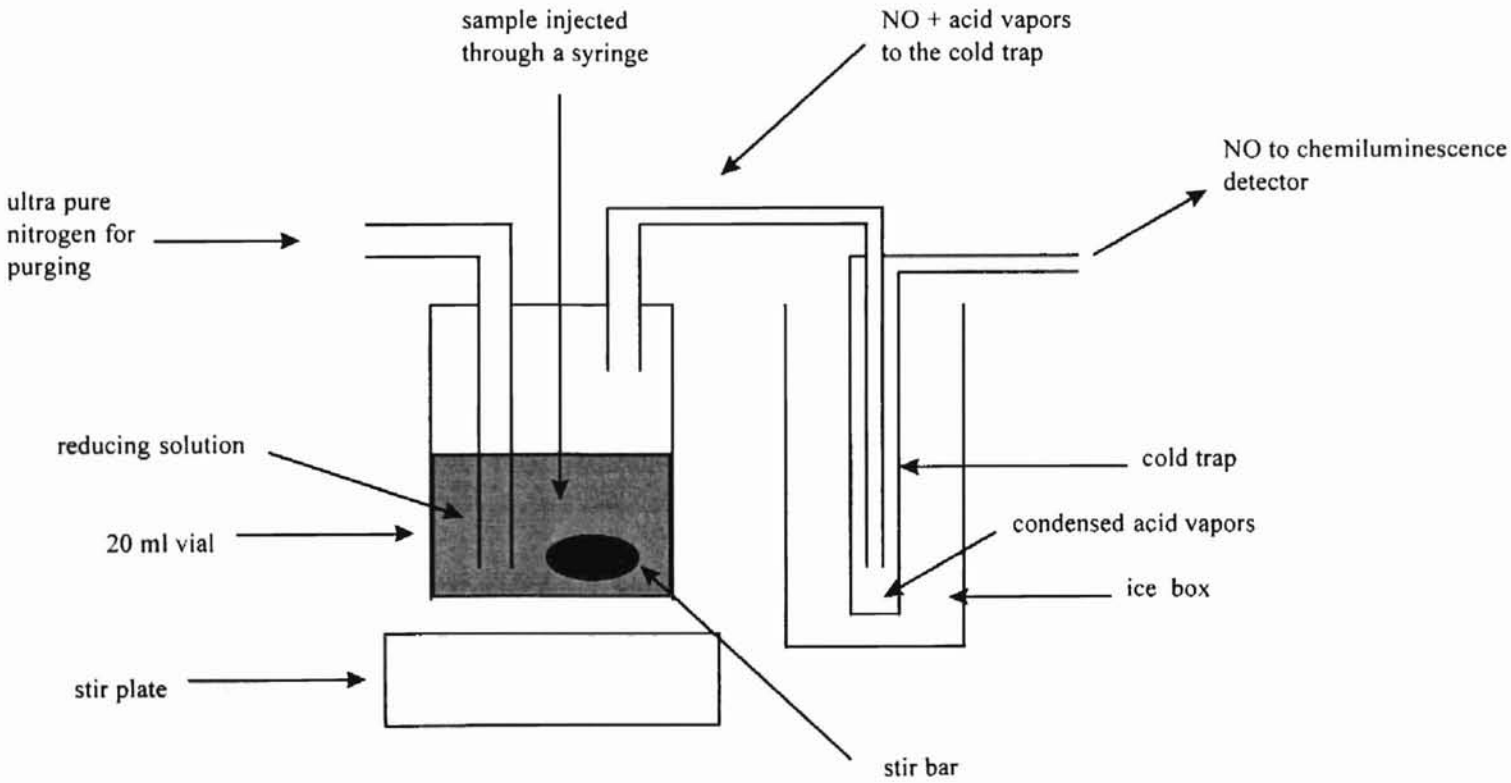

Figure 5.1 : Flow system for te analysis of nitrite and nitrate - purge method

frothing of the liquid. The vacuum valve was opened one turn to minimize the loss of liquid from the small vial.

Standard 100 μl NO_2^- samples were injected into the reducing solution. The response was recorded on a chart recorder. The detector response for standard NO_2^- samples serves as the calibration for the system. Based upon the calibration, trace amounts of NO_2^- and NO_3^- in water and biological fluids can be determined.

The experiment was repeated at different flow rates of nitrogen as well as at different stirring speeds. The flow rate and stirring speed which gave the lowest detection limit and the smallest sampling time represented the optimum experimental conditions for the system.

5.2 Results

Figure 5.2 shows the change in detector response for different flow rates of nitrogen. Compared to the detector response for 0.2 SCFH nitrogen flow rate, the response for 0.4 SCFH is 21% less for 10 nmol NO_2^- in the vial. The detector response is 26% lower at 0.6 SCFH, 36% lower at 0.8 SCFH and 42% lower at 1.2 SCFH. As the flow rate of nitrogen is increased, the detector response goes down.

The decrease in detector response with increasing flow rate of nitrogen indicates that not all of the NO produced in the vial is going into the detector. Some NO is likely lost due to the high flow rate of nitrogen and the inability of the detector to pull in all the gas. As the flow rate is increased, the amount of NO being lost increases and reduces the detector response. The flow rate has to be such that all the gas in the vial is pulled into the detector. Opening the vacuum valve one turn creates a pressure of 9.6 torr with

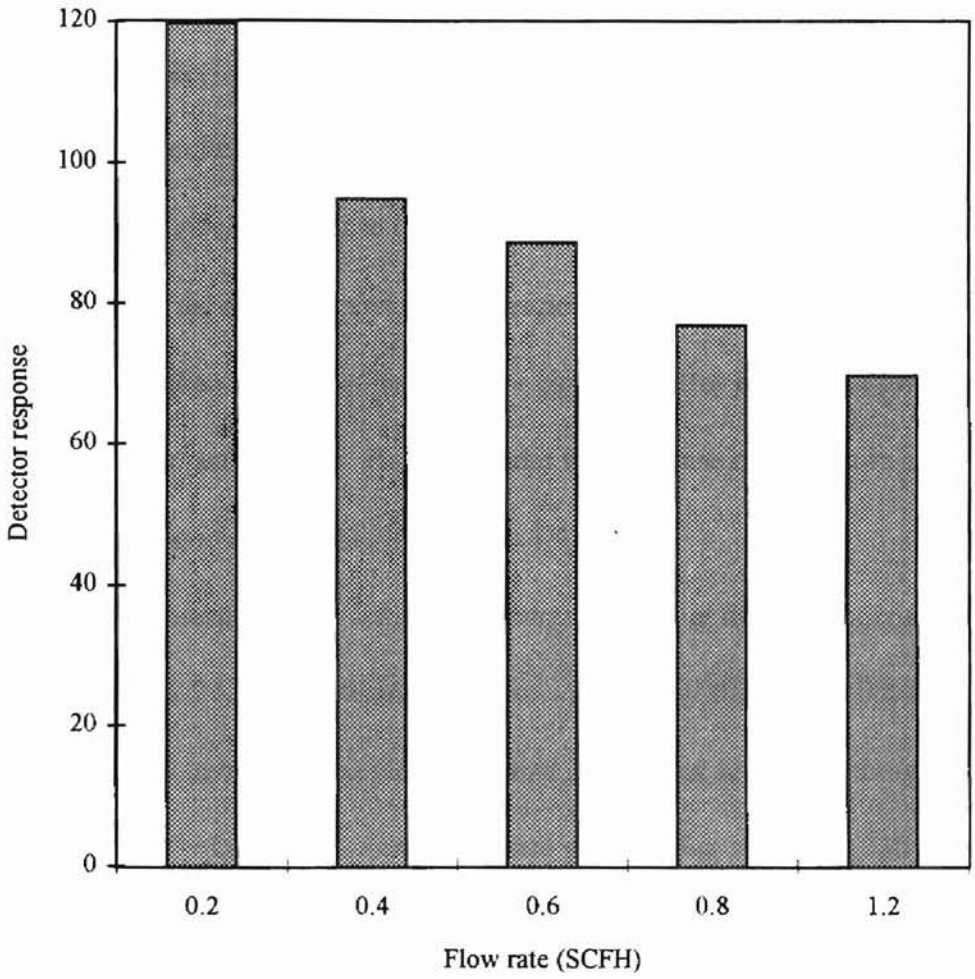

Figure 5.2 : Change in detector response with flow rate of nitrogen in glacial reducing agent at 25^0C.

a gas flow rate of 0.1 SCFH into the detector. Thus, a flow rate of 0.1 SCFH is the optimum flow rate of nitrogen.

Figure 5.3 shows the detector response for picomoles of NO going into the detector at a stirring speed of 380 rpm and nitrogen flow rate of 0.1 SCFH. The response is linear with a minimum detection of 25 picomoles. Based upon the response obtained for 1000 picomoles, the deviation from the expected response for 25 picomoles is 11%. The deviation for amounts greater than 25 picomoles is between 5% to 8%. Below 25 picomoles the detector response is not consistent and the readings are not repeatable. For 12.5 picomoles the deviation from the expected value is between 25% to 40%. For amounts lower than 25 picomoles the noise of the detector becomes significant as compared to the peak height. The area under the response curve shows a linear increase with the increase in amount of NO (Figure 5.4).

The detector response for different amounts of NO_2^- at different stirring speeds is shown in Figure 5.5. The detector response without any stirring is 10% lower for 1000 picomoles, 13% lower for 500 picomoles and 10% lower for 250 picomoles as compared to stirring at 380 rpm. The detector response with stirring speed at 1330 rpm was 182% higher than the response at 380 rpm for 1000 picomoles, 189% higher for 500 picomoles and 191% higher for 250 picomoles.

Figure 5.6 is a comparison of the areas under the response curve for the three stirring speeds with three repetitive sample injections. The area under the curve remains the same independent of stirring speed for a given NO_2^- injection. The areas for 1000 picomoles at the three stirring speed are within 4% of each other. For 500 picomoles the areas are within 2% of each other, and for 250 picomoles within 8% of each other.

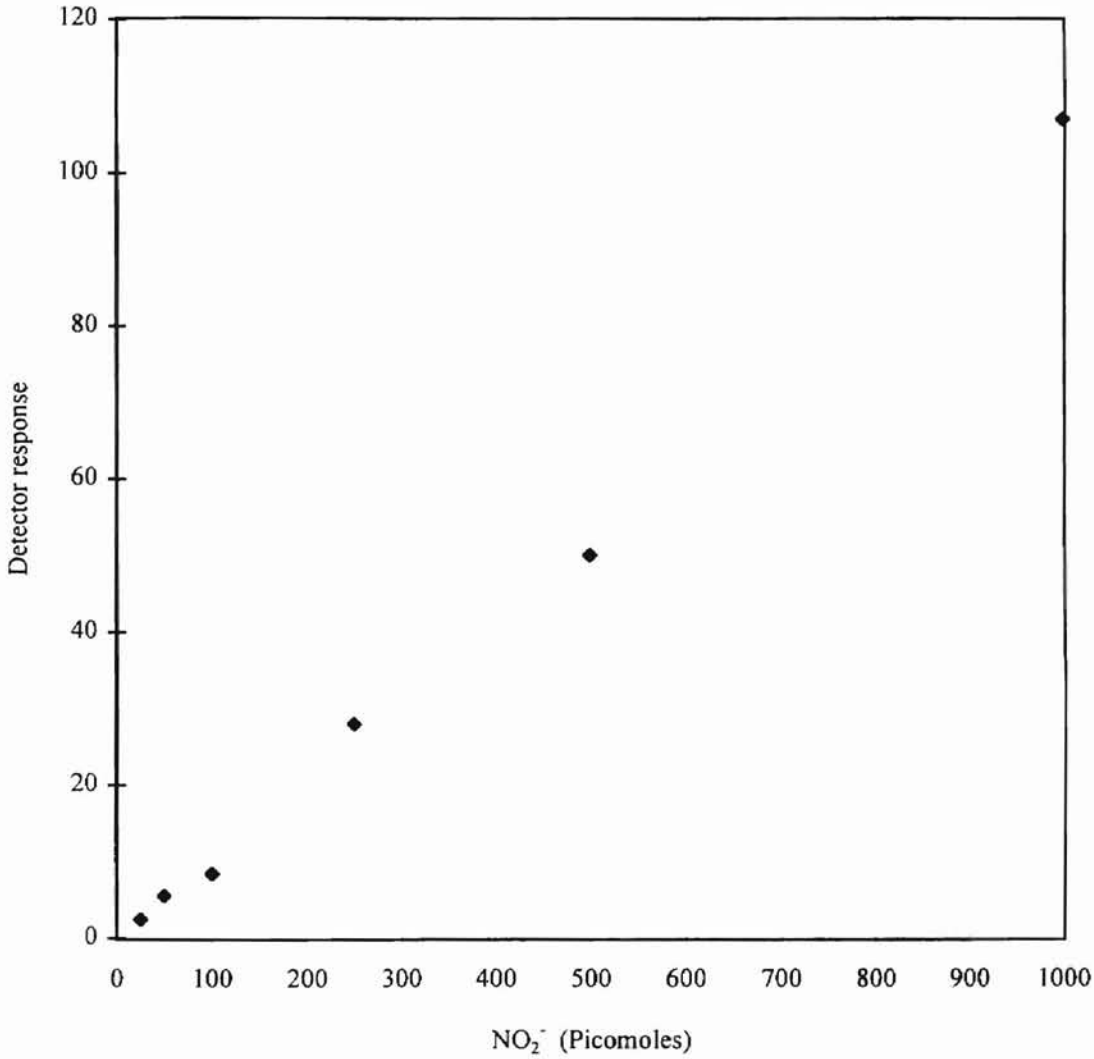

Figure 5.3 : Detector response vs NO_2^- added to glacial reducing agent at 0.1 SCFH nitrogen flow rate and 25^0C.

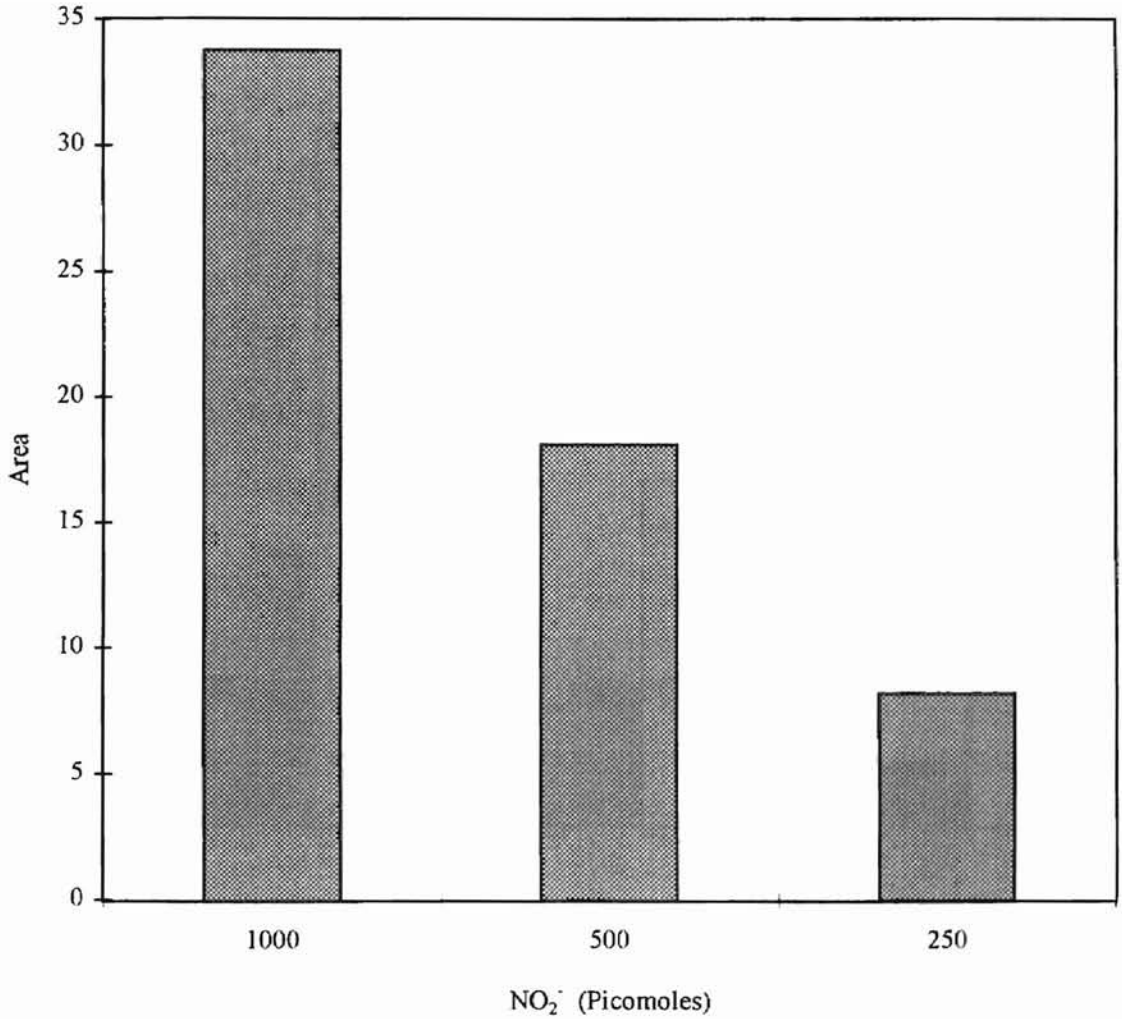

Figure 5.4 : Area under the curve vs NO_2^- added at 0.1 SCFH nitrogen flow rate and 380 rpm stirring speed.

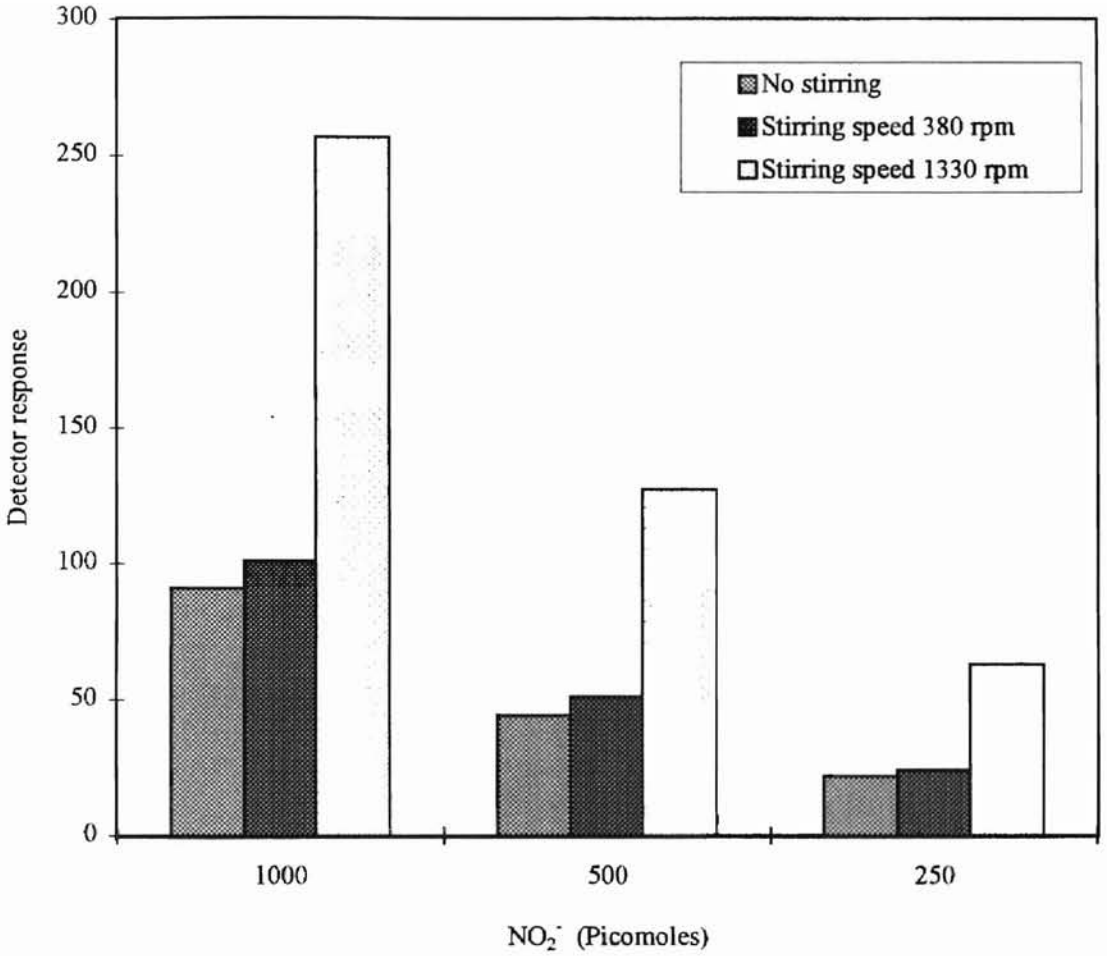

Figure 5.5 : Detector response vs NO_2^- added for different stirring speeds at a constant nitrogen flow rate of 0.1 SCFH and 25^0C.

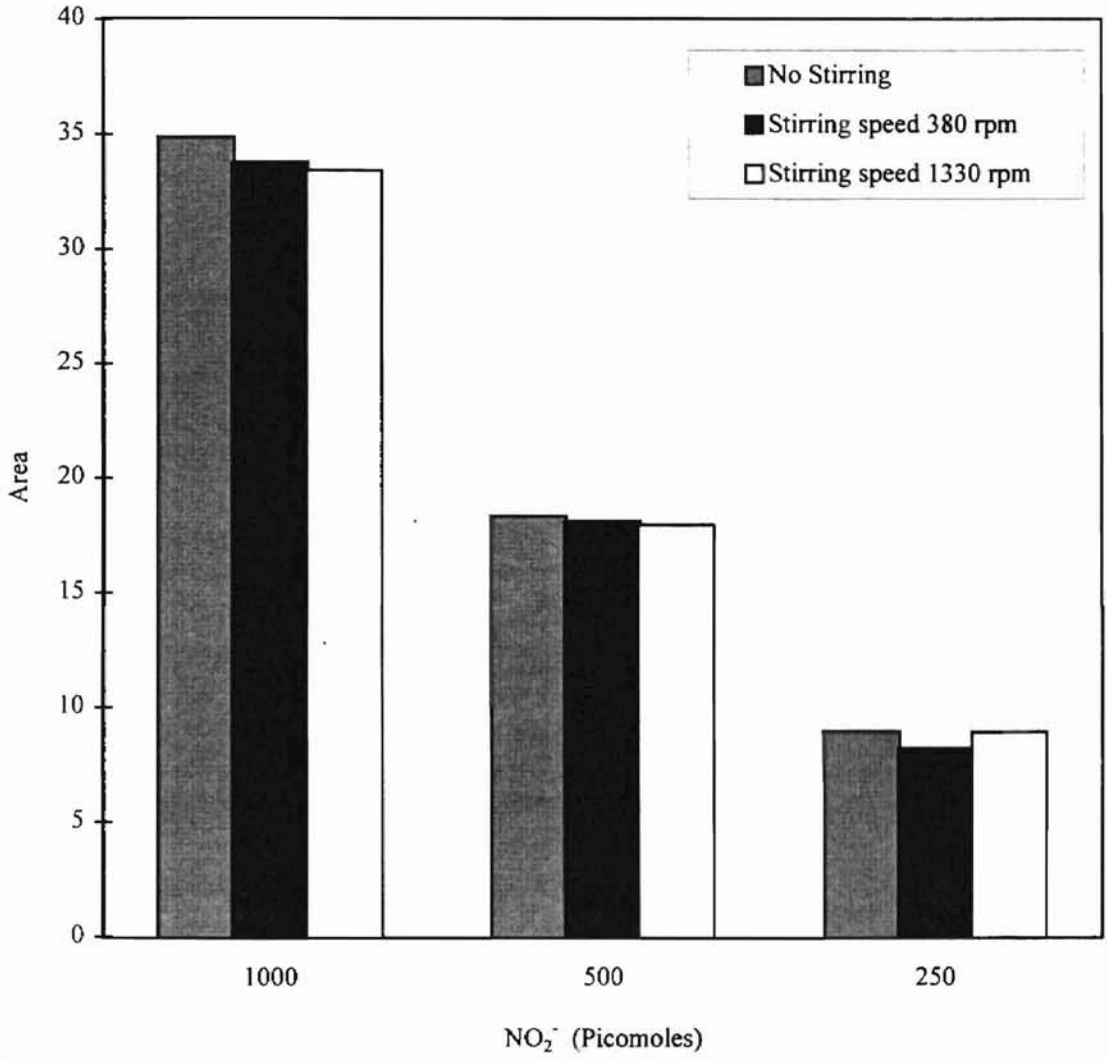

Figure 5.6 : Area under the curve vs NO_2^- added for different stirring speeds at a nitrogen flow rate of 0.1 SCFH and 25^0C.

Figure 5.7 is a comparison of the sampling time obtained without stirring with the sampling time obtained for stirring speeds of 380 rpm and 1330 rpm. The sampling time for 1000 picomoles at a stirring speed of 380 rpm is 2.3 minutes. For 500 picomoles, the sampling time is 2.2 minutes. For 250 picomoles the sampling time is 2 minutes. At 1330 rpm stirring speed the sampling time is 1.2 minutes, 1.1 minutes and 0.8 minutes for 1000 picomoles, 500 picomoles, and 250 picomoles, respectively. Thus, the sampling time decreases with increase in stirring speed, and shows very little change for different concentrations of the sample. This is consistent with the fact that NO_2^- converts instantaneously to NO upon addition to the reducing agent and that the rate of transport from the solution (via stirring and purging) is the primary means of increasing the sensitivity and decreasing the sampling time.

5.3 Conclusions

The linear increase in detector response and the linear increase in area under the response curve shows that there is complete conversion of NO_2^- to NO. The increase in detector response with an increase in stirring speed shows that the mass transfer coefficient is a strong function of stirring speed as expected. As the stirring speed increases, the mass transfer rate of NO into the detector increases. The increased rate causes the detector response to increase and improves the sensitivity of the system. Equal areas under the curve at different stirring speeds for the given concentrations indicate that there is complete conversion of NO_2^- to NO, and all the NO produced goes into the detector.

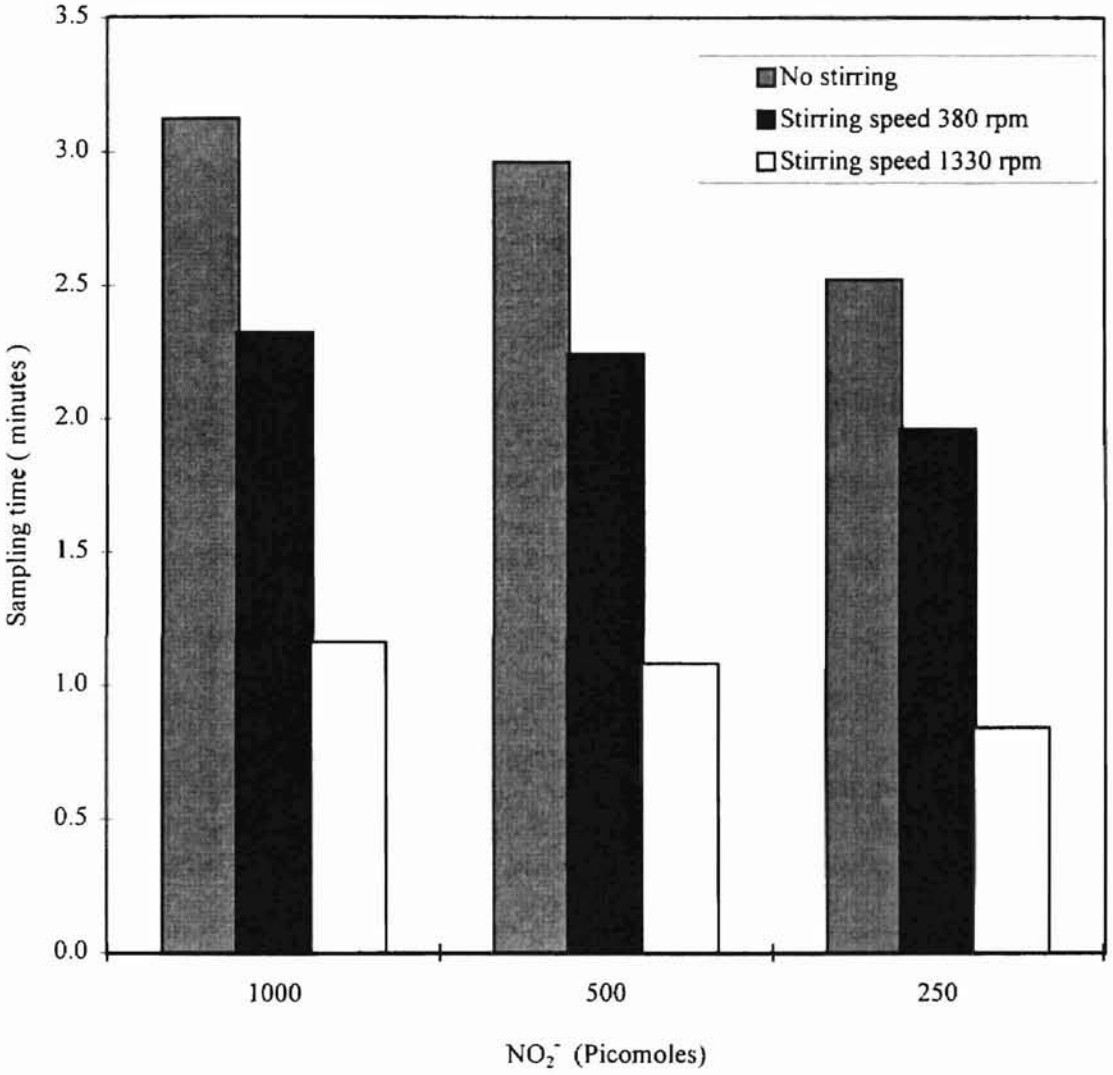

Figure 5.7 : Sampling time vs NO_2^- added for different stirring speeds at a constant nitrogen flow rate of 0.1 SCFH and 25^0C.

The lower detection limit of 25 picomoles of NO indicates higher sensitivity of the system as compared to the flow system. In addition, there is very little wastage of the reducing agent and the setup is simple and inexpensive. Among the two methods described, the above system is more advantageous as compared to the flow system. Improvements of this system can only be obtained by increasing the rate at which NO is transported from the solution.

Chapter 6

Conclusions and future scope of study

The overall objective of this study was to develop and optimize a method for measuring ppb levels of NO_2^- and NO_3^- from aqueous samples. Analysis of NO_2^- and NO_3^- in water or biological fluids is important due to its toxicity and suspected carcinogenicity in humans and other animals.

The objective was achieved by the completion of the following three aims :

1) Determination of the reaction kinetics of NO generated from NO_2^- and NO_3^-.
2) Design and optimization of a NO_2^- and NO_3^- analytical apparatus using chemiluminescence, and
3) Evaluation of the accuracy and sensitivity of concentration measurements via the chemiluminescence method.

6.1 Conclusions

The study of reaction kinetics was important for the development and optimization of the analytical system. Previous studies had not looked at the kinetics of the reaction, and thus had used long chambers to allow sufficient time for the reaction to occur.

The reaction kinetics were studied in two reducing agents. The glacial reducing agent reduced NO_2^- to NO. The NO_2^- and NO profiles and area under the curve matched closely showing that NO_2^- was converted instantaneously to NO at room temperature and long reaction chambers were not required for the reaction. Therefore, the mixing time (not reaction time) of the injected sample was of vital importance for the design of the analytical system.

In the phosphoric reducing agent, the NO_2^- concentration profile matched the NO profile showing that the conversion of NO_2^- to NO was essentially instantaneous. However, the NO_3^- profile showed that the reaction proceeds slowly at room temperature, increasing with an increase in temperature. At 77^0C the NO_3^- profile closely approximates the NO and NO_2^- profile, indicating that at higher temperatures above 77^0C the conversion of NO_3^- to NO would essentially be instantaneous. The phosphoric reducing agent was not used in the analytical system as significant amount of reducing agent was lost due to vaporization at high temperatures and would have lead to erroneous results.

The reduction of NO_3^- was achieved through cadmium reduction at room temperatures. The NO_3^- samples were reduced to NO_2^- in cadmium reduction vials and analyzed as NO_2^- samples in glacial reducing agent. The results obtained indicated that NO_3^- is completely converted to NO_2^- by the cadmium reduction vials at room temperature, thus eliminating the need to reduce NO_3^- at high temperature with phosphoric reducing agent. However, the conversion of NO_3^- to NO_2^- takes approximately 90 minutes and not 5 minutes as claimed by the manufacturer (World Precision Instruments, Inc.) of the cadmium vials.

Two analytical systems were developed and optimized for the NO_2^- and NO_3^- measurements. The first system was a flow system based on the apparatus used by Dunham(1995). The Dunham model used a long reaction coil to allow sufficient time for reaction to occur. The determination of the reaction kinetics obviated the use of a reaction coil and showed that thorough mixing of the injected sample with the reducing agent was of vital importance. Once the sample is mixed, conversion is complete. The

system was further optimized for the diameter and length of the semi-permeable tubing and also for the flow rate using the Davis & Parkinson model (1970). The model optimization showed that the key factors on which the sensitivity of the analytical system depends are the concentration of NO in the silastic tubing and the modified mass transfer coefficient. The length of the silastic tubing can be based upon two factors: The length calculated using the time required for 90 % of NO concentration to clear out of the mixing chamber and the length calculated based upon the amount of NO lost to the detector. If more than 90 % of the NO is lost for a length less than that calculated using the residence time of the CSTR, then the extra length only serves to increase the sampling time. Thus, the smaller of the two calculated lengths is the maximum length of the silastic required. The optimization analysis showed that multiple tubes of short lengths are as efficient as a single long tube. Multiple tubes of small diameter serve to increase the modified mass transfer coefficient and decrease required length of the silastic tubing. Flow system of 20 tubes and 75 cm length was the optimized system for the parameters studied. The actual length was approximately 3 times greater than the theoretically calculated length. This is likely due to the non-ideality of the injection valve (i.e. the sample is not injected as a pure pulse into the CSTR) and the calculations were based on a 90% removal rate and not a 100% rate. It is to be noted that the actual length was less than 2 times the theoretical length calculated on the basis of 99% of NO being lost. This is within the experimental error limits considering the imperfections of the injection valve and the non-ideality of the system. Thus, based upon the optimization method described in this study, an optimized system at different flow rates and number of tubes can be

developed after allowing some extra tubing to account for the non-idealities of the system.

To improve upon the sensitivity and sampling time of the flow system, a second system with a purged chamber was developed. The system had a detection limit of 25 picomoles and a sampling time of approximately one minute making the system more sensitive and faster than the flow system. The mass transfer of NO from the system was only a function of the stirring and gas purging rate.

Among the two methods of analysis developed, the analysis using the purged chamber has a higher sensitivity, smaller sampling time, and little waste of reducing agent. The setup is simple and inexpensive. Thus, the purged chamber method of analysis is more advantageous as compared to the flow system.

6.2 Future scope of study

The NO_3^- kinetics were not completely determined in the present study. The determination of NO_3^- kinetics could help develop a better analytical system and the kinetics could be used in other potential NO_3^- related studies.

The flow system provides scope for further optimization of the analytical system. The optimization method discussed in this study provides the maximum length of the tubing required. However, NO is continuously lost to the detector and an unsteady state analysis of the NO lost to the detector would serve to further clarify the required length. The low detection limit of the flow system could be due to some NO being trapped in the mixing chamber and the injection valve and methods for further improvement of the system can be explored by improving the injection system and developing a more complete flow

model. In the purged system , further methods to reduce the sampling time can be explored by increasing the rate at which NO is removed from the solution.

REFERENCES

1. Aoki, T. and Wakabayashi, M. (1995) Simultaneous flow injection determination of nitrate and nitrite in water by gas-phase chemiluminescence. *Analytica Chimica Acta* **308**, 308.

2. APHA-AWWA-WPCF 14th ed. Standard methods for the examination of water and wastewater, pp 418.

3. Baek, K.J., Thiel, B.A., Lucas, S. and Stuehr, D.J. (1993) Macrophage nitric oxide synthase subunits. *J. Biol. Chem.* **268**, 21120.

4. Beckman, J.S., Beckman, T.W., Chen, J., Marshall, P.A. and Freeman, B.A. (1990) Apparent hydroxyl radical production by peroxynitrite: Implications for endothelial injury from nitric oxide and superoxide. *Proc. Natl. Acad. Sci. USA* **87**, 1620.

5. Bendtzen, K. (1989) Immune hormones (cytokines); pathogenic role in rheumatic and endocrine diseases. *Autoimmunity* **2**, 177.

6. Bolotina, V.M., Najibi, S., Palacino, J.J., Pagano, P.J. and Cohen, R.A. (1994) Nitric oxide directly activates calcium-dependent potassium channels in vascular smooth muscles. *Nature* **368**, 850.

7. Braman, R.S. and Hendrix, S.A. (1989) Nanogram nitrite and nitrate determination in environmental and biological materials by Vanadium(III) reduction with chemiluminescence detection. *Anal. Chem.* **61**, 2715.

8. Bredt, D.S., Hwang, P.M., Glatt, C.E., Lowenstein, C., Reed, R.R. and Snyder, S.H. (1991) Cloned and expressed nitric oxide synthase structurally resembles cytochrome P-450 reductase. *Nature* **351**, 714.

9. Burleigh, D.E. (1992) N^g-nitro-L-arginine reduces nonadrinergic,noncholinergic relaxations of human, mouse, and rat. *Annu. Rev. Immunol.* **8**, 647.

10. Cleeter, M.W.J., Cooper, J.M., Darley-Usmer, V.M., Moncada, S. and Scapira, A.H.V. (1994) Reversible inhibition of cytochrome oxidase, the terminal enzyme of the mitochondrial respiratory chain, by nitric oxide. *FEBS Lett.* **345**, 50.

11. Conner, E.M. and Grisham, M.B. (1993) Nitric Oxide: Biochemistry, Physiology, and Pathology. *A Comparison of Methods in Enzymology* **7**, 3.

12. Cox,R.D. (1980) Determination of nitrate and nitrite at the parts per billion level by chemiluminescence. *Anal. Chem.* **52**, 332.

13. Cresser, M.S. (1977) Nitrate determination by reduction to ammonia and gas-phase ultraviolet absorption spectrometry. *Analyst* **102**, 99.

14. Davis,H.R. and Parkinson,G.V. (1970) Mass transfer from small capillaries with wall resistance in the laminar flow regime. *Appl. Sci. Res.* **22**, 20.

15. Dawson, T.M., Steiner, J.P., Dawson, V.L., Dinerman, J.L., Uhl, G.R. and Snyder, S.H. (1993) Immunosuppressant FK506 enhances phosphorylation of nitric oxide synthase and protects against glutamate neurotoxicity. *Proc. Natl. Acad. Sci. USA* **90**, 9808.

16. Delaney, C.A. and Eizirik, D.L. (1996) Intracellular targets for nitric oxide toxicity to pancreatic β-cells. *Braz. J. Med. Biol. Res.* **29**, 569.

17. Dinerman, J.L., Dawson, T.M., Schell, M.J., Snowman, A. and Snyder, S.H. (1994) Endothelial nitric oxide synthase localized to hippocampal pyramidal cells: Implication for synaptic plasticity. *Proc. Natl. Acad. Sci. USA* **91**, 4214.

18. Dunham,A.J., Barkley,R.M., and Sievers,R.E. (1995) Aqueous nitrite ion determination by selective reduction and gas phase nitric oxide chemiluminescence *Anal. Chem.* **67**, 220.

19. Farias-Eisner, R., Sherman, M.P., Aeberhard, E. and Chaudhuri, G. (1994) Nitric oxide is an important mediator for tumoricidal activity *in vivo*. *Proc. Natl. Acad. Sci. USA* **91**, 9407.

20. Furchgott, R.F. (1984) The role of endothelium in the responses of vascular smooth muscle to drugs. *Ann. Rev. Pharmacol.* **124**, 175.

21. Geller, D.A., Lowenstein, C.J., Shapiro, R.A., Nussier, A.K., Disilvio, M., Wang, S.C., Nakayama, D.K., Simmons, R.L., Snyder, S.H. and Billiar, T.R. (1993) Molecular cloning and expression of inducible nitric oxide synthase from human hepatocytes. *Proc. Natl. Acad. Sci. USA* **90**, 3491.

22. Grozdanovic, Z., Mayer, B., Baumgarten, H.G. and Bruning, G. (1994) *Neuroreport* **5**, 837.

23. Hibbs, J.B. Jr., Taintor, R.R., Vavrin, Z., et al. (1990) Synthesis of nitric oxide from a terminal guadino nitrogen atom of L-arginine: a molecular mechanism regulating cellular proliferation that targets intracellular iron. In S. Moncada and E.A. Higgs (Eds.). Nitric oxide from L-arginine: A bioregulatory system. Proceedings of the Symposium on Biological Importance of Nitric Oxide, London, September 14-15, 1989 (pp. 189-223). Amsterdam: Excerpta Medica.

24. Hogg, N., Darley-Usmer, V.M., Wilson, M.T. and Moncada, S. (1992) Production of hydroxyl radicals from the simultaneous generation of superoxide and nitric oxide. *Biochem. J.* **281**, 419.

25. Ignarro, L.J., Bush, P.A., Buga, G.M., Wood, K.S., Fukuto, J.M. and Raajfer, J. (1990) Nitric oxide and cyclic GMP formation upon electrical field stimulation cause relaxation of corpus cavernosum smooth muscle. *Biochem. Biophys. Res. Commun.* **170**, 843.

26. Iwamoto, J., Krasney, J.A., Morin III, F.C. (1994) Methemoglobin production by nitric oxide in fresh sheep blood. *Respiration Physiol.* **96**, 273.

27. Kieber, R.J. and Seaton, P.J. (1995) Determination of subnanomolar concentrations of nitrite in natural waters. *Anal. Chem.* **67**, 3261.

28. Lange, N.A., Ed. (1967) *Lange's Handbook of Chemistry, rev. 10th ed., McGraw Hill, New York*, p-1101.

29. Lewis, R.S. and Deen,W.M. (1994) Kinetics of the reaction of nitric oxide with oxygen in aqueous solutions. *Chem. Res. Toxicol.* **7**, 568.

30. Lobzik, L., Reid, M.B., Bredt, D.S. and Stamler, J.S. (1994) *Nature* **372**, 546.

31. Maerin, F., Mourelle, M., Guarner, F., et al. (1993) Patients with achalasia lack nitric oxide in gastro-oesophagial junction. *Eur. J Clin. Invest.* **23**, 724.

32. Manchester, K.S., Jensen, F.E., Warach, S. and Lipton, S.A. (1993) Chronic administration of Nitroglycerin decreases cerebral infarct size. *Neurology* **43**, A365.

33. Masini, F., Bianci, S., Mugnai, L., Gambassi, F., Pistelli, M., Mannaioni, P.F. (1991) *Agents Actions* **33**, 53.

34. McDonald, B., Reep, B., Lapetina, E.G. and Vedia, L.M. (1993) Glyceraldehyde-3-phosphate dehydrogenase is required for the transport of nitric oxide in platelets. *Proc. Natl. Acad. Sci. USA* **90**, 11122.

35. Moncada, S. (1994) Nitric oxide. *J Hypertension* **12** (suppl. 10), S35.

36. Moncada, S. and Higgs, E.A. (1989) Nitric oxide from L-arginine: A bioregulatory system. Proceedings of the Symposium on Biological Importance of Nitric Oxide, London. *Amsterdam: Excerpta Medica*. p-189.

37. Moncada, S., and Higgs, A. (1993) The L-arginine-nitric oxide pathway. In F.H. Epstein (Ed.) *N Engl. J Med.* **329**, 2002.

38. Moncada, S., Ferrige, A.G. and Palmer, P.M.J. (1987) Nitric oxide release accounts for the biological activity of endothelium-derived relaxing factor. *Nature* **327**, 524.

39. Moskowitz, A.H. (1977) Particle size distribution of nitrate aerosols in the Los Angeles Air Basin. *EPA/600/3-77/053*.

40. Mulik, J., Puckett, R., Williams, D. and Sawicki, E. (1976) Ion Chromatographic analysis of sulfate and nitrate in ambient aerosols. *Analytical Letters* **9(7)**, 653.

41. Panalaks, T., Iyengan, J.R., Sen, N.P. (1973) Nitrate, nitrite, and dimethylnitrosamine in cured meat products. *J. Assoc. Off. Anal. Chem.* **56**, 621.

42. Pavel, M., Zbynek, V. and Zbynek, Z. (1995) Flow-injection chemiluminescence determination of ultra low concentrations of nitrite in water. *Analytica Chimica Acta* **316**, 261.

43. Radi, R. (1996) Reactions of nitric oxide with metalloproteins. *Chem. Res. Toxicol.* **9**, 828.

44. Rand, M.J. (1992) Nitrergic transmission: Nitric oxide as a mediator of non-adrenergic, non-cholinergic neuro effector transmission. *Clin. Exp. Pharmacol. Physiol.* **19**, 147.

45. Reid, R.C., Prausnitz, J.M. and Sherwood, T.K. (1977) Pure component parameters for the Hankinson - Brobst-Thomson and the Rackett Liquid Volume Correlations. *The properties of gases & Liquids*, p-58.

46. Robb, W.L. (1968) Thin silicone membranes - their permeation properties and some applications. *Ann. N.Y. Acad. Sci.* **146**, 119.

47. Sawicki, E., Stanley, T.W., Pfaff, J. and D'Amico, A. (1963) Comparison of fifty-two spectrophotometric methods for the determination of nitrite. *Talanta* **10**, 641.

48. Shibuki, K. (1994) *7th. Seitaikinoukagaku Koushuukai Abstract.*

49. Stamler, J.S., Singel, D.J. and Loscalzo, J. (1992) Biochemistry of nitric oxide and its redox-activated forms. *Science* **258**, 1898.

50. Swann, P.F. (1975) The toxicology of nitrate, nitrite and N-Nitroso compounds. *J. Sci. Fd. Agric.* **26**, 1761.

51. Tam, F.S-F and Hiller, K. (1992) The role of nitric oxide in mediating non-adrenergic non-cholinergic relaxation in longitudinal muscle of human taenia coli. *Life Sci.* **51**, 1277.

52. Tannenbaum, S.R., Tamir, S., de Rojas-Walker, T. and Wishnok, J.S. (1991) DNA damage and cytotoxicity by nitric oxide. *Proc. ACS Symposium on N-Nitroso compounds, Wash., DC.*

53. Termin, A., Hoffmann, M., Bing, R.J. (1992) A simplified method for the determination of nitric oxide in biological solutions. *Life Sci.* **51**, 1621.

54. Toda, N., Kimura, T., Yoshida, K., Bredt, D.S., Snyder, S.H., Yoshida, Y. and Okamura. T. (1994) Human uterine arterial relaxation induced by nitroxidergic nerve stimulation. *Am. J. Physiol.* **266**, H1446.

55. USEPA (1974) Methods for the chemical analysis of water and wastes. *EPA-625-116-74-003*, pp 197.

56. Vanderwinden, J-M., Mailleux, P., Schiffmann, S.N., Vanderhaeghen, J-J and De Laet, M-H. (1992) Nitric oxide synthase activity in infantile hypertropic pyloric stenosis. *N Engl. J Med.* **327**, 511.

57. Wegner, T.N. (1972) Simple and sensitive procedure for determining nitrate and nitrite in mixtures in biological fluids. *Journal of Dairy Science* **55**, 642.

58. West, P.W. and Lyles, G.L. (1960) A new method for the determination of nitrates. *Analytica Chimica Acta* **23**, 227.

59. White, J.W. (1975) Relative significance of dietary sources of nitrate and nitrite. *Agric. Fd. Chem.* **23**, 891.

60. Yoshida, M., Akaike, T., Wada, Y., Sato, K., Ikeda, K., Ueda, S. and Maeda, H. (1994) Therapeutic effects of imidazolineoxyl N-oxide against endotoxin shock through its direct nitric oxide-scavenging activity. *Biochem. Biophys. Res. Commun.* **202**, 923.

61. Yoshizumi,K., Aoki,K., Matsouka,T., and Asakura,S. (1985) Determination of nitrate by flow system with a chemiluminescent NOx Analyzer. *Anal. Chem.* **57**, 737.

62. Zhang, J., Dawson, V.L., Dawson, T.M. and Snyder, S.H. (1994) Nitric oxide activation of poly (ADP-Ribose) synthetase in neurotoxicity. *Science* **263**, 687.

APPENDIX

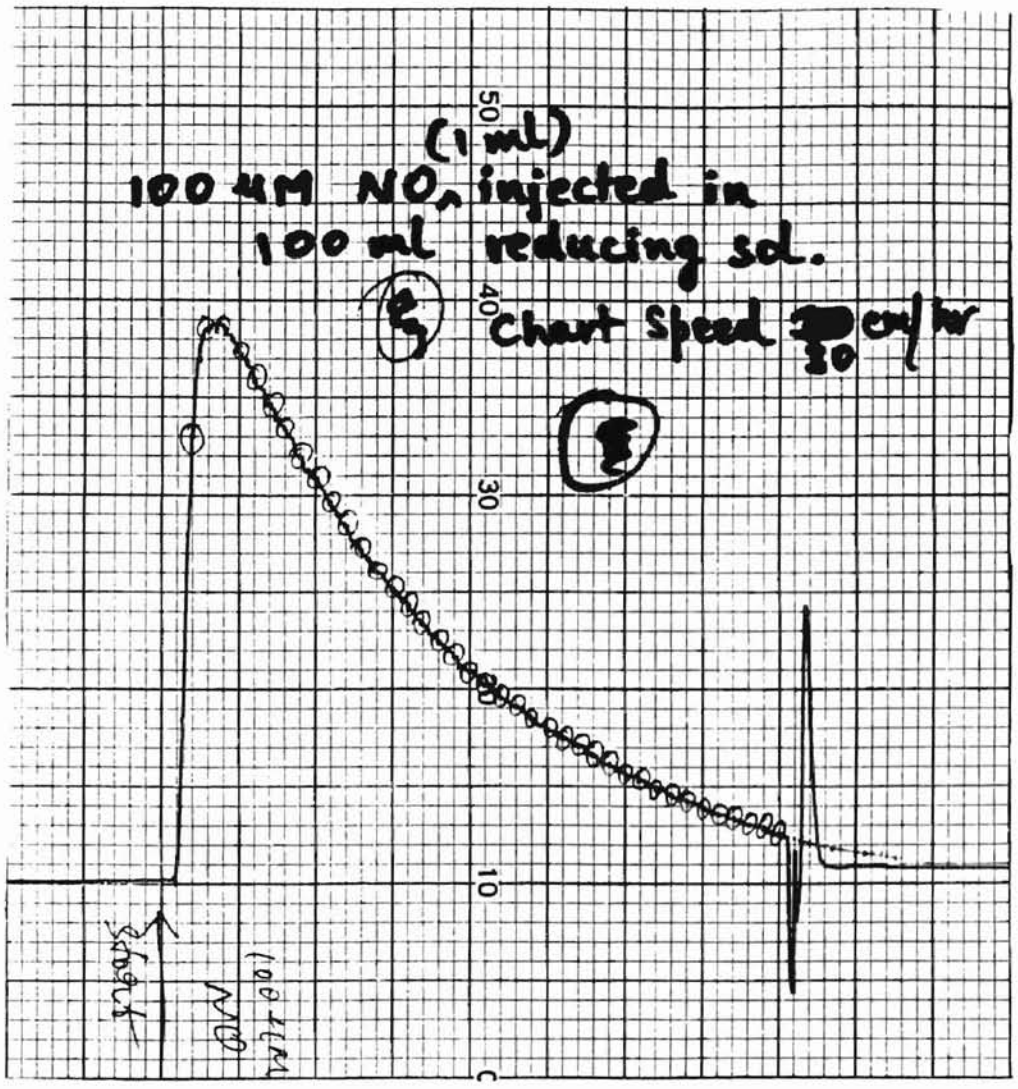

1 : Actual data obtained for the NO curve in Figure 3.6

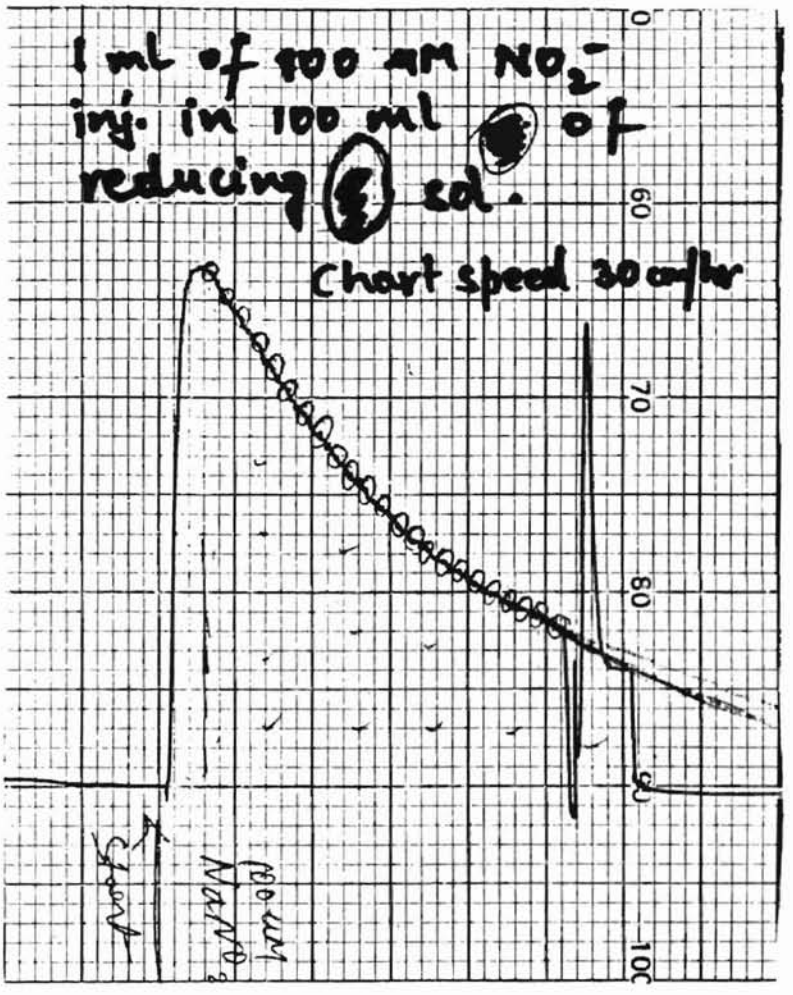

2 : Actual data obtained for the NO_2^- curve in Figure 3.6

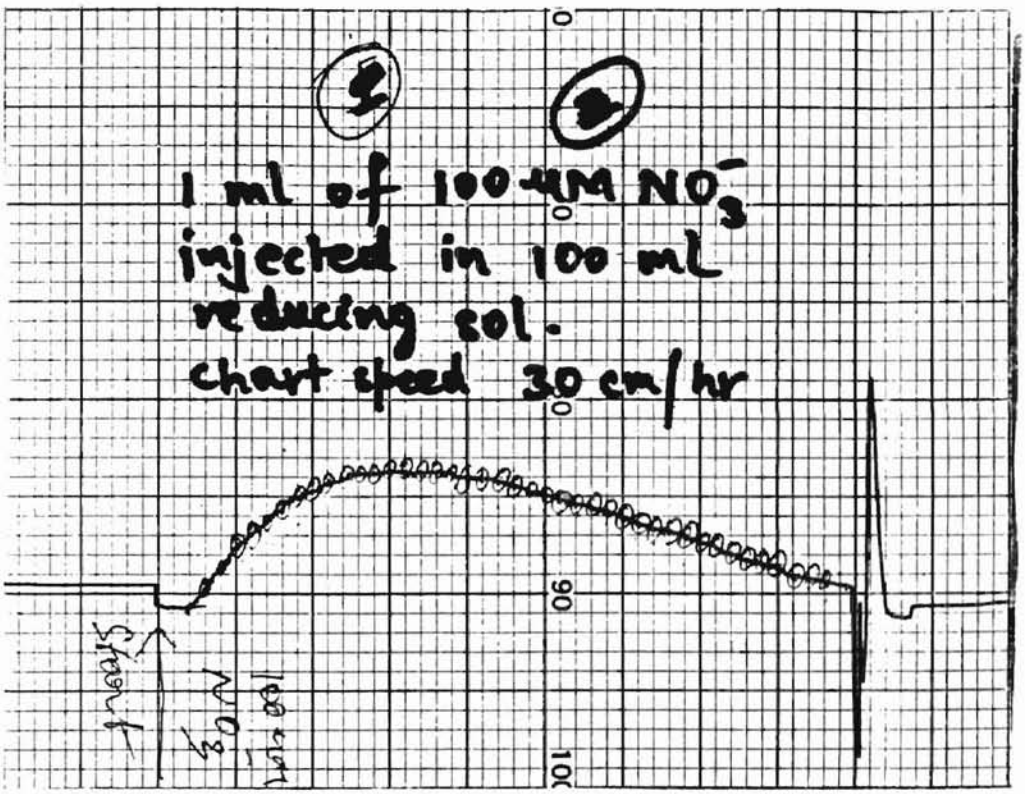

3 : Actual data obtained for the NO_3^- curve in Figure 3.6

VITA

Candidate for the degree of

Master of Science

Thesis: NITRITE AND NITRATE ANALYSIS IN WATER VIA CHEMILUMINESCENCE

Major field: Chemical Engineering

Biographical:

Personal Data: Born in Bokaro Steel City, India, on September 10, 1973, the son of Savitri and Dharm Deo Rai.

Education: Graduated from Delhi Public School R.K. Puram, New Delhi, June 1992; received Bachelor of Science (Distinction) degree in Chemical Engineering from Vinoba Bhave University, Hazaribag, India, July 1996; completed the requirement for a Master of Science degree at Oklahoma State University in May, 1998.

Experience: Intern at FCI Ltd., Sindri, India, from May 1995 to July 1995. Intern at Bokaro Steel Plant Ltd., Bokaro, India from May 1994 to August 1994. Intern at Barauni Oil Refinery Ltd., Barauni, India, from May 1993 to August 1993. Graduate Research Assistant, Department of Chemical Engineering, Oklahoma State University, August 1996 to August 1997. Teaching Assistant, Department of Chemical Engineering, Oklahoma State University, August 1997 to December 1997.

Memberships: The Honor Society of Phi Kappa Phi
AIChE (Affiliate Member).
IIChE (Affiliate Member).